FINAL REPORT

Synergistic Reductive Dechlorination of 1,1,1-Trichloroethane and Trichloroethene and Aerobic Biodegradation of 1,4-Dioxane

SERDP Project ER-2721

FEBRUARY 2019

Bruce Rittmann
Arizona State University

SERDP
DOD ▪ EPA ▪ DOE

Page Intentionally Left Blank

Page Intentionally Left Blank

REPORT DOCUMENTATION PAGE

Form Approved
OMB No. 0704-0188

1. REPORT DATE *(DD-MM-YYYY)*	**2. REPORT TYPE**	**3. DATES COVERED** *(From - To)*
31-05-2019	SERDP Final Report	05-04-2017 – 31-05-2019

4. TITLE AND SUBTITLE
Synergistic Reductive Dechlorination of 1,1,1-Trichloroethane and Trichloroethene and and Aerobic Biodegradation of 1,4-Dioxane

5a. CONTRACT NUMBER
W912HQ-17-C-0013

5b. GRANT NUMBER
N/A

5c. PROGRAM ELEMENT NUMBER

6. AUTHOR(S)
Bruce E. Rittmann, Youneng Tang, Rosa Krajmalnik-Brown, Yihao Luo, and Boya Wang

5d. PROJECT NUMBER
ER-2721; W74RDV63282715

5e. TASK NUMBER
N/A

5f. WORK UNIT NUMBER
001, 002, 003

7. PERFORMING ORGANIZATION NAME(S) AND ADDRESS(ES)
Arizona State University
660 Mill Ave., Suite 312
Tempe, AZ 84281-3679

Florida State University
874 Traditions Way, Third Floor
Tallahassee, FL 32306-4166

Aptwater, Inc.
1921 Arena Blvd.
Sacramento, CA 95834-3721

8. PERFORMING ORGANIZATION REPORT NUMBER
AWD00031373, GR15155

9. SPONSORING / MONITORING AGENCY NAME(S) AND ADDRESS(ES)
Strategic Environmental Research and Development Program
USACE Humphrey Engr. Ctr Spt Activity
7701 Telegraph Road
Alexandria, VA 22315-3860

10. SPONSOR/MONITOR'S ACRONYM(S)
SERDP

11. SPONSOR/MONITOR'S REPORT NUMBER(S) ER-2721

12. DISTRIBUTION / AVAILABILITY STATEMENT
DISTRIBUTION A. Approved for public release: distribution unlimited.

13. SUPPLEMENTARY NOTES
This Final Report supersedes the Final Report of 17 May 2019.

14. ABSTRACT

Groundwater co-contaminated with 1,4-dioxane and 1,1,1-trichloroethane (TCA) and/or trichloroethene (TCE) is common. We tested a synergistic platform featuring anaerobic TCE/TCA reduction in a H_2-based reactor followed by aerobic 1,4-dioxane biodegradation in a O_2-based membrane biofilm reactor (O_2-MBfR). For the H_2-based reduction stage, we evaluated the hydrogen-based Membrane Biofilm Reactor (MBfR) and a new hydrogen-based Membrane Palladium-film Reactor (MPfR). We conducted parallel modeling and experimental programs for the two MBfRs and an experimental program for the MPfR. Our evaluations proved that the rate and selectivity for reductive dichlorination of TCE/TCA to ethane was significantly higher with the MPfR than the MBfR. We configured the synergistic platform by linking the H_2-based MPfR with a 1,4-dioxane oxidizing O_2-MBfR in sequence. The ethane produced from reduction of TCE and TCA served as the primary electron donor for com-metabolic biodedgradation of 1,4-dioxane in the O_2-MBfR. In summary, we demonstrated proof-of-concept for removing TCE, TCA, and 1,4-dioxane without accumulation of toxic intermediates in a synergistic platform featuring a H_2-based MPfR for Pd-catalyzed TCE/TCA reduction followed by an O_2-based MBfR for biological degradation of 1,4-dioxane plus products from TCE/TCA reduction. This research advanced understanding of the fundamental factors controlling Pd-catalyzed reductive dechlorination and the co-metabolic biodegradation of dioxane derivatives.

15. SUBJECT TERMS
Reductive dechlorination of trichloroethane and trichloroethene, mono-oxygenation of 1,4-dioxane, hydrogen-based palladium-film reactor, oxygen-based membrane biofilm reactor

16. SECURITY CLASSIFICATION OF:			**17. LIMITATION OF ABSTRACT**	**18. NUMBER OF PAGES**	**19a. NAME OF RESPONSIBLE PERSON**
a. REPORT	**b. ABSTRACT**	**c. THIS PAGE**			Bruce Rittmann, PhD
UCLASS	UNCLASS	UNCLASS	UNCLASS	116	**19b. TELEPHONE NUMBER** *(include area code)* (480)727-0434

Page Intentionally Left Blank

Abstract

Introduction and objectives

Groundwater co-contaminated with 1,4-dioxane and 1,1,1-trichloroethane (TCA) and/or trichloroethene (TCE) is common. Strongly driven by the pressing needs of many DoD contaminated sites, we developed a synergistic platform that can simultaneously remove 1,4-dioxane, TCA, and TCE. The overall objectives of this project are to demonstrate proof-of-concept of this novel synergistic platform and to explore strategies to optimize this synergy.

Technical approach

We proposed and tested a synergistic platform featuring anaerobic TCE/TCA reduction in a H_2-based reactor followed by aerobic 1,4-dioxane biodegradation in a O_2-based membrane biofilm reactor (O_2-MBfR). For the H_2-based reduction stage, we evaluated the hydrogen-based Membrane Biofilm Reactor (MBfR) and a H_2-based Membrane Palladium-film Reactor (MPfR). We conducted parallel modeling and experimental programs for the two MBfRs and an experimental program for the MPfR.

Results

Our experimental evaluations of TCE/TCA reduction proved that the rate and selectivity for reductively dechlorinating TCE/TCA to ethane was significantly higher with the MPfR than with the MBfR, and modeling analyses for the H_2-based MBfR confirmed the results. The H_2-MPfR achieved TCE/TCA removals up to 96%, and selectivity towards ethane was 93%, with residual concentrations of dichloroethane (DCA) and monochloroethane (MCA) being minimal.

We then configured the synergistic platform by linking the TCE/TCA-reducing H_2-MPfR with a 1,4-dioxane-oxidizing O_2-MBfR in sequence. During 130 days of continuous operation, 1,4-dioxane and minor by-products from the H_2-MPfR were fully biodegraded through oxidation in the O_2-MBfR. Thus, all contaminants could be removed to below their Maximum Contaminant Levels or detection limits.

Benefits

In summary, we demonstrated proof-of-concept for removing TCE, TCA, and 1,4-dioxane without significant accumulation of toxic intermediates in a synergistic platform featuring a H_2-based MPfR for Pd-catalyzed TCE/TCA reduction followed by an O_2-based MBfR for biological degradation of 1,4-dioxane plus products from TCE/TCA reduction. Besides demonstrating a promising technology for groundwater treatment, this research advances understanding of the fundamental factors controlling Pd-catalyzed reductive dechlorination and the co-metabolic biodegradation of dioxane derivatives. The next steps are to advance the synergistic platform towards commercial application by a combination of modeling advancements, filling in key knowledge gaps, and pilot-scale testing.

Keywords

Synergistic platform, groundwater contamination, 1,4-dixoane, 1,1,1-trichloroethane, trichloroethene, biological degradation, Pd-catalyzed TCE/TCA reduction, co-metabolism, MBfR, MPfR, modeling.

Acknowledgements

The authors gratefully thank the U.S. Department of Defense's Strategic Environmental Research and Development Program (SERDP) for funding the research through Project ER-2721.

Table of Contents

Abstract i
Keywords ii
Acknowledgements iii
List of Figures vi
List of Tables ix
List of Acronyms x
Executive Summary xii
Introduction and objectives xii
Technical approach xii
Results xii
Benefits xiii
1. Overview 1
2. Biological Reductive Dechlorination of TCA/TCE in an H_2-MBfR 2
2.1. Background 2
2.2. Modeling evaluation 2
2.2.1. Modeling TCE reduction in the H_2-based MBfR 2
2.2.2. Modeling simultaneous reduction of TCE and TCA in H_2-Based MBfR 9
2.3. Experimental testing 10
2.3.1. Batch enrichment 10
2.3.2. MBfR operation 15
2.4. Cost analysis 17
2.5. Conclusion for biological TCA/TCE reduction 19
3. Pd-Catalytic Reduction of TCA/TCE in a H_2-MPfR 20
3.1. Background 20
3.2. MPfR setup and Pd coating 21
3.3. Testing TCA/TCE reduction 23
3.3.1. Batch kinetic tests 23
3.3.2. Continuously operated MPfR – reduction and selectivity 27

3.4. Cost analysis 33
3.5. Conclusion for catalytic TCA/TCE reduction 34
4. Biological Oxidation of 1,4-Dioxane in a O_2-MBfR 36
4.1. Background 36
4.2. Enrichment and evaluation of 1,4-dioxane degraders 37
4.3. O_2-MBfR operation 40
4.4. Modeling evaluation 43
4.4.1. Modeling 1,4-dioxane removal in O_2-based MBfR 43
4.5. Cost analysis 47
4.6. Conclusion for 1,4-dioxane degradation 48
5. Synergistic Platform for Simultaneous Removal of TCE, TCA, and 1,4-Dioxane 49
5.1. Experimental testing 49
5.2. Cost analysis 53
5.3. Conclusion for synergistic removal of TCA/TCE and 1,4-dioxane 54
6. Summary of Publications and Presentations from the Project 56
6.1. Peer-reviewed publications 56
6.2. National and international presentations 56
7. Future-research Plan 57
8. References 59
Appendix 65

List of Figures

Figure 2.1. Model components and their interactions in the H_2-based membrane biofilm. 4

Figure 2.2. Simulated distribution of (solid) biomass species along the biofilm depth for the experiment in Ziv-El et al. (2012a). 7

Figure 2.3. The effect of the TCE surface loading rate on the MBfR performance. 8

Figure 2.4. The effect of the TCE surface loading rate on the MBfR performance. 10

Figure 2.5. Dechlorinating performance of the mixed culture ZARA. Three different batch tests result with TCE, TCA and TCE + TCA as electron acceptors are shown in panels A, B and C, respectively. 12

Figure 2.6. Dechlorinating performance of the mixed culture DehaloR^2. Three different batch tests result with TCE, TCA and TCE + TCA as electron acceptors are show in panels A, B and C, respectively. 13

Figure 2.7. TCE dechlorinating performance of mixed culture SDC-9 for only TCE added. 14

Figure 2.8. Batch test results of ethene and MCA bio-reduction. 15

Figure 2.9. Schematic and picture of the MBfR system for H_2-based dechlorination of TCA and TCE. 16

Figure 2.10. Concentrations of TCE (blue dots), TCA (orange dots), cis-DCE (grey diamond), and VC (yellow triangle) in the H_2-MBfR. 17

Figure 3.1. Proposed scheme of Pd-catalytic hydrodechlorination of TCE, modified from Mori et al. (2004). 20

Figure 3.2. Schematic of the H_2-MPfR setup. 22

Figure 3.3. TCE and TCA reductions catalyzed by suspended PdNPs. The missing mass for TCE was MCA and DCA (< 3 μmole each). 24

Figure 3.4. TCE and TCA catalytic reduction batch test in the H_2-MPfR with composite membranes. The gray dash line shows the start of the H_2 supply. A: TCE only, B: TCA only, C: TCE and TCA. 26

Figure 3.5. Catalytic reductions of TCA and TCE in the H_2-MPfR with composite membranes in continuous operation. The green horizontal dash line represents the influent concentration of total chlorine in TCE and TCA. The black vertical dash line indicates HRT and pressure changes. 28

Figure 3.6. Catalytic reduction of TCE (top panel) and TCA (bottom panel) in batch test of a H_2-MPfR with polypropylene membranes. Panel A shows the mass changes of H_2, TCE, and its reduction products in the MPfR. Panel B shows the mass changes of H_2, TCA and its reductive

products in the MBfR with initial dissolved TCA concentration of 100 μM. The vertical dash line indicates the start point for H_2 supply. 29

Figure 3.7. Simultaneously TCA and TCE batch tests of a H_2-MPfR with polypropylene membranes. A had the H_2 supply pressure of 20 psig and initial concentration of 1 mM; B had the hydrogen supply pressure of 10 psig and initial concentration of 1 mM; C had the hydrogen supply pressure of 10 psig and initial concentration of 0.1 mM. 31

Figure 3.8. Selectivity differences among three batch tests having different H_2 supply pressures and initial TCA/TCE concentrations. 32

Figure 3.9. TCA and TCE catalytic reduction a H_2-MPfR with polypropylene membranes at continuous mode. The gray horizontal dash line represents the influent concentration of TCE and TCA. The black vertical dash line separates the four stages with different operating conditions noted above the graphic. 32

Figure 4.1. Schematic of aerobic 1,4-dioxane biodegradation, modified from (Mahendra et al. 2007). Yellow highlights the initial monooxygenation reactions. 36

Figure 4.2. The growth curve of *R. ruber* 219 with different electron-donor conditions.38

Figure 4.3. Results of batch tests with *R. ruber* 219. (A) Growth and dioxane oxidation by *R. ruber* 219 with acetate as the primary electron donor. (B) Growth with ethane as the sole electron donor and carbon source. (C) Growth with dioxane as the sole electron donor and carbon source. 39

Figure 4.4. Wetland sediments enriched dioxane oxidation culture with ethane as the primary electron donor..... 40

Figure 4.5. *R. ruber* 219 inoculated O_2-MBfR performance of dioxane removal in continuous (A) and batch (B) modes. 42

Figure 4.6. The 1,4-dioxane concentration in the O_2-MBfR. The first black dash line indicates the day when we re-inoculated the reactor. 43

Figure 4.7. Model components and their interactions in the O_2-MBfR. 44

Figure 4.8. The effect of surface loading rate on the performance of the O_2-based MBfR with two sub-stages: (A) Effluent concentrations of sub-stage 1; (B) Effluent concentrations of sub-stage 2. 46

Figure 5.1. The schematic of running H_2-MPfR and O_2-MBfR in sequence. 49

Figure 5.2. The 1,4-dioxane concentration in the O_2-MBfR fed with the effluent from the H_2-MPfR during the 130 days of sequential operation. The vertical black dash line indicates the day when the influent concentrations of all the three substrates were decreased. The red dots indicate the total chlorinated solvent (CS) concentration in both H_2-MPfR and O_2-MBfR..... 51

Figure 5.3. Concentration of chlorinated solvents in H_2-MPfR and O_2-MBfR when operated in

series. The vertical back dashed line indicates the stage changing from I to II..... 52

Figure 5.4. A short batch to test the 1,4-dioxane degrading activity of the O_2-MBfR without ethane as primary electron donor. 52

List of Tables

Table 2.1. Comparison of simulated results to experimental effluent concentrations and relative microbial fractions in Ziv-El et al. (2012a)[2] 5

Table 2.2. Estimated capital and operating expense for H_2-Based MBfR (100 gpm flow at 0.20 mg/L TCE, 40 kg TCE/yr). 18

Table 3.1. The coating and operating parameters for the H_2-MPfR..... 23

Table 3.2. Estimated capital and operating expense for H_2-Based MPfR (100 gpm flow at 13 mg/L TCE, or 2610 kg TCE/yr) 34

Table 4.2. Estimated capital and operating expense for a two-stage O_2-Based MBfR (100 gpm flow with modeled H_2-based MBfR effluent, 25.9 kg 1,4-dioxane/yr) 47

Table 5.1. Concentrations of dissolved VOCs at steady states of Stages I and II in the reactors continuously operated in sequence. 51

Table 5.2. Estimated capital and operating expense for an O_2-Based MBfR following the H_2-based MPfR at 100 gpm flow rate, 3500 kg 1,4-D/yr..... 54

List of Acronyms

1,4-D	1,4-dioxane
BAP	biomass associated products
BES	bromoethanesulfate
Cl^-	chloride
Conc.	concentration
CS	chlorinated solvent
DCA	dichloroethane
DCE	dichloroethane
DoD	Department of Defense
EPA	Environmental Protection Agency
EPS	extracellular polymeric substances
gpm	gallon per minute
MCA	monochloroethane
Pd	palladium
gpm	gallon per minute
H_2	hydrogen
HCO_3^-	bicarbonate
HRT	hydraulic retention time
IB	inert biomass
ID	inner diameter
k_1	fraction of electrons used for biomass synthesis
k_2	fraction of electrons used for UAP production
k_3	fraction of electrons used for EPS production
k_{det}	detachment coefficient
K_s	half-maximum-rate concentration
MBfR	membrane biofilm reactor
MCA	monochloroethane
MCL	maximum contamination level
MPfR	membrane palladium-film reactor
OD	outer diameter
Pd	palladium
PdNPs	palladium nano-particles
k_{det}	detachment coefficient
BES	bromoethanesulfate
PdNPs	palladium nano-particles
OD	outer diameter
R. ruber 219	*Rhodococcus ruber* strain 219
R. ruber 219	*Rhodococcus ruber* strain 219
TCA	trichloroethane

TCE	trichloroethene
UAP	utilization associated products
VC	vinyl chloride
VOCs	volatile organic compounds
WWTP	wastewater treatment plant
Y	yield coefficient

Executive Summary

Introduction and objectives

Groundwater co-contaminated with 1,4-dioxane and 1,1,1-trichloroethane (TCA) and/or trichloroethene (TCE) is common, since 1,4-dioxane was widely used as a stabilizer for chlorinated solvents. While TCE and TCA are among Department of Defense's (DoD) most frequently found contaminants of concern in groundwater, 1,4-dioxane is a contaminant of emerging concern. Strongly driven by the pressing needs of many DoD contaminated sites, we developed a synergistic platform that can simultaneously remove 1,4-dioxane, TCA, and TCE. The overall objectives of this project are to demonstrate proof-of-concept of this novel synergistic platform and to explore strategies to optimize this synergy by both experimental and computer modeling methods.

Technical approach

We proposed and tested a synergistic platform featuring anaerobic TCE/TCA reduction in a H_2-based reactor followed by aerobic 1,4-dioxane biodegradation in a O_2-based membrane biofilm reactor (O_2-MBfR). For the H_2-based reduction stage, we evaluated the hydrogen-based Membrane Biofilm Reactor (MBfR) and a new hydrogen-based Membrane Palladium-film Reactor (MPfR). We conducted parallel modeling and experimental programs for the two MBfRs and an experimental program for the MPfR.

Results

Our experimental evaluations of TCE/TCA reduction proved that the rate and selectivity for reductively dechlorinating TCE/TCA to ethane was significantly higher with the MPfR than with the MBfR, and modeling analyses for the H_2-based MBfR confirmed that the system had slow kinetics because of the relatively large half-maximum-rate concentration (K_s) for vinyl chloride (VC), an intermediate of TCE reduction. For the H_2-MPfR, continuous operation at an HRT of 15 hours and a TCE/TCA surface loading of 50 mmol/m^2-day achieved TCE/TCA removals up to 96%, and selectivity towards ethane was 93%, with residual concentrations of dichloroethane (DCA) and monochloroethane (MCA) being minimal. Our cost analysis of pilot-scale systems suggests that the H_2-based MPfR for Pd-catalytic treatment of TCE/TCA requires significantly lower capital and operating costs than the H_2-based MBfR on the bases if mass of TCE treated.

Based on the promising results with the MPfR, we configured the synergistic platform by linking the TCE/TCA-reducing H_2-MPfR with a 1,4-dioxane-oxidizing O_2-MBfR in sequence. During 130 days of continuous operation, the ethane produced from reduction of TCA and TCE in the H_2-MBfR served as the endogenous primary electron donor for promoting co-metabolic biodegradation of 1,4-dioxane in the O_2-MBfR. In addition, minor by-products from the H_2-MPfR, including DCA and MCA, were fully biodegraded through oxidation in the O_2-MBfR. Thus, all contaminants could be removed to below their Maximum Contaminant Levels or the

detection limit. For practical application, we suggest a full-scale system containing 256 commercial membrane modules in the MPfR and 318 commercial membrane modules in the O_2-MBfR to treat a flow of 100 gpm. The estimated capital and annual operating costs of the combined system are $6.6 M and $0.48 M/year for the 100-gpm capacity.

Benefits

In summary, we demonstrated proof-of-concept for removing TCE, TCA, and 1,4-dioxane without significant accumulation of toxic intermediates in a synergistic platform featuring a H_2-based MPfR for Pd-catalyzed TCE/TCA reduction followed by an O_2-based MBfR for biological degradation of 1,4-dioxane plus products from TCE/TCA reduction. This novel synergistic platform overcomes the drawbacks of existing treatment methods of TCE/TCA (toxic intermediates accumulation) and 1,4-dioxane (slow degradation due to low biomass concentration). It also provides a solution for simultaneous and synergistic removal of 1,4-dioxane, TCA, and TCE from groundwater. As shown in the figure below, the end product of the TCA and TCE reduction in the first stage (ethane) is used as the primary substrate in the second stage to promote growth of 1,4-dioxane-degrading bacteria.

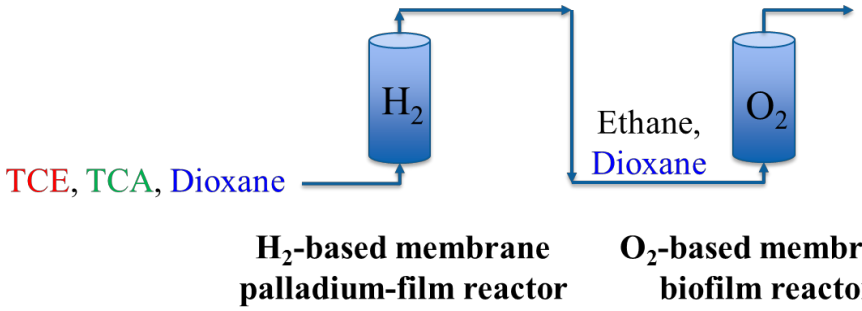

The platform is a pump-and-treat system, but the principles of the system can also be utilized for in-situ remediation, in which, the upstream TCA and TCE product (ethane) is used downstream for 1,4-dioxane degradation. For the pump-and-treat system, the next steps are to advance the synergistic platform towards commercial application for environmentally relevant contaminant concentrations by a combination of modeling advancements, filling in key knowledge gaps, and pilot-scale testing. For in-situ remediation, the next steps are to test in-situ technologies that can efficiently reduce TCA and TCE all the way to ethane.

Besides demonstrating a promising technology for groundwater treatment, this research advances understanding of the fundamental factors controlling Pd-catalyzed reductive dechlorination and the co-metabolic biodegradation of dioxane derivatives.

1. Overview

Groundwater co-contaminated with 1,4-dioxane and 1,1,1-trichloroethane (TCA) and/or trichloroethene (TCE) is common. While TCE and TCA are among the Department of Defense's (DoD's) most frequently found contaminants of concern in groundwater, 1,4-dioxane is a contaminant of emerging concern. Strongly driven by the pressing needs of many DoD contaminated sites, we developed a synergistic platform that can simultaneously remove 1,4-dioxane, TCA, and TCE. The overall objectives of this one-year limited-scope project are to demonstrate proof-of-concept of this novel synergistic platform and to explore strategies to optimize this synergism by both experimental and computer modeling methods. Specific objectives include: 1) reducing TCE (trichloroethene) to ethane in the first stage, 2) reducing TCA (1,1,1-trichloroethane) to ethane in the first stage, 3) enhancing co-metabolism of dioxane (1,4-dioxane) by using ethane as the primary donor substrate in the second stage, 4) running the two stages in series, 5) generalizing results through mathematical modeling, and 6) cost analysis.

We proposed and tested a synergistic platform featuring anaerobic TCE/TCA reduction in a H_2-based reactor followed by aerobic 1,4-dioxane biodegradation in a O_2-based membrane biofilm reactor (O_2-MBfR). For the H_2-based reduction stage, we evaluated the hydrogen-based Membrane Biofilm Reactor (MBfR) and a new hydrogen-based Membrane Palladium-film Reactor (MPfR). We conducted parallel modeling and experimental programs for the two MBfRs and an experimental program for the MPfR.

The results proved that this synergistic platform overcomes the drawbacks of existing treatment methods of TCE/TCA (toxic intermediates accumulation) and 1,4-dioxane (slow degradation due to low concentrations of bioamss), and it provides a solution for simultaneous removal of 1,4-dioxane, TCA, and TCE from groundwater.

The platform is a pump-and-treat system, but the principles of the system can also be utilized for in-situ remediation, in which, the upstream TCA and TCE product (ethane) is used downstream for 1,4-dioxane degradation. For the pump-and-treat system, the next steps are to advance the synergistic platform towards commercial application for environmentally relevant contaminant concentrations by a combination of modeling advancements, filling in key knowledge gaps, and pilot-scale testing. For in-situ remediation, the next steps are to test in-situ technologies that can efficiently reduce TCA and TCE all the way to ethane.

This report includes experimental and modeling evaluations of a H_2-MBfR for biological TCA/TCE reduction (Section 2), a H_2-MPfR for Pd-based catalytic TCA/TCE reduction (Section 3), an O_2-MBfR for 1,4-dioxane biodegradation (Section 4), and a synergistic platform featuring the H_2-MPfR and O_2-MBfR operated in sequence for simultaneous removal of TCA, TCE, and 1,4-dioxane (Section 5), publications and presentations from this project (Section 6), and a future research plan (Section 7).

2. Biological Reductive Dechlorination of TCA/TCE in an H_2-MBfR

2.1. Background

Biological processes have been widely tested for TCE and TCA removal due to their low cost. In particular, reductive dechlorination of TCE to ethene *in-situ* (Adamson et al. 2003), in microcosms (Delgado et al. 2014a), and in the H_2-based MBfR has been widely documented (Chung and Rittmann 2007, Chung et al. 2008, Ziv-El et al. 2012a, Ziv-El et al. 2012b). Ziv-El et al. (2012a) reported conditions for a H_2-based MBfR leading to the accumulation and activity of *Dehalococcoides*, the only known bacteria that can metabolically reduce VC to ethene (He et al. 2003). These conditions included suppressing competing processes such as methanogenesis and acetogenesis. Nearly complete reduction of TCA to monochloroethane (MCA) in the H_2-based MBfR was demonstrated (Chung and Rittmann, 2008).

The main challenges of these kind of anaerobic processes include maintaining strictly anaerobic conditions, a long start-up period, necessarily long hydraulic retention time (HRT; usually more than 24 hours), weak occupation of dechlorinating microorganisms (particularly *Dehalococcoides*) in the biofilm, competition for H_2 by methanogenesis and homoacetogenesis, and the potential accumulation of more toxic daughter products. For example, vinyl chloride (VC), a daughter product of TCE reduction, is more toxic than TCE; its maximum contamination level (MCL) is 2 ppb, a value even lower than that of TCE (5 ppb) (U.S. EPA, 2015). Furthermore, the more-chlorinated ethenes inhibit biotransformation of the less-chlorinated ethenes (Yu et al. 2005), and co-occurrence of TCE and TCA leads to mutual inhibition of TCE and TCA towards biological reduction of each other as well as their intermediates (Grostern et al. 2009, Chan et al. 2011).

Therefore, the application of simultaneous bioreduction of TCE and TCA is not a secure technology in practice. The goal of this task is to evaluate the feasibility of TCE and TCA reduction in a H_2-MBfR through modeling evaluation and experimental testing.

2.2. Modeling evaluation

2.2.1. Modeling TCE reduction in the H_2-based MBfR

We developed a mathematical model to simulate TCE reductive dechlorination in the H_2-based MBfR. (This work was submitted as a manuscript to *Biotechnology and Bioengineering*: Wang, B., Krajmalnik-Brown, R., Zhou, C., Luo, Y., Rittmann, B.E., Tang, Y. Modeling the interactions among trichloroethene reduction, methanogenesis, and homoacetogenesis in a H_2-based biofilm). In this section, we briefly summarize the model development and evaluation, and then we use the model to predict TCE reduction in a pilot-scale H_2-based MBfR over a wide range of TCE loading rates. The submitted manuscript, which is appended, provides more details.

The model considers the interactions among TCE reduction, methanogenesis, and homoacetogenesis. It has six solid biomass species (*Dehalococcoides*, *Geobacter,* methanogens, homoacetogens, inert biomass (IB), and extracellular polymeric substances (EPS)) and 10 dissolved chemical species (TCE, dichloroethane (DCE), VC, ethene, H_2, methane, acetate, HCO_3^-, utilization associated products (UAP), and biomass associated products (BAP)). Figure 2.1 summarizes the interactions among all the microbiological and chemical species.

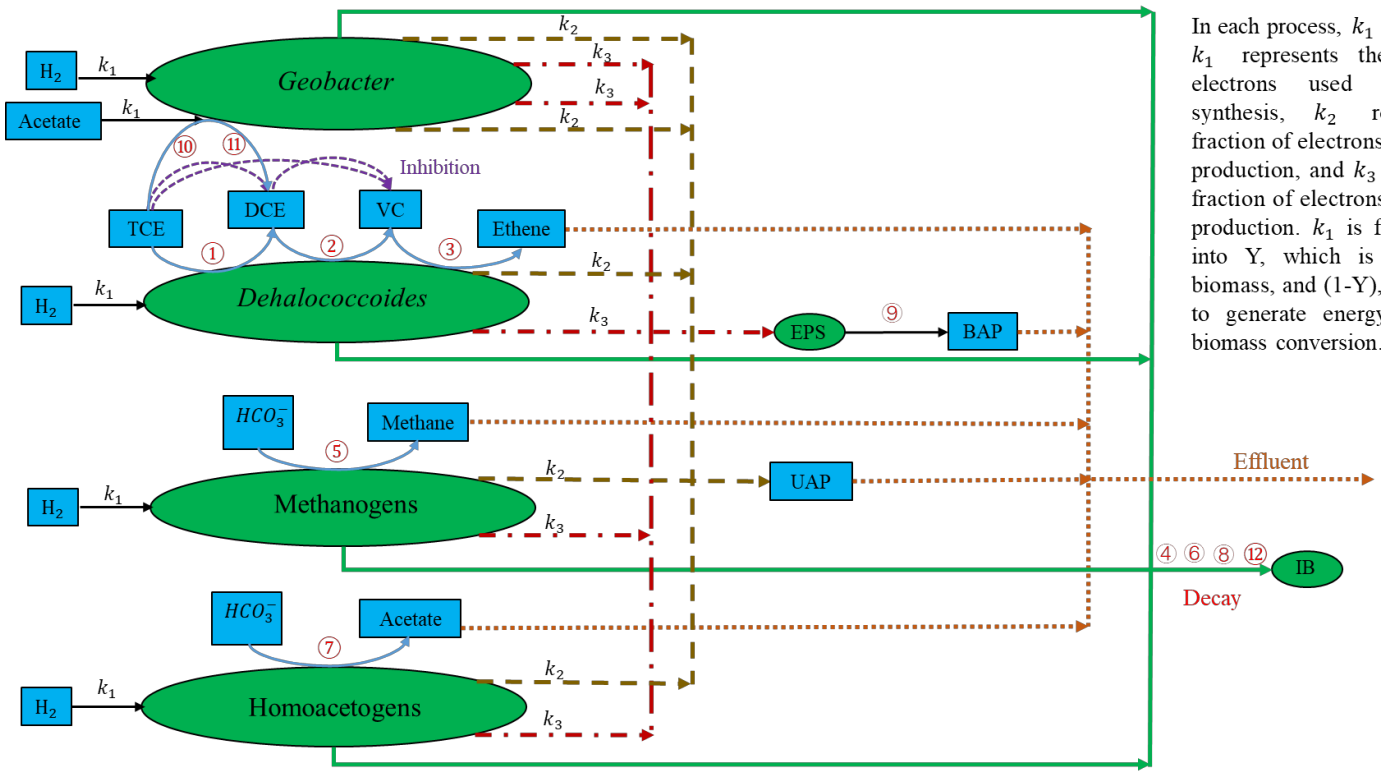

Figure 2.1. Model components and their interactions in the H_2-based membrane biofilm.

Notes:

1) The blue square symbols represent dissolved chemical species and green round symbols represent solid biomass species.
2) This figure is from the submitted manuscript: Wang, B., Krajmalnik-Brown, R., Zhou, C., Luo, Y., Rittmann, B.E., Tang, Y. Modelling the interactions among trichloroethene reduction, methanogenesis, and homoacetogenesis in a H_2-based biofilm, submitted to *Biotechnology and Bioengineering*.
3) Processes ①, ②, ③ refer to the stepwise TCE reduction by *Dehalococcoides* using H_2 as the electron donor; ④, ⑥, ⑧, ⑫ refer to biomass inactivation; ⑤ refers to methanogenesis; ⑦ refers to homoacetogenesis; ⑨ refers to EPS hydrolysis; ⑩ and ⑪ refer to TCE reduction by *Geobacter* using H_2 and acetate as the electron donor, respectively.

To evaluate the model, we used mid-range parameter values reported in the literature and conditions reported for a bench-scale experiment with a H_2-based MBfR and TCE reductive dechlorination (Ziv-El et al., 2012a). The reactor was operated to treat a synthetic groundwater contaminated by TCE until steady state was achieved. The experimental results and simulated results are compared in Table 2.1.

Table 2.1. Comparison of simulated results to experimental effluent concentrations and relative microbial fractions in Ziv-El et al. (2012a)[2]

	Experiment Results	Simulation Results
TCE (mM)	<0.00001	0.0039
DCE (mM)	0.013	0.00062
VC (mM)	0.10	0.071
Ethene (mM)	0.21	0.25
Methane (mM)	Not measured	0.0067
Acetate (mM)	4.5	2.20
Dehalococcoides (%)[1]	43.3	49.3
Methanogens (%)[1]	0.4	1.1
Homoacetogens (%)[1]	17.3	17.7
Geobacter (%)[1]	39.0	32.0

Notes:

1. To be consistent with Ziv-El et al. (2012a), the fraction of each solid biomass species is mass of one active biomass species in the biofilm divided by the mass of total active biomass species in the biofilm.
2. This table is from the submitted manuscript: Wang, B., Krajmalnik-Brown, R., Zhou, C., Luo, Y., Rittmann, B.E., Tang, Y. Modelling the interactions among trichloroethene reduction, methanogenesis, and homoacetogenesis in a H_2-based biofilm, submitted to *Biotechnology and Bioengineering*.

Overall, the experimental results and the model simulations were consistent. *Dehalococcoides* (43% in experiment and 49% in the model) and *Geobacter* (39% in experiment and 32% in model) dominated the biofilm; this corresponded very well with complete TCE reduction (>98% removal of 0.325 mM TCE in experiment and model). Accumulation of DCE was minimal (0.013 mM in the experiment and 0.00062 mM in the model), but more VC accumulated (0.10 mM in experiment and 0.071 mM in model). The accumulation of DCE and VC can be explained by the fact that *Geobacter* does not reduce DCE and VC; thus, *Geobacter* converts TCE to DCE, but not further. The higher accumulation of VC than DCE can be explained by the ~30 times higher half-maximum-rate concentrations for VC than for DCE.

Acetate was zero in the influent, but increased in the effluent (4.5 mM in the experiment, and 2.2 mM in the model). High acetate accumulation occurred because the maximum acetate-production rate by homoacetogens is about one order of magnitude higher than the maximum acetate-utilization rate by *Geobacter*. Methanogens were negligible (<1%) in the experiment and the model, because they were outcompeted by homoacetogens, since methanogens have a smaller maximum specific growth rate and a higher decay rate.

Figure 2.2 shows the model-generated biomass distribution along the biofilm depth of 15 μm, the steady-state thickness. The biofilm could be divided into three layers, each characterized by one dominant type of active microorganism. Homoacetogens dominated Layer 1, which was next to the membrane and closest to the H_2 source. In this layer, *Dehalococcoides* and *Geobacter* were suppressed due to the low concentration of TCE and DCE. *Dehalococcoides* outcompeted homoacetogens and dominated in Layer 2 because of the presence of TCE and DCE in this layer. *Geobacter* was dominant in Layer 3 due to the high TCE concentration.

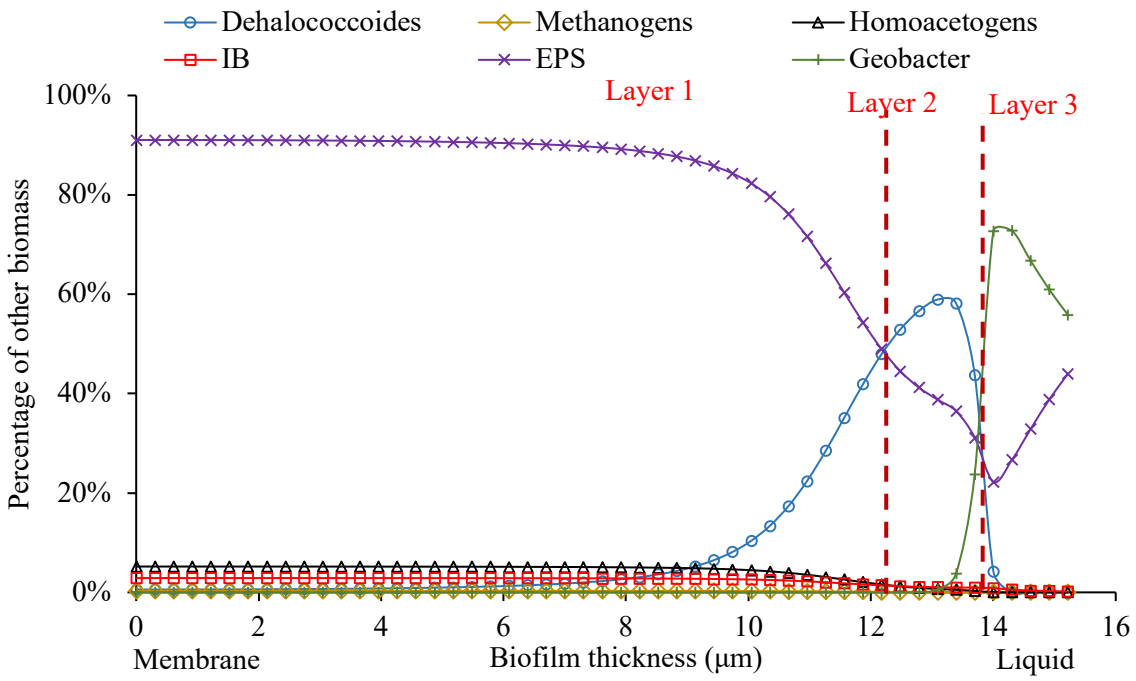

Figure 2.2. Simulated distribution of (solid) biomass species along the biofilm depth for the experiment in Ziv-El et al. (2012a). Note: This figure is from the submitted manuscript: Wang, B., Krajmalnik-Brown, R., Zhou, C., Luo, Y., Rittmann, B.E., Tang, Y. Modelling the interactions among trichloroethene reduction, methanogenesis, and homoacetogenesis in a H_2-based biofilm, submitted to *Biotechnology and Bioengineering*.

We next used the model to simulate the performance of a pilot-scale H_2-based MBfR (Tang et al., 2010) treating a groundwater that contained a typical TCE concentration of 1.5 μM (Freeberg et al. 1987, Hirvonen et al. 1996). The reactor's performance was affected by three major operating conditions: TCE loading rate, H_2 pressure, and the biofilm detachment rate (Rittmann, 2007). During the simulation, we varied the TCE surface loading between 7.8×10^{-4} and 7.8 mmol/m^2-day while fixing the H_2 pressure at a low value (*i.e.*, 1.1 atm) and the biofilm detachment rate at a typical value, 36 cm^{-1}day^{-1} (Tang et al. 2012). A low H_2 pressure was used to minimize the growth of H_2-utilization bacteria other than TCE-reducing bacteria.

The simulated effluent concentrations of chemical solutes are plotted in Figure 2.3. Based on this figure, 1.2×10^{-2} mmol/m^2-day was selected as the design surface loading and later used for cost analysis. When the TCE loading was smaller than 1.2×10^{-2} mmol/m^2-day (HRT = 2.4 hour; the black dash vertical line in Fig. 2.3), the effluent concentrations of TCE and DCE were below the MCLs set by EPA. Under no modeled conditions could the effluent VC concentration meet the MCL. At the optimum loading, substantial acetate (1.1 mM) was produced due to homoacetogenesis; considerable H_2 (0.5 mM) existed in the effluent due to over-supply; and a

small amount of ethene (0.013 μM) was produced. Methane production was negligible. The simulation results suggest that a H_2-based MBfR cannot completely dechlorinate TCE under typical operating conditions and with the parameter values used here. In particular, the effluent concentration of VC could not meet the MCL due to VC's high half-maximum-rate concentration (K_s) with *Dehalococcoides*.

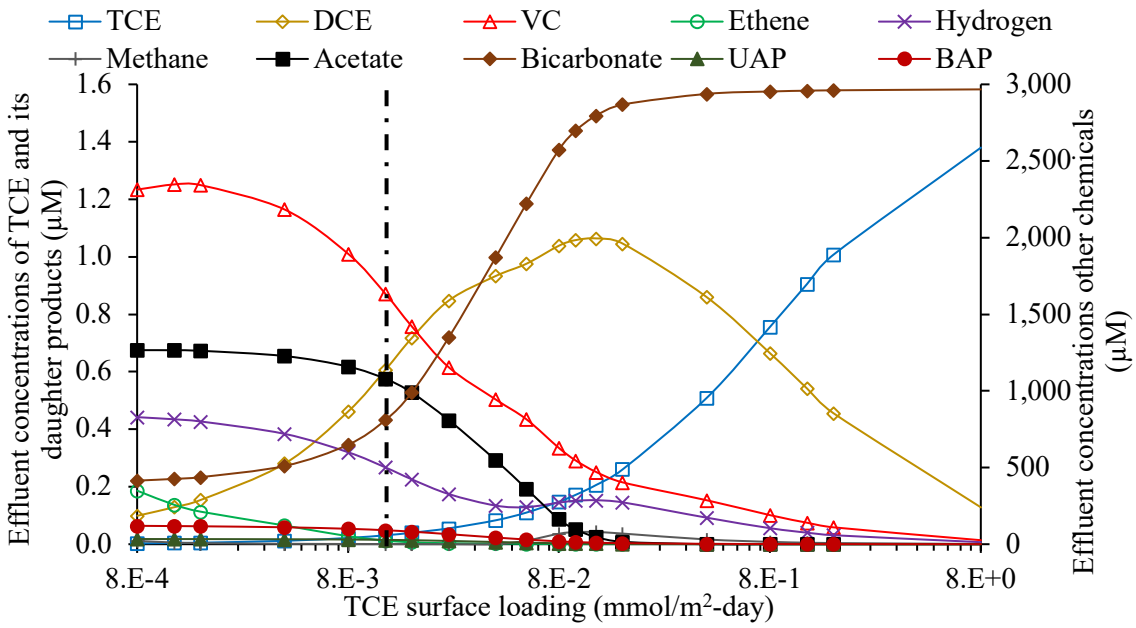

Figure 2.3. The effect of the TCE surface loading rate on the MBfR performance. Note: MCLs for TCE, DCE, and VC are 0.038, 0.72, and 0.032 μM, respectively.

We then simulated the same reactor for TCE removal over a range of operating conditions. (We are preparing a manuscript to discuss operating strategies for complete biological dechlorinating of TCE.) In brief, we found that the best TCE removal occurred when the H_2 pressure was low (0.05 atm), the detachment rate was low (1.0 $cm^{-1}day^{-1}$), and the half-maximum rate concentration of VC was decreased from the mid-range value (1.8×10^{-2} mg/L or 290 μM) to the minimum value reported in the literature (1.6×10^{-4} mg/L or 2.6 μM) (Haston and McCarty 1999). With this best condition, the effluent concentrations of TCE, DCE, and VC could meet all EPA MCLs at a maximum TCE surface loading of 1.2×10^{-2} mmol/m^2-day. Coincidentally, this loading rate was the same as that used to evaluate the MBfR at typical operating conditions (the previous paragraph). Therefore, we used 1.2×10^{-2} mmol/m^2-day as the design loading for the cost analysis that follows.

2.2.2. Modeling simultaneous reduction of TCE and TCA in H_2-Based MBfR

To simulate simultaneous reduction of TCE and TCA, we expanded the model developed in Section 2.2.1 by adding the TCA reduction process. The expanded model had 7 solid biomass species (*Dehalococcoides*, *Geobacter*, *Dehalobacter*, methanogens, homoacetogens, IB, and EPS) and 14 dissolved chemical species (TCE, DCE, VC, ethene, TCA, DCA, CA, ethane, H_2, methane, acetate, HCO_3^-, UAP, and BAP).

Besides the inhibition among chlorinated ethenes (*i.e.,* more-chlorinated ethenes inhibit less-chlorinated ethenes) (Yu et al. 2005), inhibition among chlorinated ethanes and chlorinated ethenes also was included. TCA inhibits the reduction of TCE, DCE, and VC (Chan et al., 2011). In contrast, TCE, DCE, and VC inhibit TCA reduction, and DCE and VC inhibit DCA reduction (Grostern et al. 2009). The inhibition to TCA and DCA reductions by chlorinated ethenes is uncompetitive, while other inhibitions are competitive (Grostern et al. 2009). We were not able to evaluate this model against experimental results, since experimental studies are not available in the literature.

The model was used to simulate the performance of the H_2-MBfR treating a groundwater containing a typical TCE concentration of 1.5 μM (Freeberg et al. 1987, Hirvonen et al. 1996) and a typical TCA concentration of 60 μM (Scheutz et al. 2011) in contaminated groundwater. During the simulation, the H_2 pressure and the detachment coefficient (k_{det}) were fixed at 1.1 atm and 36 $cm^{-1}day^{-1}$, respectively, which were the same conditions as those for the TCE model. By varying the flow rate, the reactor performance at a range of the TCE and TCA surface loading rates (1.2×10^{-3} – 0.12 mmol TCE/m^2-day and 4.8×10^{-2} – 4.8 mmol TCA/m^2-day) was simulated.

The model results for the chlorinated chemicals, ethene, and ethane are shown in Figure 2.4. The black vertical dash line (TCE surface loading rate = 1.9×10^{-2} mmol/m^2-day, TCA surface loading rate = 7.6×10^{-2} mmol/m^2-day; HRT = 1.5 hour) represents the optimum loading rate, since TCE, DCE, and TCA are below their MCLs. Under no conditions could the concentration of VC go below its MCL. Therefore, the H_2-MBfR could not achieve complete dechlorination of TCE and TCA with practical operating conditions. Interestingly, the co-existence of TCA favored TCE removal: The optimum TCE surface loading increased from 1.2×10^{-2} mmol/m^2-day (when only TCE existed) to 1.9×10^{-2} mmol/m^2-day (when both TCE and TCA co-existed). This is explained by the fact that TCA promoted the growth of *Dehalobacter,* which also reduces TCE (Scheutz et al., 2011).

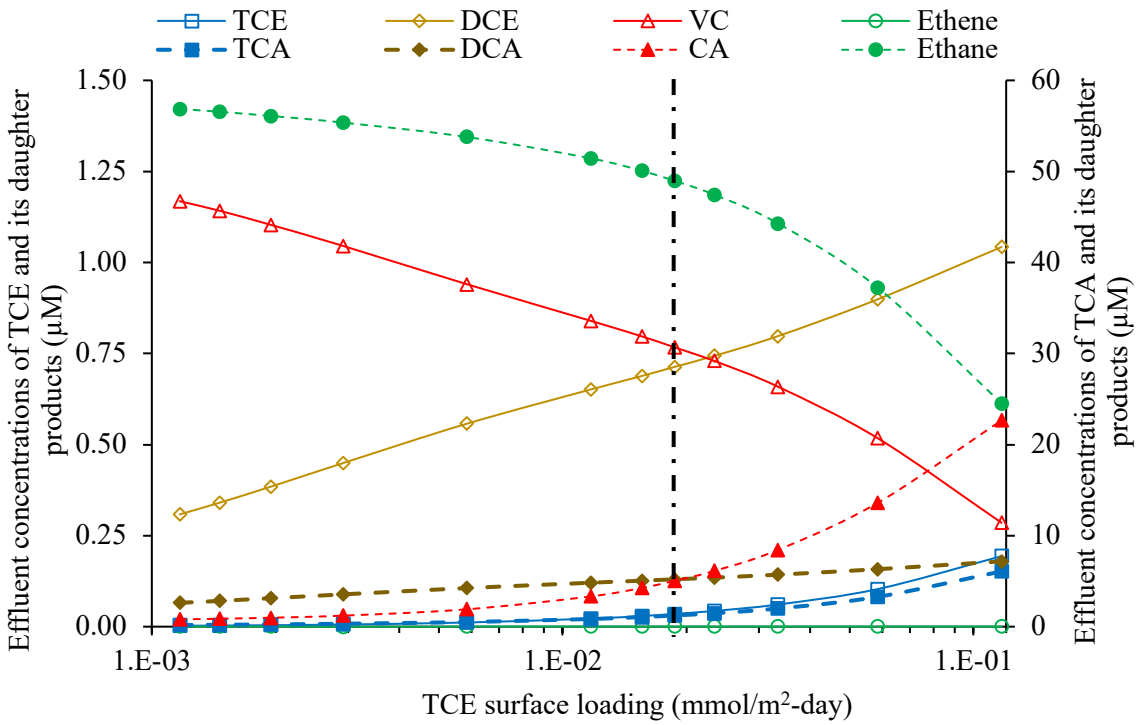

Figure 2.4. The effect of the TCE surface loading rate on the MBfR performance. Note: The TCA surface loading is 40 times of the TCE surface loading. MCLs are 1.5 μM (TCA), 0.038 μM (TCE), 0.72 μM (DCE), and 0.032 μM (VC).

2.3. Experimental testing

2.3.1. Batch enrichment

We tested three dechlorinating cultures for their abilities to reductively dechlorinate TCE, TCA, and TCE+TCA in batch bottles using H_2 (over 90% in the headspace) as the electron donor and 10 mM acetate, 10 mM methanol, or 10 mM lactate as carbon sources; also, 2 mM of bromoethanesulfate (BES) was added to inhibit the methanogens. The inoculum cultures were ZARA (Delgado et al. 2014b), DehaloR^2 (Ziv-El et al. 2011), and SDC-9 (Vainberg et al. 2009), and we tested duplicate serum bottles for all conditions. All three were active in TCE reduction to DCE, but only SDC-9 was able to further reduce DCE to VC. All three were not able to reduce TCA to DCA, and the presence of TCA slowed down the TCE reduction rate.

Figure 2.5 shows the dechlorination performance for the mixed culture ZARA. The data are presented for the serum bottles with the fastest TCE removal, although the results were similar for the other bottles. When TCE was added as the sole electron acceptor, ZARA initially could reduce 99% of 92 μmole of TCE to cis-DCE within 14 days; after the second spike of 95 μmole, TCE was totally reduced within 9 days (Fig. 2.5A). Further reduction of cis-DCE to VC or ethene was not observed within the 60-day enrichment. When TCA was added as the only electron

acceptor, ZARA did not reduce TCA at all in the 50-day enrichment (Fig. 2.5B). When TCA and TCE were added together (Fig. 2.5C), ZARA was still able to reduce TCE to cis-DCE, although the reduction rate was slower (99% of 94 μmole TCE reduced within 20 days) compared to adding TCE alone (Fig. 2.5A). No further reductions of TCE or TCA were observed during the 50-day enrichment.

The mixed culture DehaloR^2 showed similar results as ZARA when TCE and TCA were added separately (Fig. 2.6A and B for the bottle with the fastest rates). When TCA and TCE were added together, DehaloR^2 had a much slower TCE reduction rate (99% of 101 μmole TCE reduced within 28 days, Fig. 2.6C) compared to with TCE alone (99% of 105 μmole TCE reduced within 9 days, Fig. 2.6A).

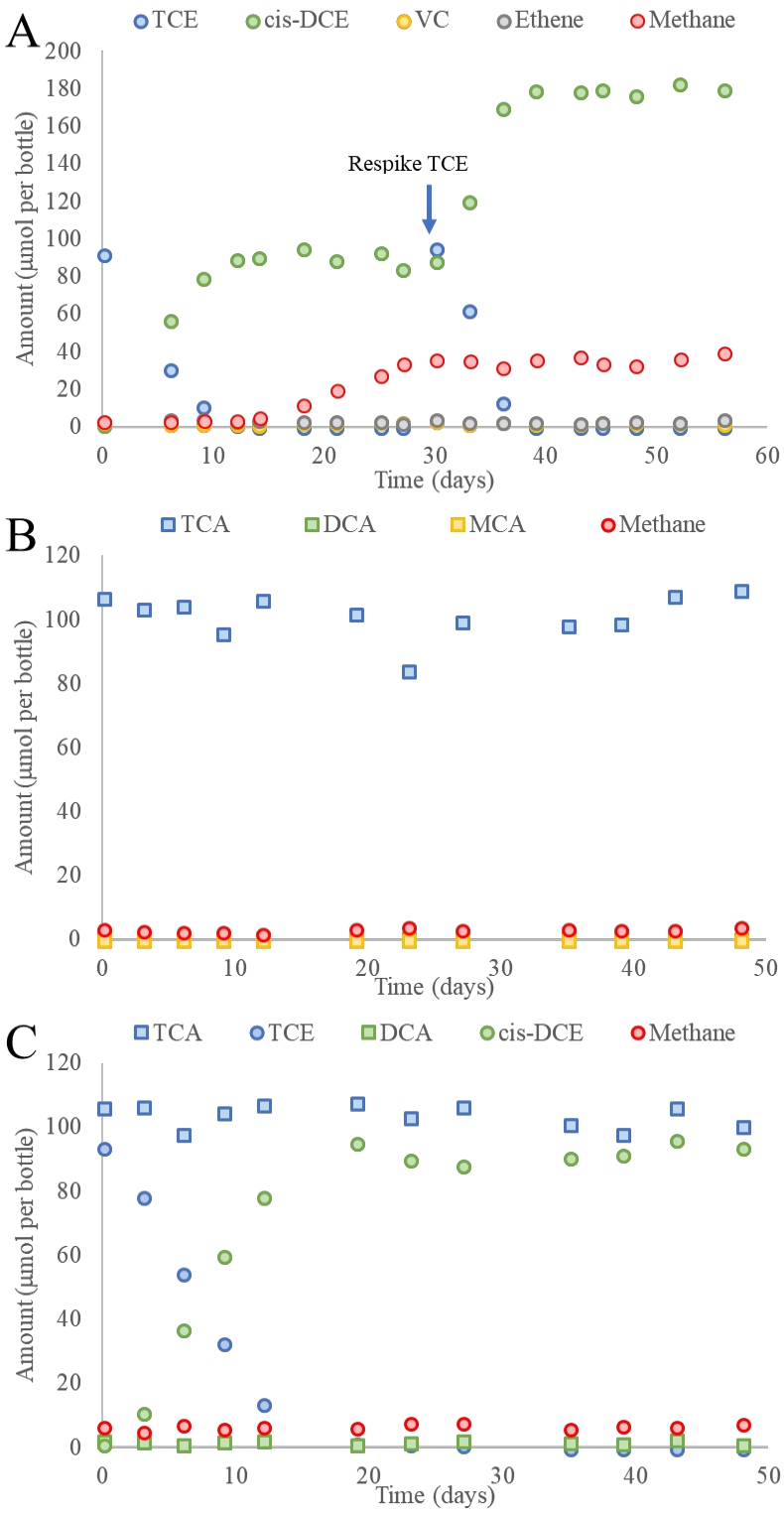

Figure 2.5. Dechlorinating performance of the mixed culture ZARA. Three different batch tests result with TCE, TCA and TCE + TCA as electron acceptors are shown in panels A, B and C, respectively.

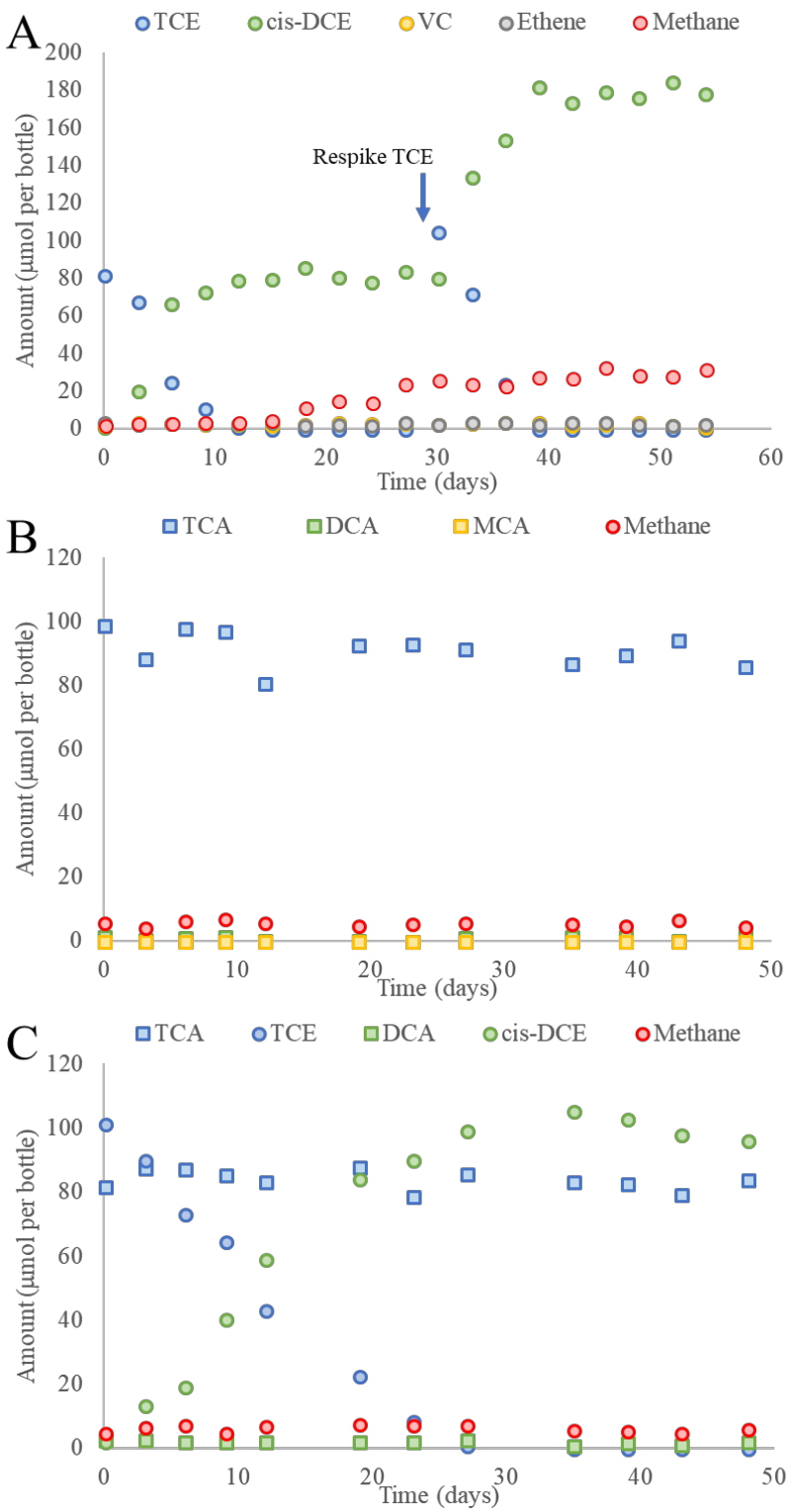

Figure 2.6. Dechlorinating performance of the mixed culture DehaloR^2. Three different batch tests result with TCE, TCA and TCE + TCA as electron acceptors are show in panels A, B and C, respectively.

For the mixed culture SDC-9, about 0.1 mmol TCE was completely converted to cis-DCE within 12 days, and VC started to accumulate (Fig. 2.7). After we respiked 0.1 mmol TCE into the bottles on the 30th day, TCE was converted to cis-DCE within 7 days, and VC slowly accumulated (280 µM or 14% of the initial TCE in two weeks). 10 mM lactate was added to the bottle on the 43th day, but it did not have an effect on cis-DCE reduction.

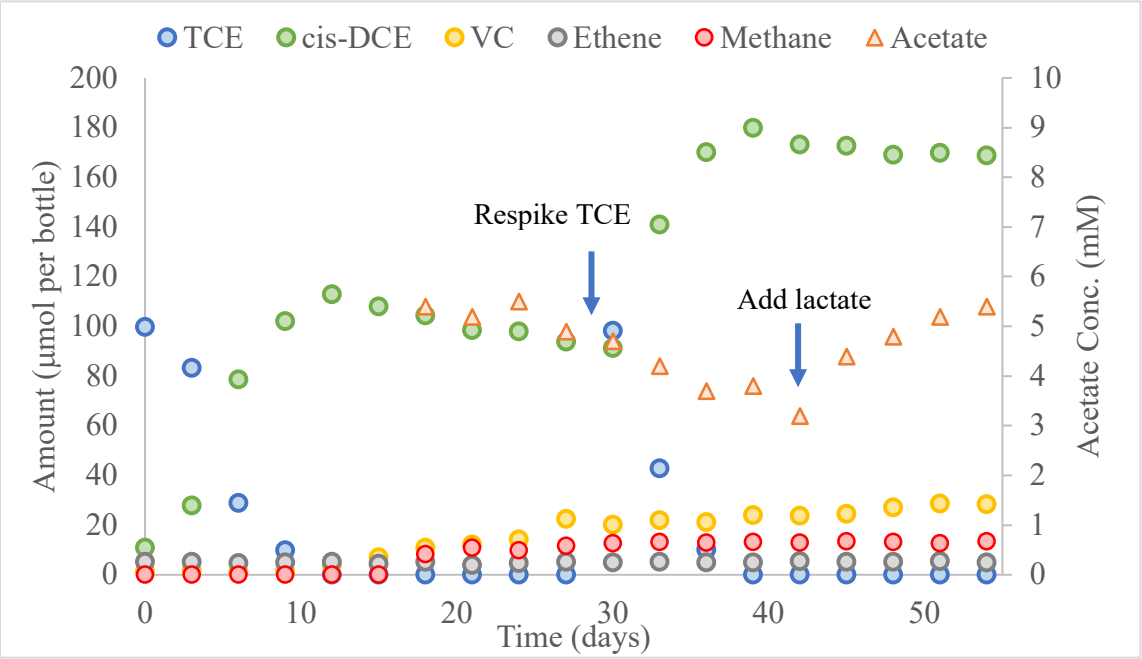

Figure 2.7. TCE dechlorinating performance of mixed culture SDC-9 for only TCE added.

Along with the batch tests of TCA and TCE reductions, tests for ethene and MCA reductions also were carried out in serum bottles with the three cultures and two other inocula: wastewater treatment digester sludge and wetland sediments. All the test bottles showed the same results: Ethene and MCA were not reduced to ethane with these cultures, but methane was generated (Fig. 2.8).

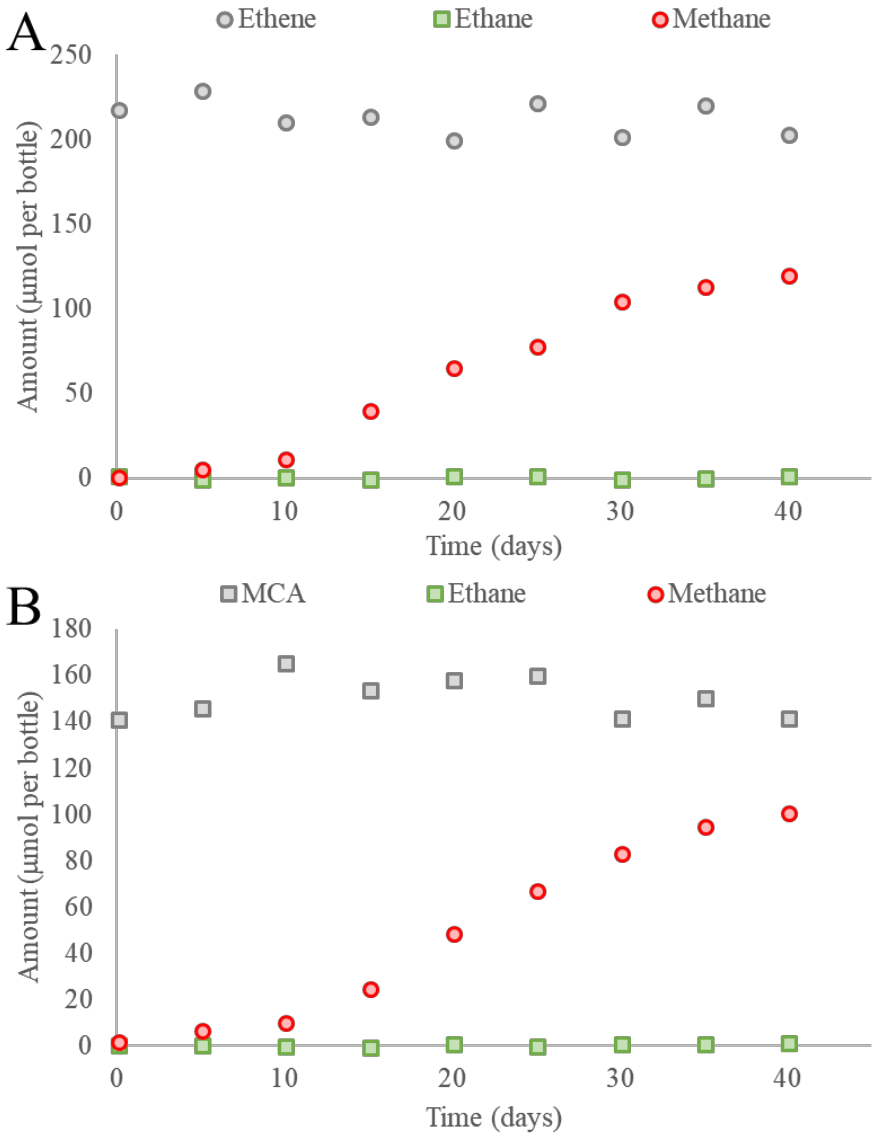

Figure 2.8. Batch test results of ethene and MCA bio-reduction.

2.3.2. MBfR operation

A schematic and picture of the H_2-based MBfR used for TCE and TCA bioreduction are shown in Figure 2.9, and details of the reactor and its characteristics are described by Liu et al. (2018). The MBfR consisted of a 380-mL glass bottle, Viton or Teflon tubing, and Teflon stopcocks. The glass bottle contained five bundles of 32 hollow-fiber membranes (Composite bubble-less gas-transfer membrane, Model MHF 200TL Mitsubishi Rayon Co., Ltd, Tokyo, Japan), each 14-cm long; this gave a total membrane surface area of 160 cm^2. The reactor was positioned with an inclination about 40° to keep the effluent at the top and to avoid gas being trapped in the reactor.

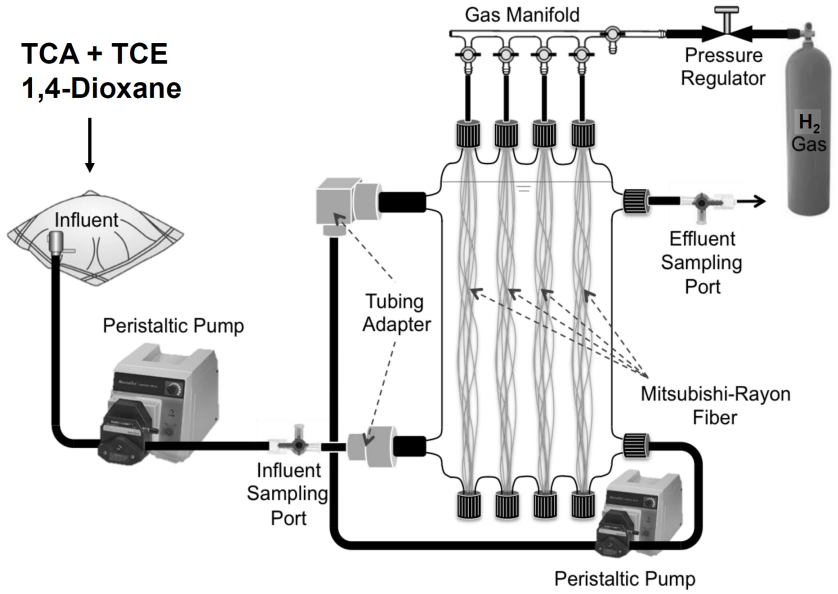

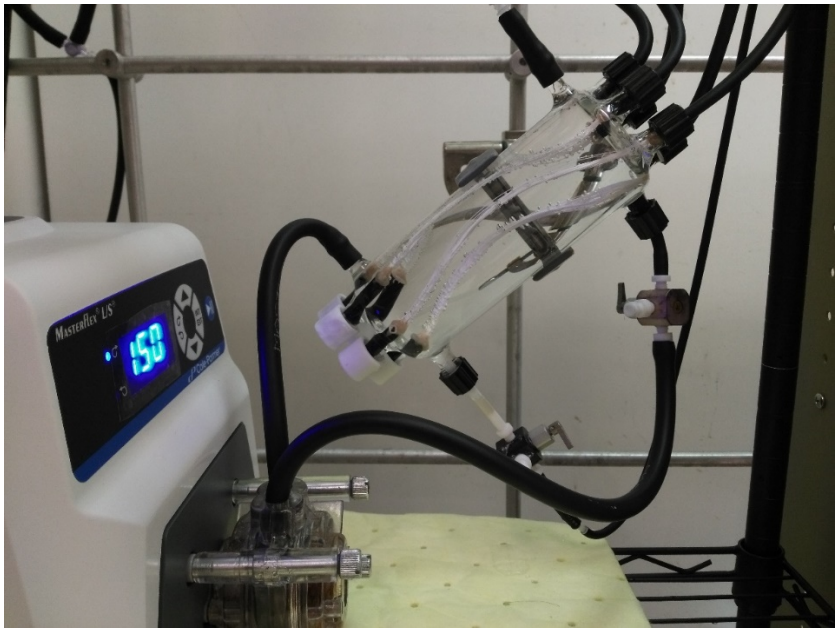

Figure 2.9. Schematic and picture of the MBfR system for H_2-based dechlorination of TCA and TCE.

At the beginning of the experiments with the H_2-based MBfR, the dechlorinating culture ZARA was inoculated into MBfR together with 0.1 mM each of TCE and TCA as electron acceptors. Figure 2.10 shows the results for TCE dechlorination in the H_2-based MBfR during batch operation. Dechlorinating activity was negligible in 10 days, and no intermediates were

observed. Low dechlorinating activity may have been caused by a low density of biomass active in dechlorination. Thus, we re-inoculated the MBfR with dechlorinating culture ZARA on the 10th and 20th days of batch experiment. Reduction intermediates and chloride were not observed in the next 29 days. As the low dechlorinating activity might have been caused by TCA inhibition, we changed the medium on Day 30 to be the same as what we used in batch bottles and removed TCA, using 0.1 mM TCE as the only electron acceptor. After re-inoculating DehaloR^2 on the 35th day, we started to observe TCE dechlorination to cis-DCE from the 40th day. 99% of the 0.1 mM TCE was converted to cis-DCE within 40 days after the second respike of TCE. Further cis-DCE reduction was not observed until Day 155. To strengthen the dechlorinating biofilm, we re-inoculated the MBfR with dechlorinating culture SDC-9 (10 mL active culture) on the 155th day. 99% of the TCE was reduced to cis-DCE, and the VC slowly accumulated up to 2 μM in 20 days. Methane generation was minimal.

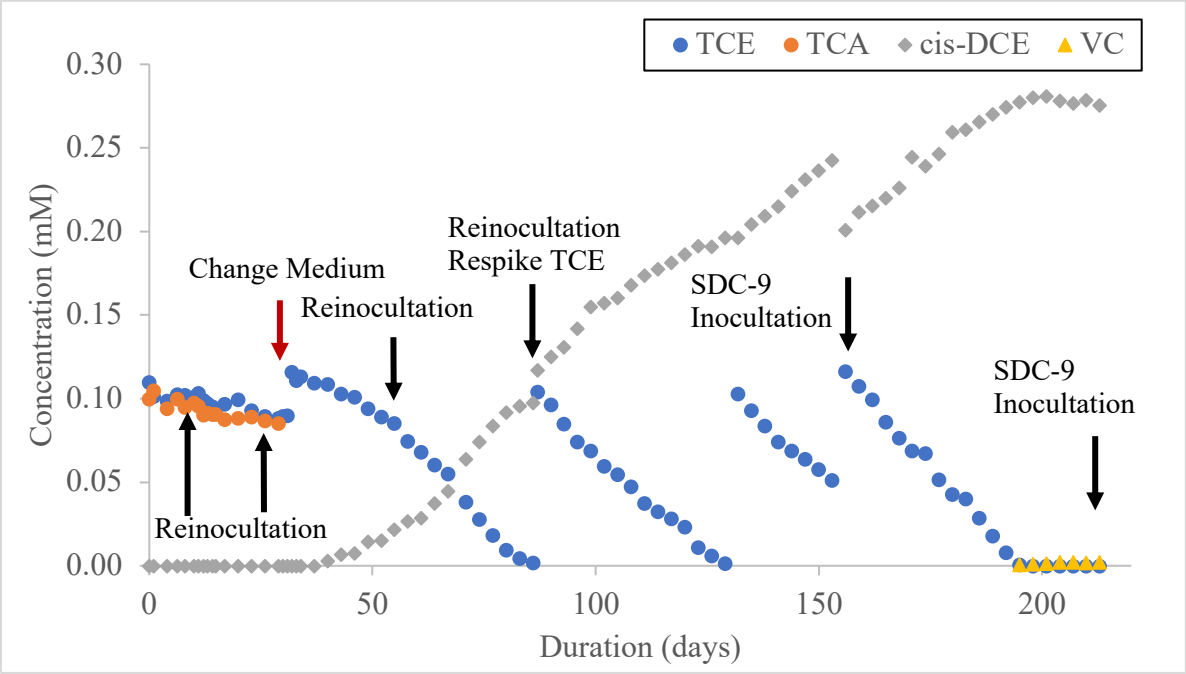

Figure 2.10. Concentrations of TCE (Blue dots), TCA (Orange dots), cis-DCE (Grey diamond), and VC (Yellow triangle) in the H_2-MBfR.

2.4. Cost analysis

APTwater, LLC developed and launched a commercial scale H_2-based MBfR for nitrate treatment (called ARoNITE, where ARo stands for Autotrophic Reduction of). APTwater has programs for equipment sizing and capital and operating cost estimation. The design loading in section 1.2.1 (1.2×10^{-2} mmol/m^2-day) was used to design a full-scale system with a typical flow rate of 100 gallon/minute and a typical TCE concentration of 200 μg/L TCE. At this design loading and applying APTwater's MBfR module containing 170 m^2 membrane area,

approximately 416 modules would be required. The expected capital and operating costs of this system are shown in Table 2.2. The number of modules and the total costs at this flow rate are large compared to an MBfR for nitrate treatment or to conventional TCE treatment (air stripping, activated carbon, advanced oxidation).

Table 2.2. Estimated capital and operating expense for H_2-Based MBfR (100 gpm flow at 0.20 mg/L TCE, 40 kg TCE/yr).

Capital Cost		
	Equipment	$3,000,000
	Site improvements and design	$425,000
	Start-up costs	$70,000
	Contingency	$700,000
	Total installed cost	$4,200,000
	Installed cost per kg TCE/yr	$105,000
Annual Operating Cost		
	Labor	$26,700
	Consumables	$8,500
	Parts and Maintenance	$59,915
	Module Replacement	$114,000
	Power	$28,800
	Total annual costs	$238,000
	Total operating cost per kg TCE	$5950

Note: Basis assumptions are power at $0.10/kw-hr, natural gas at $4/mBTU, and membrane module life at 10 yrs.

2.5. Conclusion for biological TCA/TCE reduction

We examined TCE and TCA reductions in the H_2-MBfR through modeling evaluation and experimental testing. The modeling simulations suggest that the H_2-based MBfR cannot completely dechlorinate TCE and/or TCA under typical operating conditions, as the effluent concentration of VC did not meet its MCL due to the high half-maximum-rate coefficient (K_s) of *Dehalococcoides* for VC. When only TCE is applied in the H_2-MBfR, the optimized TCE surface loading is 1.2×10^{-2} mmol/m^2-day, since both TCE and DCE could meet the EPA MCLs at this loading. When TCE and TCA co-exist in the H_2-MBfR, the optimized surface loading of TCE is 1.9×10^{-2} mmol/m^2-day, at which TCE, DCE, and TCA could meet the MCLs. Under no condition could VC meet its MCL. H_2-based MBfR treatment with these low loadings result in a relatively large and costly system.

The experimental results from batch bottles and H_2-MBfR reinforce the conclusions from the modeling simulations. DCE conversion to VC was remarkably slower than TCE conversion to DCE, and addition of TCA further retarded the whole dechlorination process. From a practical perspective, slow dechlorination and accumulation of toxic intermediates mean that a more rapid and reliable method is needed for reduction of TCE and TCA.

3. Pd-Catalytic Reduction of TCA/TCE in a H_2-MPfR

3.1. Background

An alternative to biological catalysis, Pd-based catalysis, has been applied in a variety of water-treatment strategies. Palladium nano-particles (PdNPs), supported-Pd, and Pd-based bimetallic catalysts can activate H_2 and catalyze the reductive transformation of a number of drinking-water contaminants: *e.g.,* halogenated organics, oxyanions, and nitrosamines (Lowry and Reinhard 1999, Heck et al. 2009, Chaplin et al. 2012). In particular, reductive dechlorination of TCA and TCE, though more widely reported through enzymatic processes, also can be catalyzed by Pd (Lowry and Reinhard 2001, Mori et al. 2004, Davie et al. 2008). As illustrated in Figure 3.1, one or more carbon-bound chlorine atoms are replaced with atomic hydrogen. The reactants -- H_2 and TCA/TCE -- are adsorbed to the surface of metallic Pd, forming adsorbed atomic H and alkane with higher reactivities. The H atoms then replace all or part of the Cl atoms on the TCE. Eventually, the selected products, including ethane, MCA, DCA, detach from the Pd surface. In general, ethane is the primary product of Pd-catalyzed TCA/TCE reduction, although some undesired by-products, like DCE, DCA, and MCA, may also form in parallel. Since Pd-based reduction is a surface reaction, the specific surface area (related to particle size) significantly affects the reaction kinetics and selectivity (Nutt et al. 2005, Chaplin et al. 2012). Environmental conditions (*e.g.,* gas versus aqueous phase TCE, pH, and H_2 supply) also are key parameters.

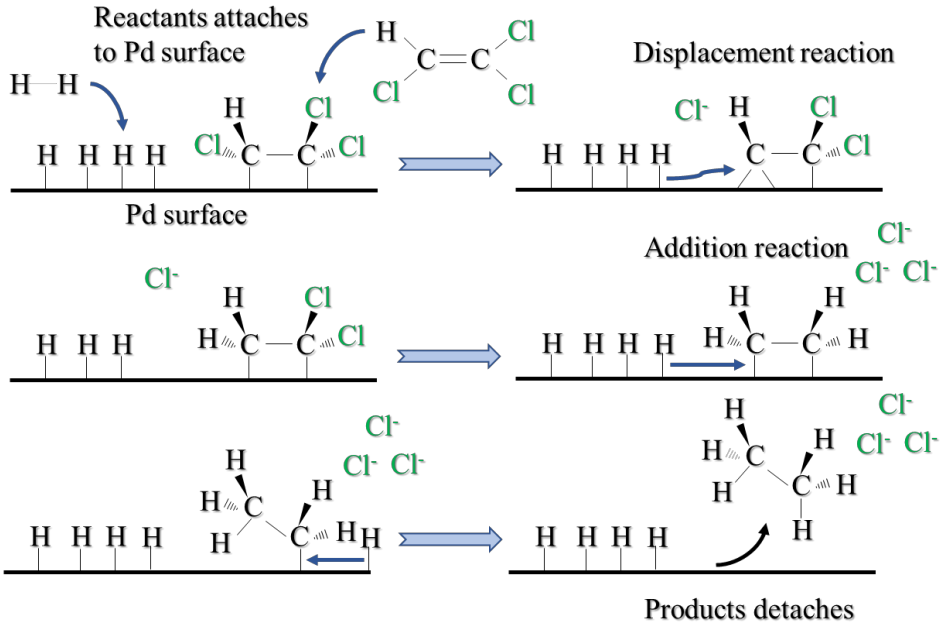

Figure 3.1. Proposed scheme of Pd-catalytic hydrodechlorination of TCE, modified from Mori et al. (2004).

3.2. MPfR setup and Pd coating

We evaluated PdNPs as the catalyst for the reductive dichlorination of TCE and TCA. We carried out preliminary tests with suspended PdNPs and then coated the PdNPs onto the bubbleless gas-transfer membranes to create the MPfR.

The preliminary batch test with suspended PdNPs was carried out in a 160-mL serum bottle having 100 mL medium and 60 mL headspace. The temperature was 23°C, and the medium pH was ~7 established with a 10-mM phosphate buffer.

Continuous catalytic reduction was carried out in a H_2-MPfR having the same dual-tube configuration (illustrated in Fig. 3.2) as in a previous study (Zhou et al. 2016a). The MPfR had a total working volume of 80 mL (60 mL liquid phase and 20 mL headspace) and contained two bundles of 30 identical hollow-fiber membranes in two glass tubes (6 mm internal diameter and 27 cm length). We evaluated two types of membranes in separated tests: One was the composite gas-transfer membrane, 280 μm OD, 180 μm ID, wall thickness 50 μm; Model MHF 200TL Mitsubishi Rayon Co., Ltd, Tokyo, Japan; the other was nonporous polypropylene fiber, 200 μm OD, 100–110 μm ID, wall thickness 50–55 μm; Teijin, Ltd., Japan. H_2 gas (>99.9%) was supplied to both ends of each fiber bundle at a pressure controlled by a pressure regulator. A solute's concentration inside the MPfR was equal to its effluent concentrations due to mixing from a recirculation rate of 150 mL/min created by a peristaltic pump. A 30-mL serum bottle was set between two tubes to create gas-liquid interface; this enabled the volatile organic compounds (TCA, TCE, reduction products) to reach equilibrium of partitioning between the liquid phase and the headspace where gaseous samples were collected.

To coat the fibers with PdNPs, we filled the reactor with the medium containing ~10 mg L^{-1} of soluble Pd^{II} added as Na_2PdCl_4. The medium had been autoclaved and deoxygenated before use. The PdNPs spontaneously formed through autocatalytic reduction from Pd^{II} to Pd^0 and attached to the membrane surfaces under continuous H_2 supply within 12 hours. The estimated loading of the PdNPs coated to the membrane was ~65 mg/m^2. Detail parameters describing the MPfR are listed in Table 3.1.

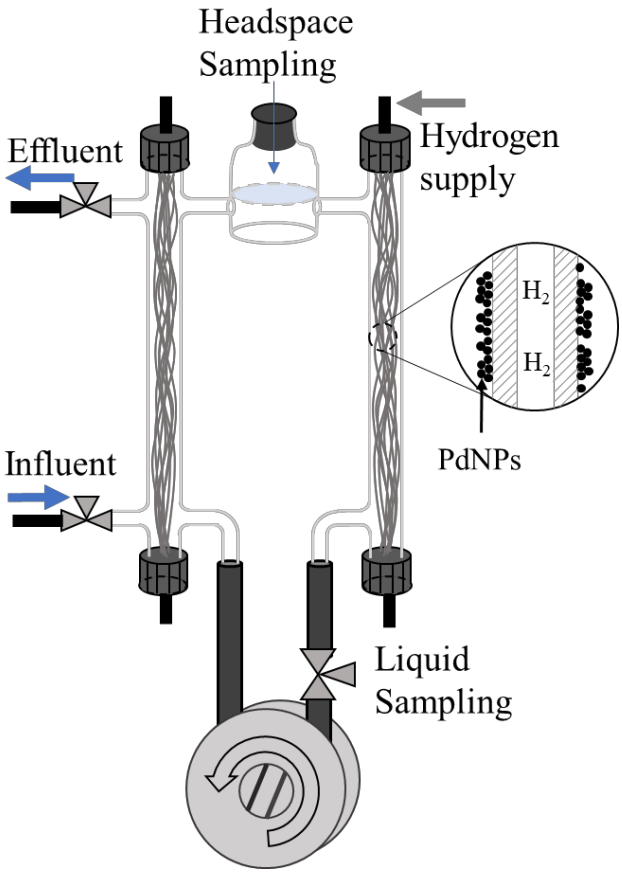

Figure 3.2. Schematic of the H_2-MPfR setup.

Table 3.1. The coating and operating parameters for the H_2-MPfR

MPfR parameters					
		Value	Unit 1	Value	Unit 2
Coating	Palladium conc.	0.1	mmol/L	10.6	mg/L
	H_2 pressure	3	psig	1.2	atm
	Membranes type	Polypropylene membrane			
	Membranes area	0.0115	m^2	115	cm^2
	Coated Pd	0.007	mmol	0.74	mg
		0.60	$mmol/m^2$	63.4	mg/cm^2
Operation	Flow rate	0.10	mL/min	144	mL/d
	H_2 pressure	10	psig	1.69	atm
	TCE influent	100	μmol/L	13	mg/L
	TCE loading	1.25	$mmol/m^2$-day	165	mg/m^2-day
	TCE flux	1.24	$mmol/m^2$-day	163	mg/m^2-day
	TCA influent	100	μmol/L	13	mg/L
	TCA loading	1.25	$mmol/m^2$-day	167	mg/m^2-day
	TCA flux	1.22	$mmol/m^2$-day	163	mg/m^2-day

3.3. Testing TCA/TCE reduction

3.3.1. Batch kinetic tests

Two preliminary batch tests were performed to assess abiotic TCE and TCA dechlorination catalyzed by suspended PdNPs. We added 40 μmole TCE into a serum bottle containing 100 ml liquid medium plus 0.5 mM suspended PdNPs and 60 ml headspace containing 0.4 atm H_2 and 0.8 atm N_2. Figure 3.3 shows that TCE was converted into ethene (6.4 μmole, or 16% of the initial TCE) and ethane (32.1 μmole, or 80% of the initial TCE) within an hour, while other by-products

were present at trace levels (MCA, DCA < 0.1 μmole, or < 0.25% of the initial TCE). For the same conditions, 45 μmole TCA was converted to ethane (43.1 μmole, or 95.8% of the initial TCA) and DCA (1.9 μmole, or 4.2% of the initial TCA). The batch tests confirm that reduction of TCA and TCE can be catalyzed by PdNPs in ambient conditions (23°C, circumstantial pH).

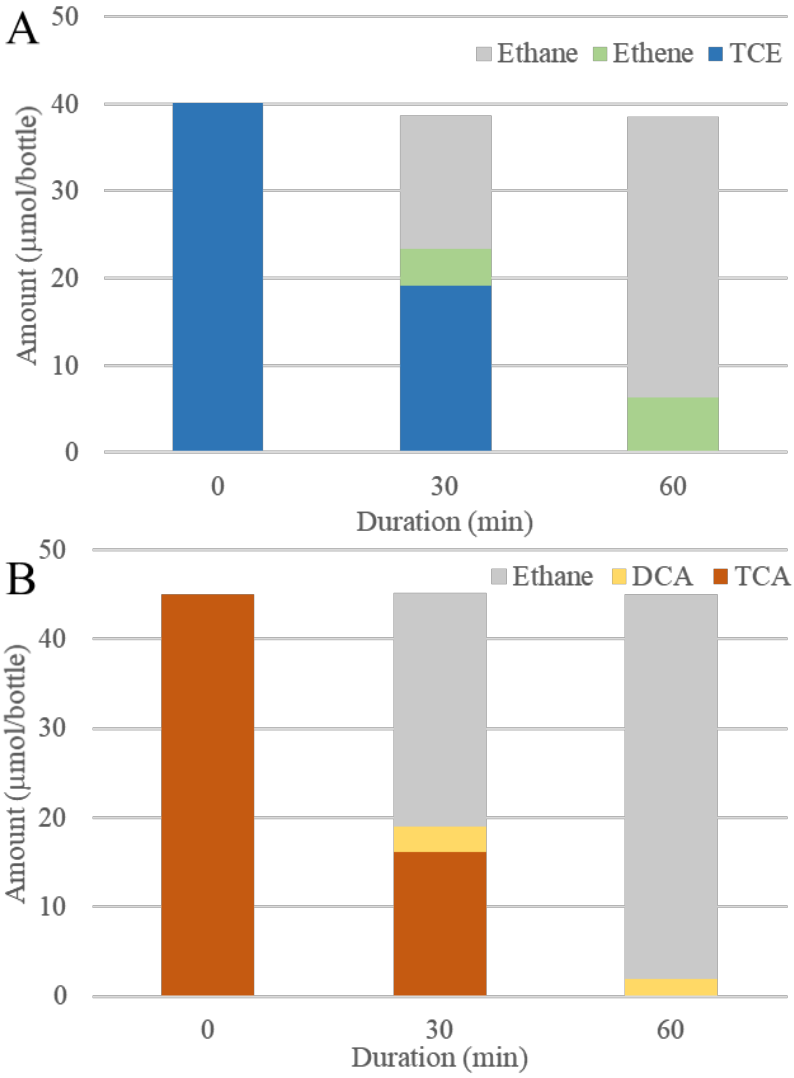

Figure 3.3. TCE and TCA reductions catalyzed by suspended PdNPs. The missing mass for TCE was MCA and DCA (< 3 μmole each).

The first H_2-MPfR was built with the composite bubble-less gas-transfer membranes. We first tested TCE and TCA reductions in this H_2-MPfR in batch mode with a H_2-supply pressure of 3 psig (~1.2 atm total pressure). Figure 3.4A shows that the initial 1 mM TCE was rapidly

reduced to ethane (88%) and MCA (10%) within about 70 mins once H_2 was supplied. The maximum rate of TCE reduction was 0.54 μmol/min for the whole reactor, which corresponded to 146 μmol/min·g-Pd. The H_2 accumulation in the reactor meant that the reduction reaction did not need all the H_2 that could be delivered from the membrane, which means that H_2 was being wasted.

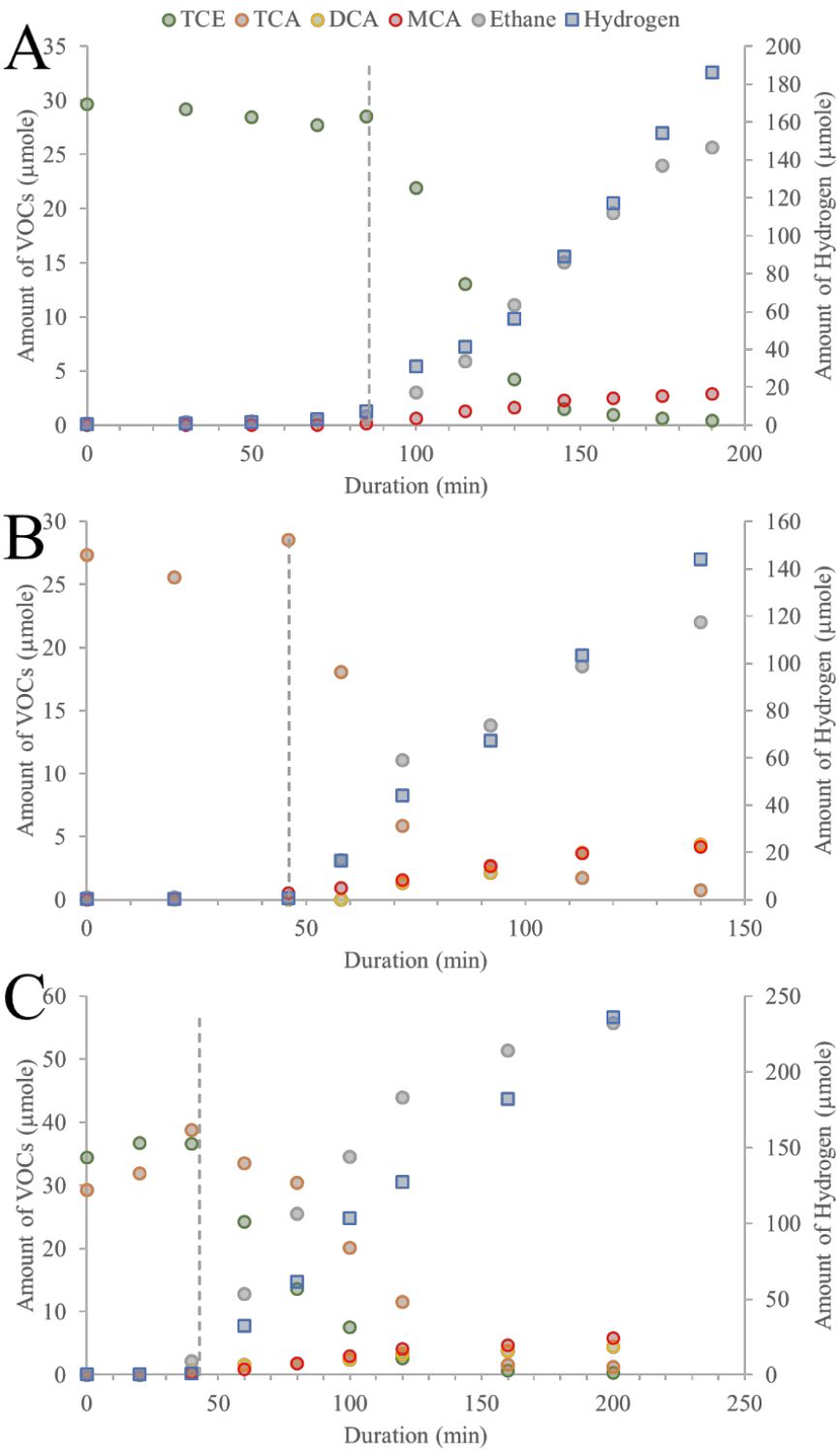

Figure 3.4. TCE and TCA catalytic reduction batch test in the H_2-MPfR with composite membranes. The gray dash line shows the start of the H_2 supply. A: TCE only, B: TCA only, C: TCE and TCA.

Figure 3.4B shows that 1 mM TCA was converted to ethane (75%), DCA (12%), and MCA (12%) within 120 mins. Furthermore, 1 mM TCE and 1 mM TCA together were converted to ethane (75%), DCA (13%), and MCA (12%) within 180 mins (Fig. 3.4C). These tests confirm that TCE and TCA reductions catalyzed by the PdNPs coated on the H_2-delivery membranes were as efficient as the suspended PdNPs.

3.3.2. Continuously operated MPfR – reduction and selectivity

After the batch tests, the H_2-MPfR was operated in the continuous mode with different hydraulic retention times (HRTs) and H_2-supply pressures. Figure 3.5 presents the results of the initial 30 days of operation divided into five stages. The influent concentrations of TCA and TCE were 1 mM, which means that the influent Cl concentration was 6 mM. In the first stage, the H_2-MPfR was supplied with 3 psig H_2 with an HRT of 12 h. To optimize the reactor operating conditions, we kept decreasing the HRT: from 12 h to 6.8 h, 3.8 h, and finally 2.6 h. The effluent concentrations of TCE (from 10 μM to 20 μM, 40 μM, and 70 μM with decreasing HRT), TCA (from 40 μM to 100 μM, 200 μM and 280 μM), and DCA (from 40 μM to 50 μM, 75 μM and 80 μM) increased, and the effluent chloride concentration decreased from 5.3 to 5.0, 4.7, and 4.3 μM. The total Cl in the effluent was stable at around 80% of the influent chlorine throughout. The other 20% of chlorine was lost, since some of the TCA, TCE, and reduced products were stripped out of the reactor by the excess H_2.

The trends with HRT show that, when the HRT was less than 6.8 h, the H_2 supply became insufficient for full reductions of TCE and TCA (the H_2 partial pressure in the headspace was lower than 0.1%). In the last stage, when we increased the H_2 pressure to 5 psig (from 3 psig), the concentrations of all the chlorinated hydrocarbons ions decreased very fast, but so did the concentration of Cl^-; the latter supports that excess H_2 probably stripped TCA and TCE out of the reactor.

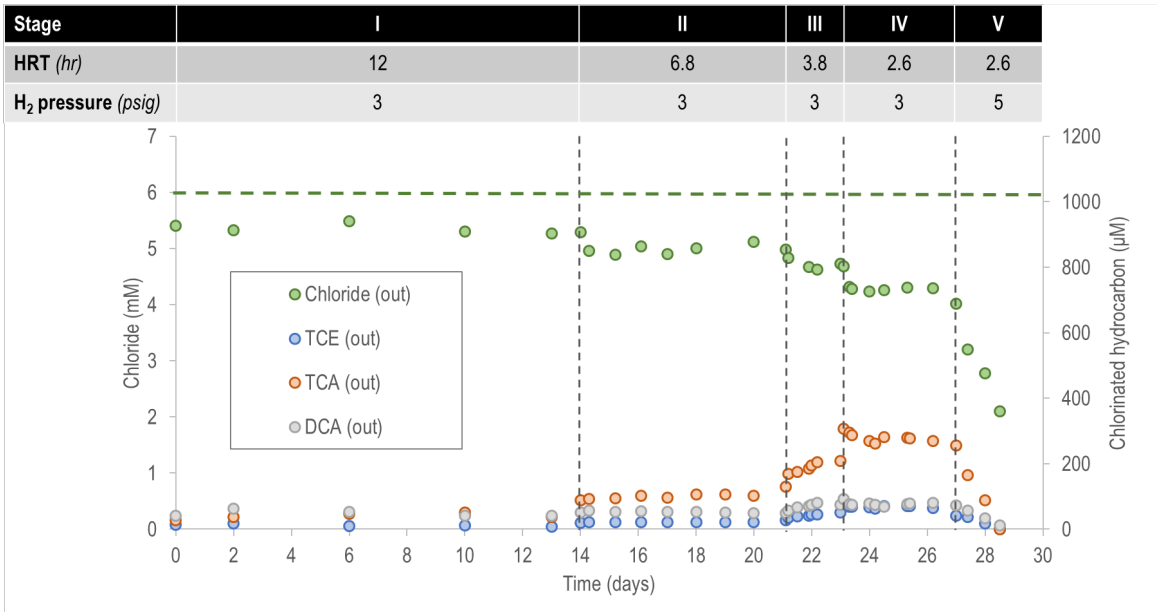

Figure 3.5. Catalytic reductions of TCA and TCE in the H_2-MPfR with composite membranes in continuous operation. The green horizontal dash line represents the influent concentration of total chlorine in TCE and TCA. The black vertical dash line indicates HRT and pressure changes.

The previous results indicate that the H_2-delivery capacity of the composite membranes was too high to preclude over-supply of H_2, which wasted H_2 and led to stripping of TCE and TCA. Therefore, we changed to the polypropylene membranes, which have a lower delivery rate (about 10% of the composite membrane). Figure 3.6 shows the results of separate TCE- and TCA-reduction batch tests using polypropylene membrane at the H_2 pressure of 10 psig and initial concentrations of 0.1 mM. TCE was rapidly reduced to ethane (84%) and MCA (12%) within about 100 minutes with the maximum reaction rate of ~20 μmol/min/g-Pd. TCA also was converted to ethane (70%), DCA (16%), and MCA (11%) within 100 mins, with the maximum reaction rate of 17 μmol/min/g-Pd. The total mass of hydrocarbons (black triangles) had 100% mass-balance closure at the beginning and the end of the batch experiment. The transient loss of the total mass (as low as 38% and 25% for separated reduction of TCE and TCA, respectively) probably was due to reaction intermediates that were transiently attached on the PdNPs. Compared to the composite membrane, the H_2 delivered by polypropylene in the first 40 minutes was well matched to the reaction rate, which mean that H_2 was not wasted and did not cause stripping of TCE or TCA.

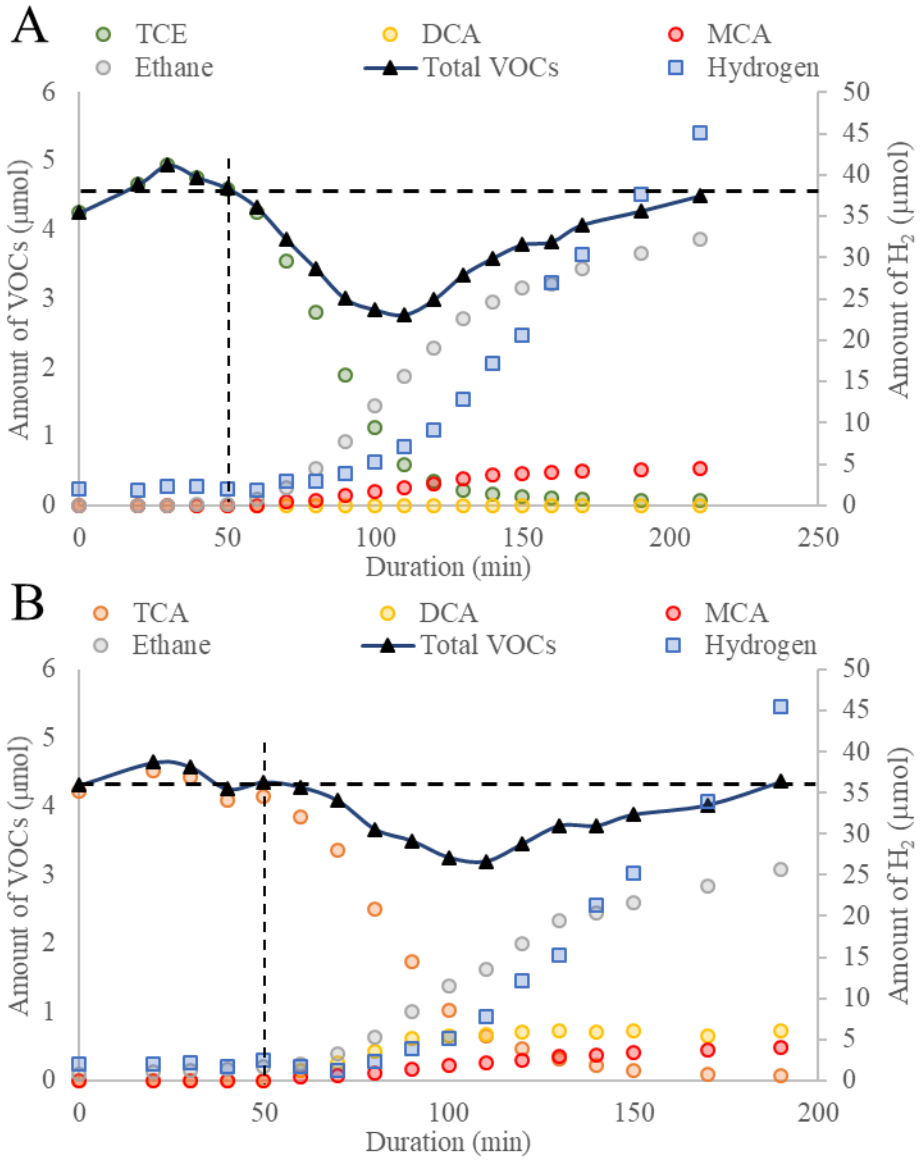

Figure 3.6. Catalytic reduction of TCE (top panel) and TCA (bottom panel) in batch test of a H_2-MPfR with polypropylene membranes. Panel A shows the mass changes of H_2, TCE, and its reduction products in the MPfR. Panel B shows the mass changes of H_2, TCA and its reductive products in the MBfR with initial dissolved TCA concentration of 100 µM. The vertical dash line indicates the start point for H_2 supply.

Simultaneous TCE and TCA reductions were tested for different H_2-supply pressures (20 and 10 psig) and with TCA and TCE initial concentrations of 1 and 0.1 mM. Figure 3.7 shows the results for three batch tests. All compounds had the same trends: the reaction rate was higher when the initial concentration or the H_2 pressure was higher.

Product selectivity was affected by the initial TCE and TCA concentrations. Figure 3.8 summarizes the selectivity for the three batch tests. A H_2-pressure change from 10 to 20 psig did not significantly affect selectivity with initial TCE and TCA concentrations of 1 mM each, but lowering the initial concentration of TCA or TCE led to higher selectivity towards ethane, from 58% to 69%.

We then operated the polypropylene-fiber H_2-MPfR in continuous mode with an HRT of 15 hours and influent TCE and TCA concentrations set at 1 mM. Figure 3.9 presents the results. In the stage 1, the influent featured TCE, TCA, and deionized (DI) water only, and the medium pH in the reactor was around 7. The results show that more than 96% of the TCE and TCA were removed at a surface loading of 50 mmol/m^2-day. The selectivity towards ethane was as high as 93%. The main by-products in the effluent were DCA and MCA, accounting for about 3% and 4% of total TCE and TCA, respectively. In stage 2, we added a phosphate buffer to control the pH at ~7. The pH shift to 7 did not have a significant effect on TCE and TCA reductions.

In stage 3, we increased the surface loading to 75 mmol/m^2-day, with the same influent concentration and H_2 supply, by decreasing the HRT to 10 hours. The effluent concentrations of TCE and TCA did not change, DCA increased from 60 μM to 160 μM (3% to 8% of total TCE and TCA), and MCA increased from 80 μM to 100 μM (3% to 5% of total TCE and TCA). In the last stage, we fed the reactor with the medium used for biodegrading 1,4-dioxane in an O_2-MBfR (reported in the next section); the influent TCE and TCA concentrations were 1 mM, and the 1,4-dioxane concentration was 0.5 mM. The additional compounds in the medium (ammonia, calcium, magnesium, trace metals, and 1,4-dioxane) had no observable effect on TCE and TCA reductions. The chlorine mass balance during the continuous was stable around 98 ± 5%.

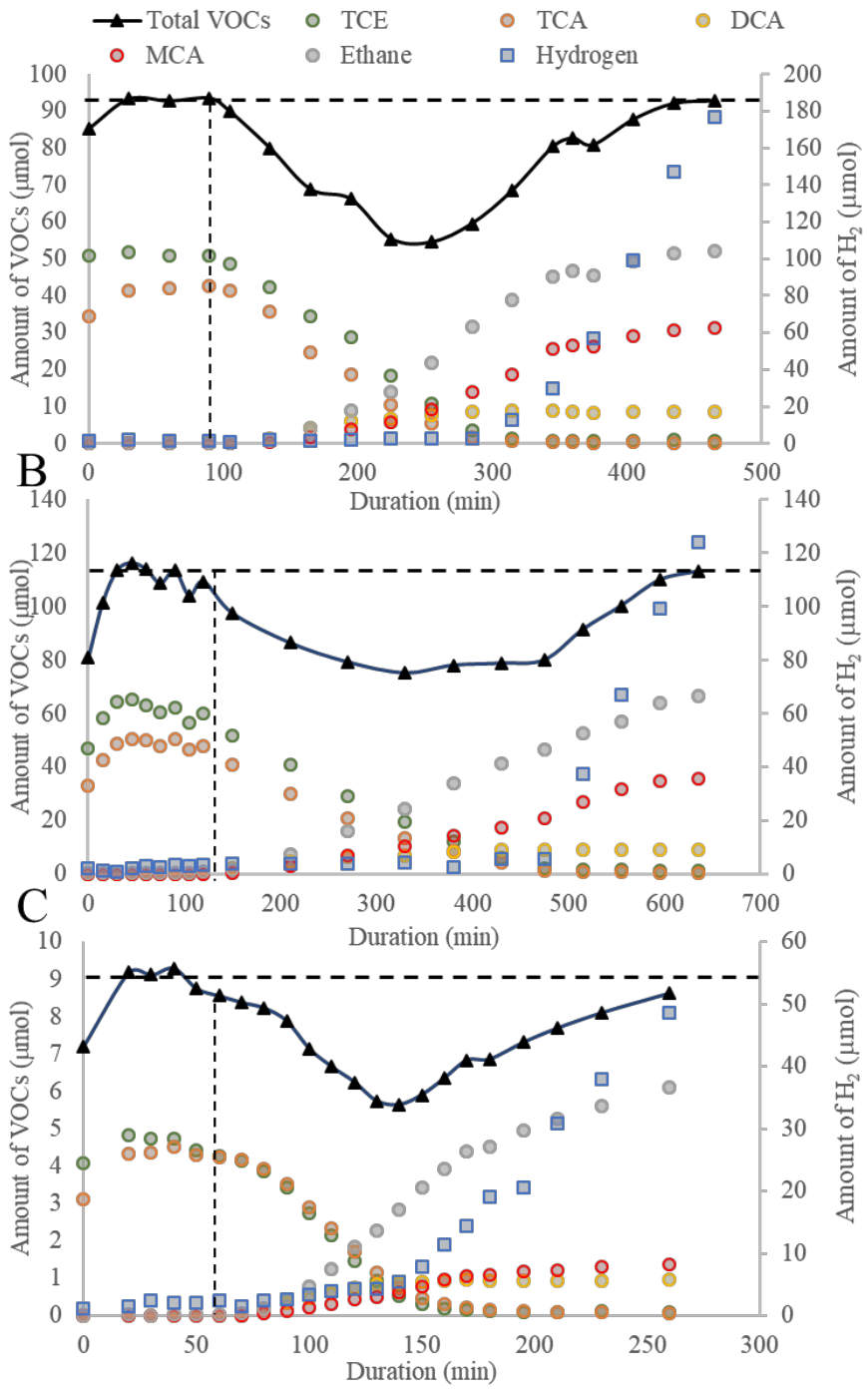

Figure 3.7. Simultaneously TCA and TCE batch tests of a H_2-MPfR with polypropylene membranes. A had the H_2 supply pressure of 20 psig and initial concentration of 1 mM; B had the hydrogen supply pressure of 10 psig and initial concentration of 1 mM; C had the hydrogen supply pressure of 10 psig and initial concentration of 0.1 mM.

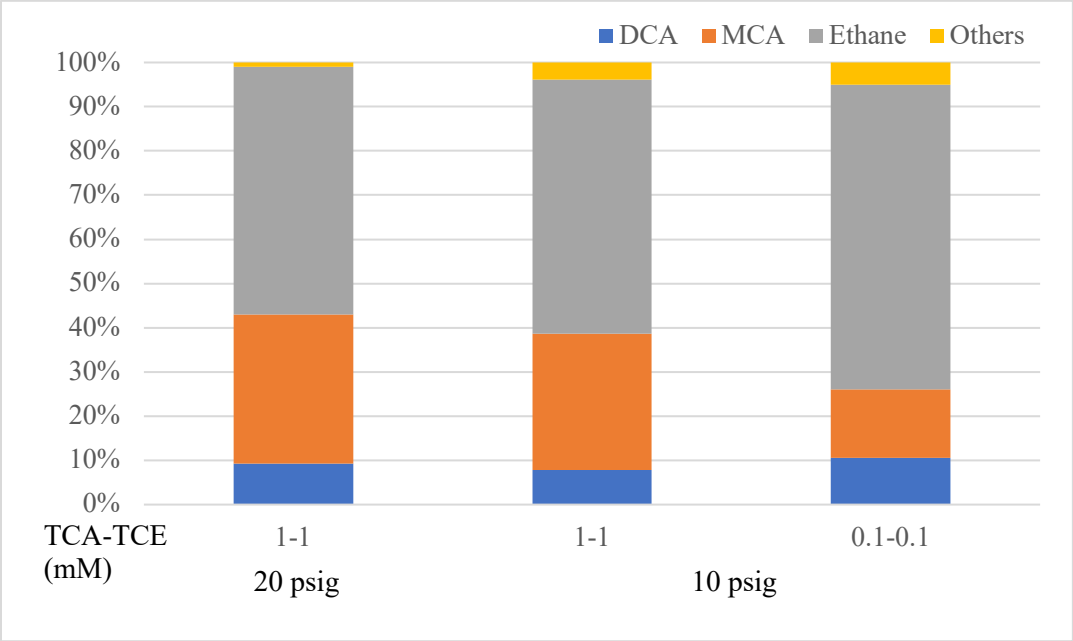

Figure 3.8. Selectivity differences among three batch tests having different H_2 supply pressures and initial TCA/TCE concentrations.

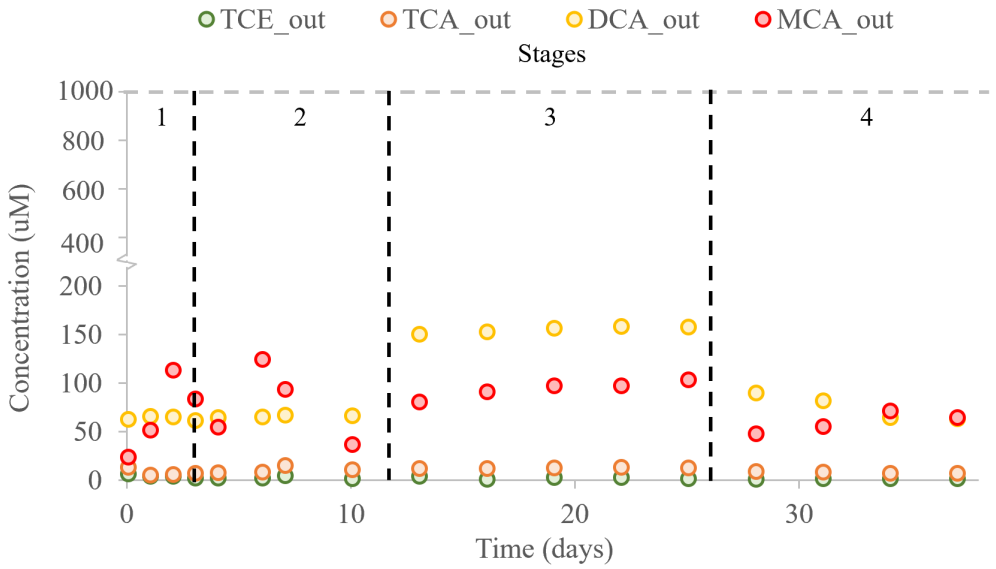

Figure 3.9. TCA and TCE catalytic reduction a H_2-MPfR with polypropylene membranes at continuous mode. The gray horizontal dash line represents the influent concentration of TCE and TCA. The black vertical dash line separates the four stages with different operating conditions noted above the graphic.

3.4. Cost analysis

To estimate the capital and operating cost of a H_2-based MPfR, we used the coating and operating parameters in Table 3.1 to determine the amount of Pd required per commercial membrane module similar in size to APTwater's modules; we incorporated that extra cost of the Pd and the coating step into the cost models. All MCLs can be met with this scenario. The loading information in Table 3.1 results in 256 modules being required to treat 100 gal/min at 13 mg/L TCE, but the influent concentration is 65-fold higher than the 0.20 mg/L used for cost analysis for the H_2-based MBfR. A large-quantity quote (≥100 kg) for Na_2PdCl_4 of $18/gram was obtained from Strem Chemicals. This calculation results in about 11 grams Pd per module and $550 in Na_2PdCl_4 per module. Because of the extra potential of Pd fouling, the module life was assumed to seven years, versus the uncoated module at ten years. Using the same power ($0.10/kw-hr) and natural gas ($4/mBTU) costs as for the H_2-based MBfR, Table 3.2 summarizes the operating and capital cost of the H_2-based MPfR. Compared to the biological H_2-based MBfR, the H_2-based MPfR for Pd-catalytic treatment of TCE/TCA requires substantially less capital on the basis of kg TCE/yr treated ($1,320 vs $105,000) and operating cost on the basis of kg TCE basis ($110 vs $6,000).

Table 3.2. Estimated capital and operating expense for H_2-Based MPfR (100 gpm flow at 13 mg/L TCE, or 2610 kg TCE/yr)

Capital Cost		
	Equipment	$2,500,000
	Site improvements and design	$315,000
	Start-up costs	$70,000
	Contingency	$550,000
	Total installed cost	$3,435,000
	Installed cost per kg TCE/yr	$1320
Annual Operating Cost		
	Labor	$26,700
	Consumables	$14,800
	Parts and maintenance	$51,300
	Module replacement	$182,000
	Power	$18,000
	Total annual costs	$293,000
	Total operating cost per kg TCE	$110

3.5. Conclusion for catalytic TCA/TCE reduction

We tested reduction of TCE and TCA catalyzed by PdNPs suspended in serum bottles and coated on fibers in an MPfR. In the presence of H_2 as the electron donor, both types of PdNPs rapidly catalyzed reductive transformation of TCA and TCE, mostly to ethane, which is the most desired product. Other byproducts -- mainly DCA and MCA -- were minor and are expected to be oxidized together with 1,4-dioxane in the next stage (reported in the next section).

In the H_2-MPfR, the reaction rate was controlled by the H_2-supply pressure, and the selectivity towards ethane was controlled by the surface loading of TCA and TCE. When the H_2-MPfR was

continuously operated at an HRT of 15 hours and TCE and TCA surface loadings of 50 mmol/m^2-day, TCE and TCA removals were 96%, and the selectivity towards (desired) ethane was 93%, with DCA and MCA residuals being small. Compared to the H_2-based MBfR, the H_2-based MPfR offered many benefits: Pd-catalyzed TCE and TCA reductions were initiated without a lag phase, were significantly faster, produced less partly dechlorinated intermediates, and mostly generated ethane, which is the desired substrate to stimulate aerobic 1,4-dioxane biodegradation in the second stage.

The estimated cost of a 100-gpm full-scale system further supports the advantage of the H_2-based MPfR for reductive dechlorination of TCE and TCA: TCE can be treated at significantly lower capital and operational cost per kg TCE/yr capacity. Based on these promising results, we decided to evaluate the Pd-catalytic MPfR as the first stage of the synergistic platform, the topic of Section 5.

4. Biological Oxidation of 1,4-Dioxane in a O_2-MBfR

4.1. Background

The first bacterial species shown to biodegrade 1,4-dioxane and grow on it as a sole electron and carbon donor was *Pseudonocardia dioxanivorans* CB1190 (Parales et al. 1994, Mahendra et al. 2007). On the basis of the intermediates identified during dioxane biodegradation, Mahendra et al. (2007) proposed the complete biodegradation pathway shown in Figure 4.1. In this pathway, we highlight the two steps of monooxygenation, as they are the key steps that convert dioxane from a stable cyclic ether to metabolically labile organic intermediates.

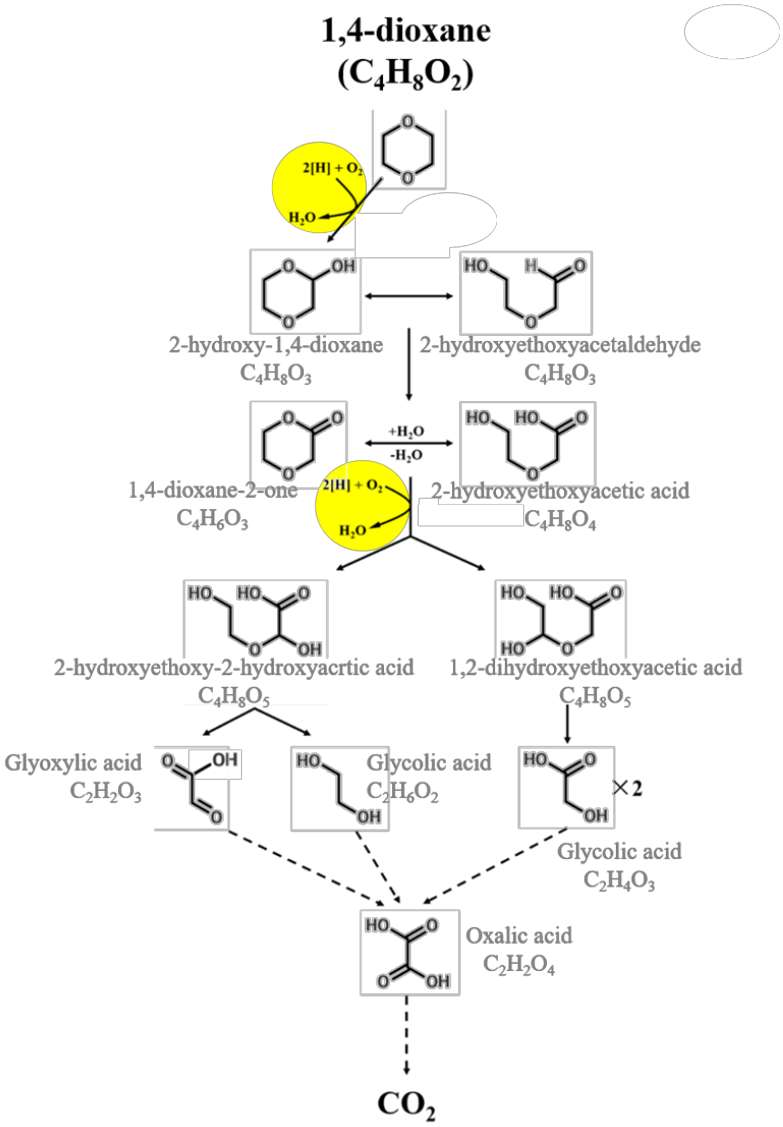

Figure 4.1. Schematic of aerobic 1,4-dioxane biodegradation, modified from (Mahendra et al. 2007). Yellow highlights the initial monooxygenation reactions.

Besides *P. dioxanivorans* CB1190, a few other aerobic microorganisms can use dioxane as sole electron and carbon donor: e.g., *Rhodococcus ruber* strain 219, *Acinetobacter baumannii* DD1, *Xanthobacter flavus* DT8, *Afipia* sp. strain D1 (Bernhardt and Diekmann 1991, Chen et al. 2016, Isaka et al. 2016, Zhou et al. 2016b). Most research on dioxane biodegradation indicates that dioxane biodegradation is co-metabolic, which means that a growth-supporting primary substrates is needed, such as tetrahydrofuran (THF), methane, propane, toluene, or ethanol (Burback and Perry 1993, Vainberg et al. 2006, Kim et al. 2009). In co-metabolic dioxane degradation, the microorganisms cannot use dioxane as the sole electron donor and carbon source for growth.

In this section, we first attempted to enrich a mixed culture for dioxane biodegradation from different inocula (wastewater treatment plan aerobic sludge, landfill leaches, oil contaminated soil, and wetland sediments) with and without primary electron donors. Second, we used a pure culture of *R. ruber* strain 219 to perform kinetic experiments on dioxane biodegradation. Third, we utilized the enriched mixed culture and a *R. ruber* strain 219 pure culture as inocula to set up an O_2-based MBfR for dioxane biodegradation. Finally, we operated the O_2-based MBfR in continuous mode to evaluate and optimize high-rate dioxane removal.

4.2. Enrichment and evaluation of 1,4-dioxane degraders

To enrich a dioxane-oxidizing culture, we tried different inocula: a pure culture of *Rhodococcus ruber* 219, aerobic sludge from a wastewater treatment plant (WWTP), landfill leachate, and wetland sediments. Added electron donors were acetate and ethane.

Figure 4.2 shows the results of the batch tests to measure the growth and 1,4-dioxane degradation capability of *R. ruber* 219 under aerobic conditions (the medium was aerated with pure O_2). Initial conditions were 5 mM acetate, 5 mM acetate with 0.5 mM 1,4-dioxane, or 1 mM 1,4-dioxane only (although 0.4 mM acetate came from the transfer source). *R. ruber* 219 growing with acetate as the only electron donor had a generation time of about 13 hours. *R. ruber* 219 growth was slower (20 hours later than the test without 1,4-dioxane to reach the maximum optical density) when 0.5 mM 1,4-dioxane was added, probably because monooxygenation reactions consume electron equivalents for acetate.

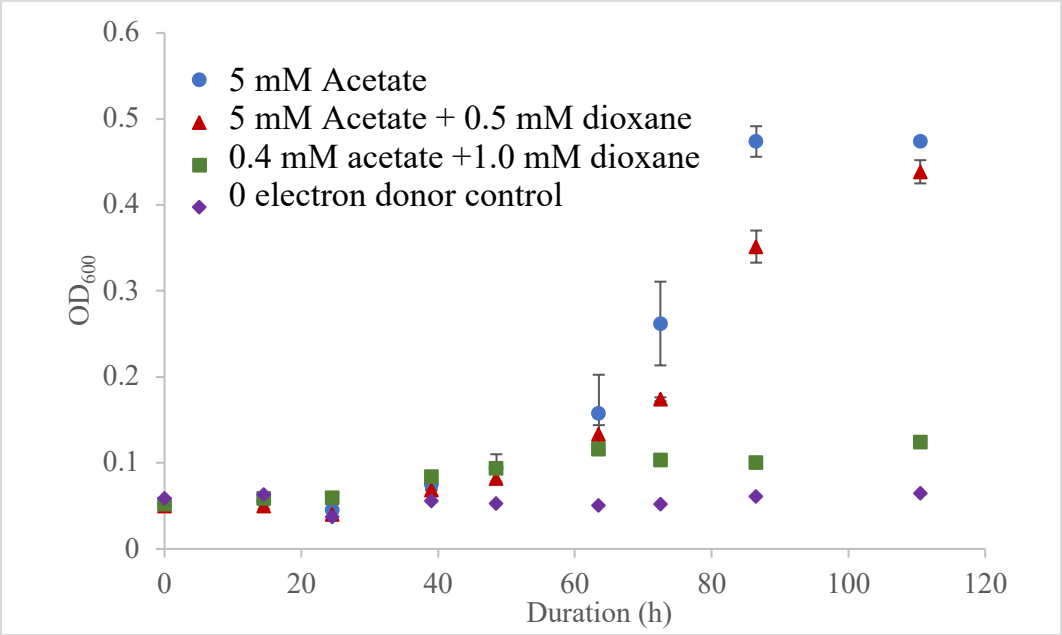

Figure 4.2. The growth curve of *R. ruber* 219 with different electron-donor conditions.

In Figure 4.3A, the pure culture *R. ruber* 219 achieved more than 90% removal of 0.4 mM dioxane with acetate as the primary electron donor. Figure 4.3B shows that *R. ruber* 219 did not use ethane as a primary electron donor for growth or 1,4-D degradation through co-metabolism. Also, Figure 4.3C shows that *R. ruber* 219 was not able to use dioxane as the only electron donor for growth. These batch tests show that *R. ruber* 219 had the capability of 1,4-dixoane degradation with acetate as primary electron donor, but not with ethane or with 1,4-dixoane alone as a sole electron donor.

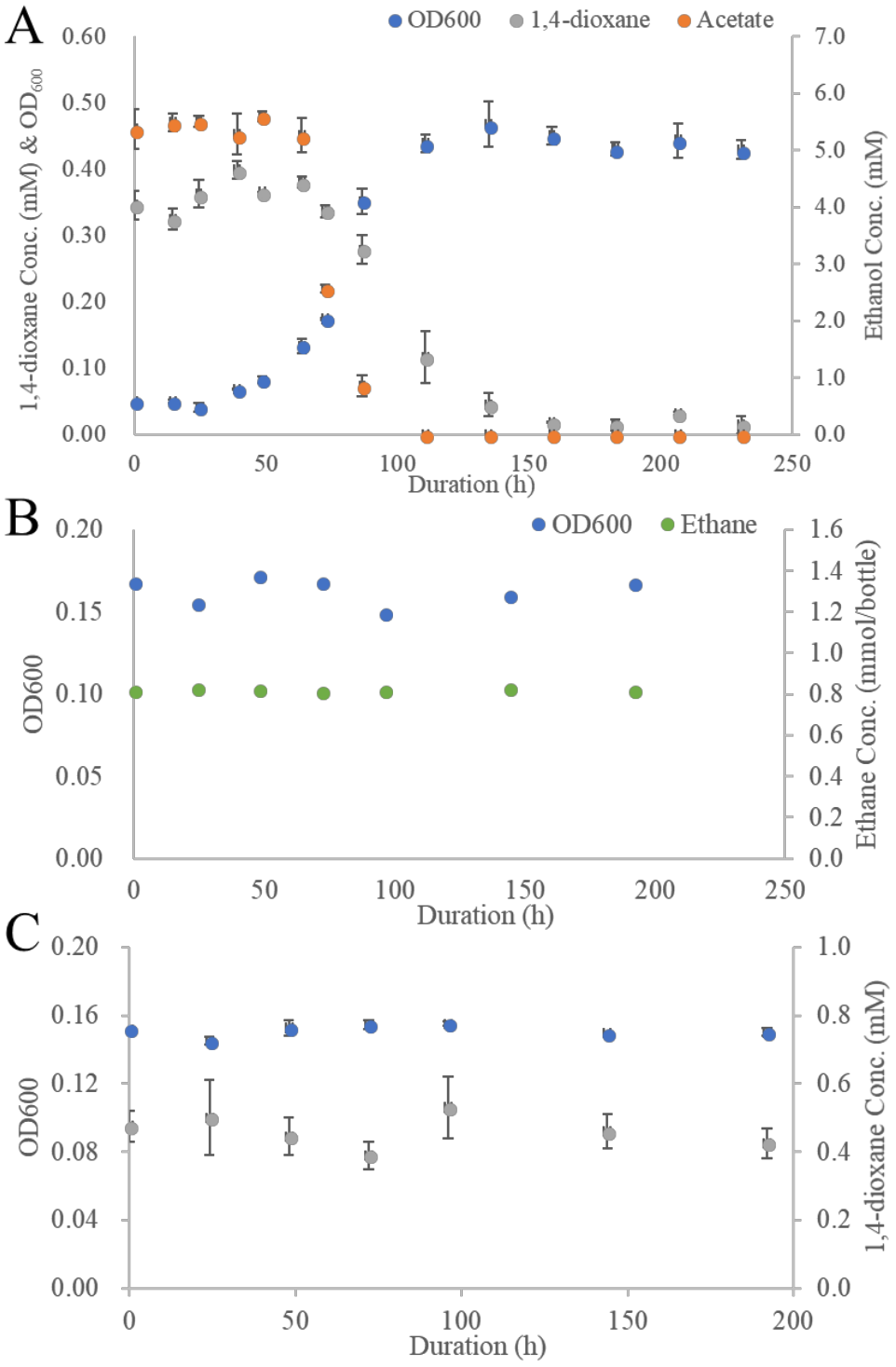

Figure 4.3. Results of batch tests with *R. ruber* 219. (A) Growth and dioxane oxidation by *R. ruber* 219 with acetate as the primary electron donor. (B) Growth with ethane as the sole electron donor and carbon source. (C) Growth with dioxane as the sole electron donor and carbon source.

We eventually succeeded in enriching an ethanotrophic mixed culture from the wetland sediments as the inoculum. The enriched ethanotrophic mixed culture was able to oxidize ethane at a rate of 11 μmol/day, shown in Fig. 4.4. In the presence of ethane as the primary electron donor, the mixed culture also was able to degrade dioxane.

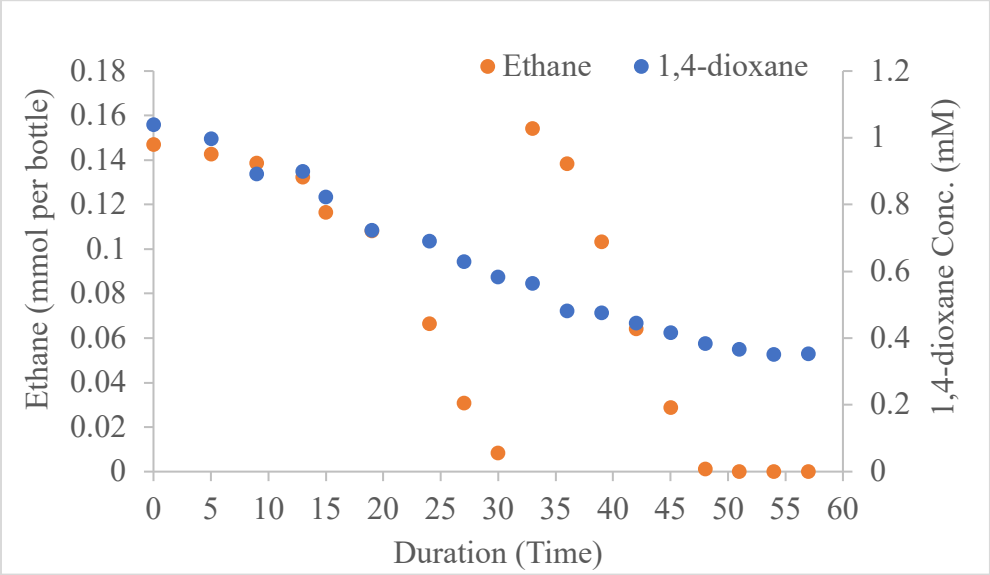

Figure 4.4. Wetland sediments enriched dioxane oxidation culture with ethane as the primary electron donor.

4.3. O_2-MBfR operation

We set up an O_2-MBfR and inoculated it with the pure culture *R. ruber* 219. The configuration of the O_2-MBfR was identical to the H_2-MBfR, except that the fiber lumen was pressurized with gaseous O_2, not H_2. In the initial enrichment stage, the O_2-MBfR was fed with 2.5 mM acetate and set at a long HRT of 24 hour to promote the biofilm growth. Figure 4.5A shows that the O_2-based MBfR soon attained the capability for complete acetate removal. We then increased the influent concentration to about 12 mM. In the second stage, we operated the O_2-MBfR at sequential batch mode and started to feed the reactor with acetate and 1,4-dioxane. The trend, in Fig. 4.5B, was similar to the batch bottles: 1,4-dioxane was removed only in the presence of acetate as the primary electron donor.

Oxidation of 1,4-dioxane slowed after a few acetate re-spikes. To test if this biofilm could maintain a stable 1,4-dioxane oxidation capability, we switched the reactor to the continuous mode. In the continuous mode, the influent concentration of acetate was 10 mM, 1,4-dioxane was 200 μM, and the HRT was 48 hours. During continuous operation, we observed that 1,4-dioxane removal was gradually decreasing, probably due to the loss of monooxygenation capability.

Another possible reason was that the bacteria capable of 1,4-dioxane oxidation (including *R. ruber* 219 and probably other species that gradually colonized the biofilm during the O_2-MBfR operation) gradually lost their dominant position in the biofilm or even were washed out, as the high acetate-to-dioxane ratio might have been favorable to other faster growing bacteria that utilized acetate but not 1,4-dioxane. To decrease the acetate-to-dioxane ratio, we increased the influent 1,4-dioxane concentration form 200 μM to 300 μM and decreased the acetate concentration form 11 mM to 5 mM and then to 2 mM during continuous operation. The negligible decrease of 1,4-dioxane concentration in the effluent for four weeks reveals that the lost capacity of 1,4-dioxane removal was not recovered. Thus, *R. ruber* 219 or other 1,4-dioxane oxidizers had been washed out before we made the concentration change. Overall, the results show that the pure culture *R. ruber* 219 did not maintain stable 1,4-dioxane-removing capability in an O_2-MBfR.

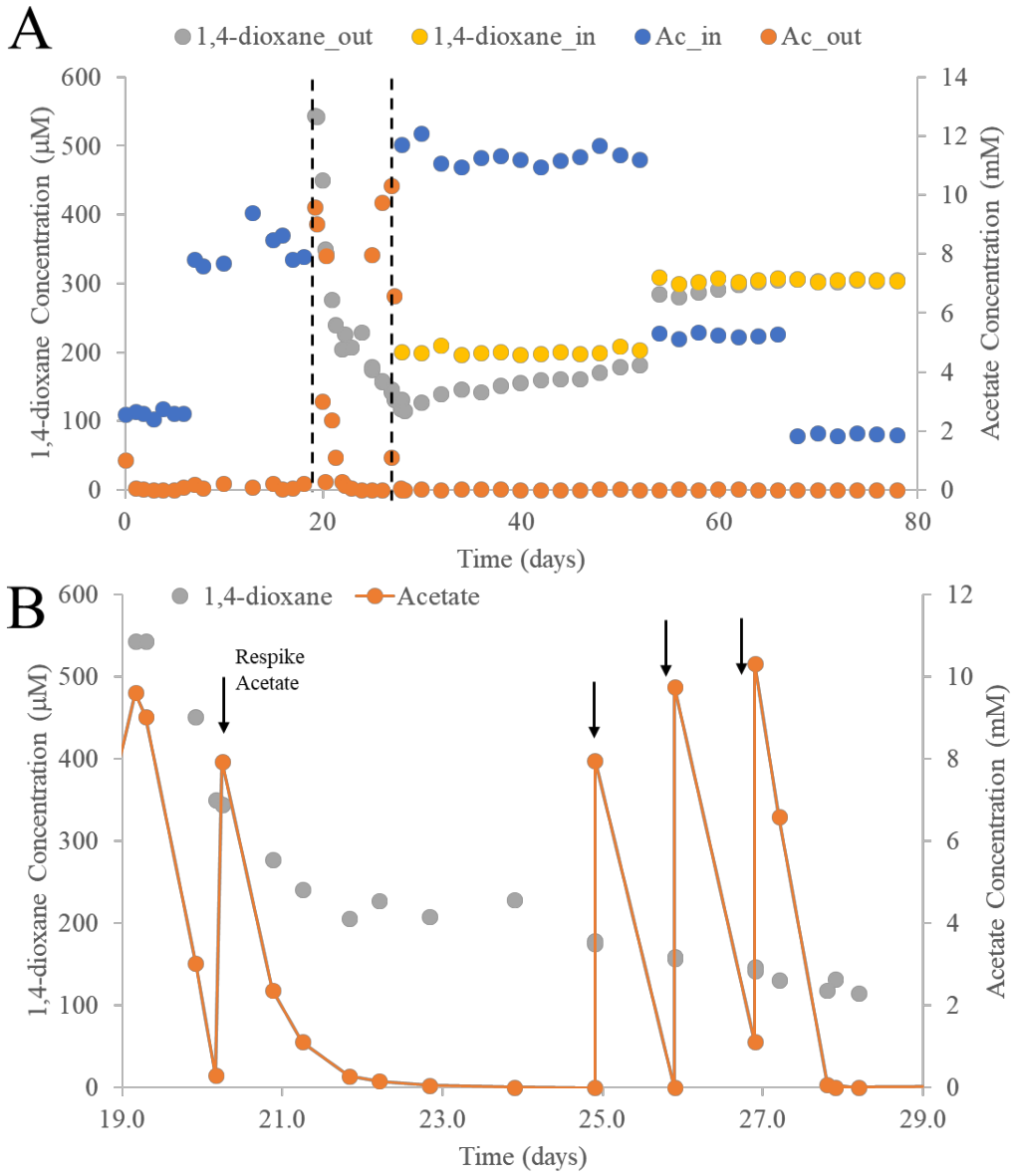

Figure 4.5. *R. ruber* 219 inoculated O_2-MBfR performance of dioxane removal in continuous (A) and batch (B) modes.

We then operated an O_2-MBfR fed with medium containing 0.5 mM 1,4-dioxane and saturated with ethane (up to 58 mg/L or 1.9 mM soluble ethane after sparkling with pure ethane gas). The O_2-MBfR was inoculated with wetland sediment. In the first stage, 1,4-dioxane removal was initiated after 18 days and gradually reached 7% within the following 6 days, summarized in Fig. 4.6. Once ethane was fully consumed in the reactor, 1,4-dioxane began to be consumed rapidly. By Day 38, 1,4-dioxane removal reached steady state at over 99%, and the removal remained

almost over 99% for over four weeks.

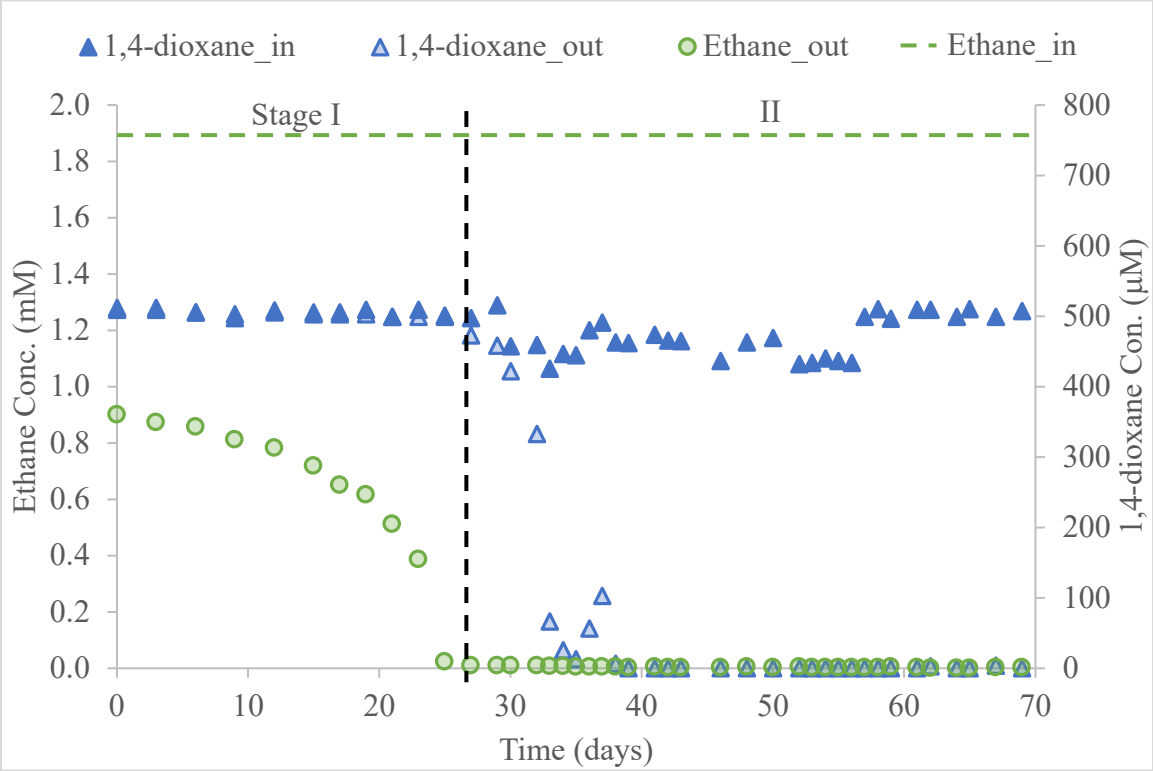

Figure 4.6. The 1,4-dioxane concentration in the O_2-MBfR. The first black dash line indicates the day when we re-inoculated the reactor.

4.4. Modeling evaluation

4.4.1. Modeling 1,4-dioxane removal in O_2-based MBfR

To simulate 1,4-dioxane removal in the O_2-based MBfR, we developed a model by adapting the TCE model framework in Section 2.2. In addition to 1,4-dioxane, other chemicals that might come from the first stage of the treatment train (the H_2-based MBfR or the H_2-based MPfR) were also considered in the model. When the first stage was the H_2-based MBfR, the model had 6 solid biomass species (1,4-dioxane- and acetate-co-oxidizing bacteria (DA-COB), 1,4-dioxane- and ethene-co-oxidizing bacteria (DE-COB), hydrogen-oxidizing bacteria (HOB), VC- and ethene-co-oxidizing bacteria (VE-COB), IB, and EPS) and 8 dissolved chemical species (O_2, 1,4-dioxane, H_2, VC, acetate, ethene, UAP, and BAP). The interactions among all the microbiological and chemical species were summarized in Figure 4.7.

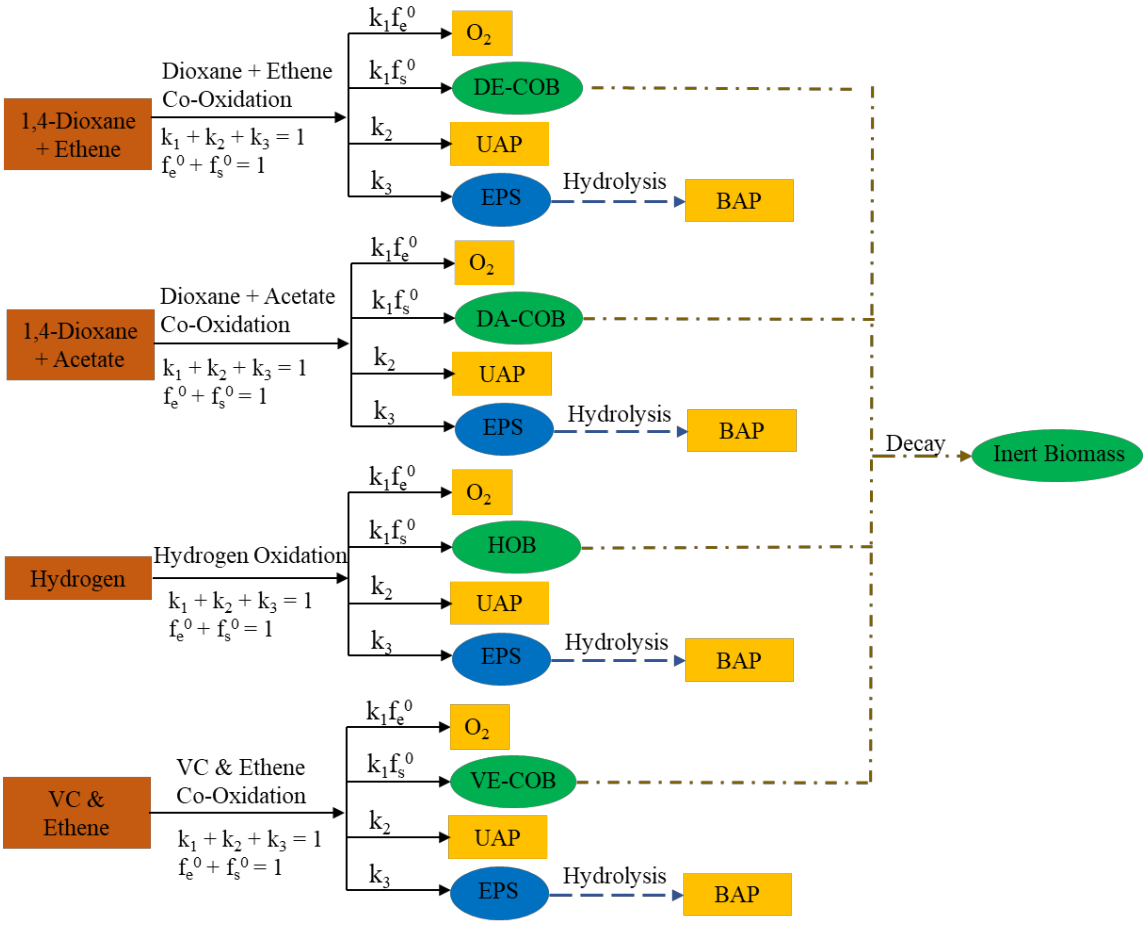

Figure 4.7. Model components and their interactions in the O_2-MBfR.

Since some kinetic parameters were not available in the literature, we made some assumptions for the parameters. For example, we assumed that the 1,4-dioxane co-oxidation kinetic value was the same as its counterpart in the oxidation of 1,4-dioxane only. Based on the assumptions, we simulated the performance of the O_2-based MBfR treating the effluent from the H_2-based MBfR operated at the design operating conditions determined in Section 2.2.1 (TCE surface loading at 1.2×10^{-2} mmol/m^2-day and flow rate at 0.28 m^3/day for one commercial-scale MBfR module). The 1,4-dioxane concentration was assumed to be 1.5 μM, a typical groundwater concentration at the 1,4-dioxane releasing sites (Zenker et al. 2003, Adamson et al. 2014). We varied the 1,4-dioxane loading rate from 6.4×10^{-4} to 0.11 mmol/m^2-day by changing the reactor volume (i.e., number of commercial-scale MBfR modules), while fixing the O_2 pressure and the detachment coefficient (k_{det}) at 1.1 atm and 36 cm^{-1}day^{-1}, which were the same as those for the H_2-based MBfR. When the surface loading was smaller than 7.3×10^{-4} mmol/m^2-day (HRT = 1.6 day), the effluent concentrations of 1,4-dioxane and VC met the drinking water standards (MCL set by the U.S. EPA for VC and MCL set by CA EPA for 1,4-dioxane since there was no federal regulation for 1,4-

dioxane (Crawford et al. 2012).

To evaluate if the loading rate could be further increased by dividing the O_2-MBfR into two identical sub-stages, the two-stage scenario was simulated by gradually decreasing the 1,4-dioxane loading rate until the 1,4-dioxane and VC met the drinking water standards. As shown in Figures 4.8, 1,4-dioxane and VC could meet the drinking water standards when the 1,4-dioxane surface loading rate was below 2.0×10^{-2} mmol/m^2-day. Therefore, by using a two-stage O_2-MBfR, the design loading rate increased to 2.0×10^{-2} mmol/m^2-day, which was later used for the cost analysis. The model can be adapted to simulate effluent coming out of the MPfR in the future.

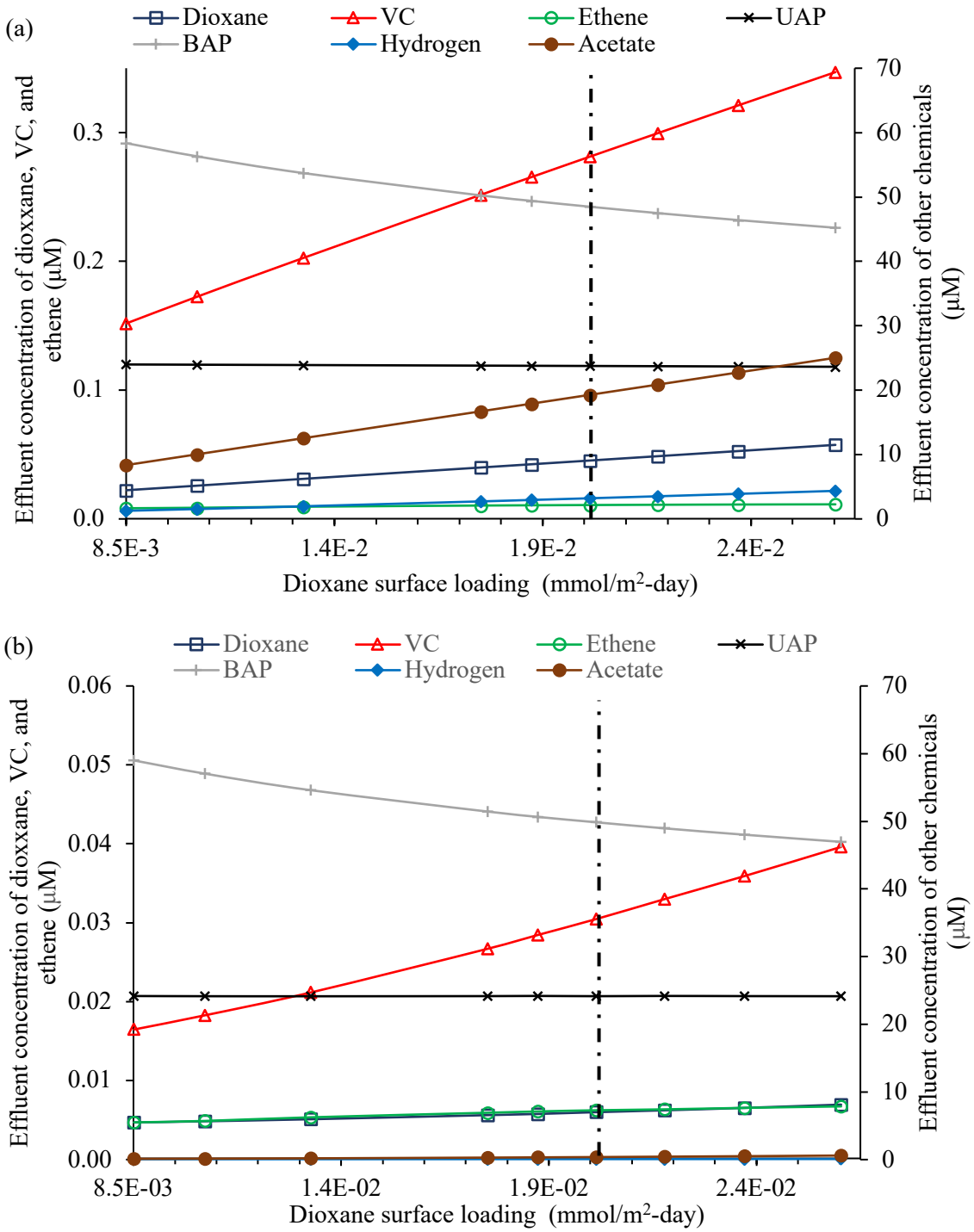

Figure 4.8. The effect of surface loading rate on the performance of the O_2-based MBfR with two sub-stages: (a) Effluent concentrations of sub-stage 1; (b) Effluent concentrations of sub-stage 2. Notes: 1) Drinking water standards for 1,4-dioxane and VC are 0.011 μM and 0.032 μM, respectively. 2) The X-axis represents the overall surface loading rate of the two sub-stages.

4.5. Cost analysis

To estimate the capital and operating cost of a two-stage O_2-based MBfR following the H_2-based MBfR, we used the design loading rate of 2.0×10^{-2} mmol/m^2-day (described above) and modified APTwater's design models for O_2 in place of H_2. Using APTwater's commercial membrane module at 170 m^2 membrane area per module, the resulting module requirement is 196 modules per sub-stage (392 total for two stages). The estimated capital and annual operating cost for such a system is shown in Table 4.2. Power was assumed at \$0.10/kw-hr and liquid oxygen at \$1.80/CCF. Total oxygen requirement was estimated at 67 kg/day.

Table 4.2. Estimated capital and operating expense for a two-stage O_2-Based MBfR (100 gpm flow with modeled H_2-based MBfR effluent, 25.9 kg 1,4-dioxane/yr)

Budgetary Capital Cost		
	Equipment	\$2,700,000
	Site improvements and design	\$410,000
	Start-up costs	\$70,000
	Contingency	\$640,000
	Total installed cost	\$3,820,000
	Installed cost per kg 1,4-D/yr	\$148,000
Annual Operating Cost		
	Labor	\$26,700
	Consumables (oxygen)	\$13,300
	Parts and maintenance	\$47,700
	Module replacement	\$107,000
	Power	\$26,900
	Total annual costs	\$222,000
	Total operating cost per kg 1,4-D	\$8,560
Note: On the one hand, the cost would be higher at more typical influent 1,4-dioxane concentrations. On the other hand, the cost would be lower at optimized operating conditions.		

4.6. Conclusion for 1,4-dioxane degradation

In this task, we successfully enriched from a wetland sediment an ethanotrophic consortium capable of degrading 1,4-dioxane along with ethane as the primary electron donor. We then inoculated the O_2-MBfR with the ethanotrophic sludge. During continuous operation of the O_2-MBfR fed with 0.5 mM 1,4-dioxane along with saturated (1.9 mM) ethane at an HRT of 13 hours, ethane was gradually removed, and substantial 1,4-dioxane removal began once ethane was fully consumed (after 25 days). 1,4-dioxane removal then rapidly became > 99% within 10 days and stayed at this level for over one month. This corresponds to removing an influent concentration of 1,4-dioxane of 4400 μg/L to an effluent concentration below our detection limit (20 μg/L). The mathematic simulation further predicts that 1,4-dioxane can meet the drinking water standards when the 1,4-dioxane surface loading rate is below 2.0×10^{-2} mmol/m^2-day. Together, the experimental and modeling results confirm that 1,4-dioxane was able to be efficiently degraded by an ethanotrophic biofilm in O_2-MBfR.

5. Synergistic Platform for Simultaneous Removal of TCE, TCA, and 1,4-Dioxane

5.1. Experimental testing

Successful TCE/TCA reduction in the H_2-MPfR and 1,4-dioxane oxidation in the O_2-MBfR add support to the proposed concept of the synergistic platform through operation of the H_2-MPfR and the O_2-MBfR in sequence. We linked the two reactors by connecting the effluent port of the H_2-MPfR to the influent port of O_2-MBfR; this is illustrated in Fig. 5.1. Gaseous VOC concentrations of both reactors were measured through the gas sampling ports 1 and 2. Concentrations of 1,4-dioxane and anionic chloride (Cl^-) concentration were measured through two liquid sampling ports.

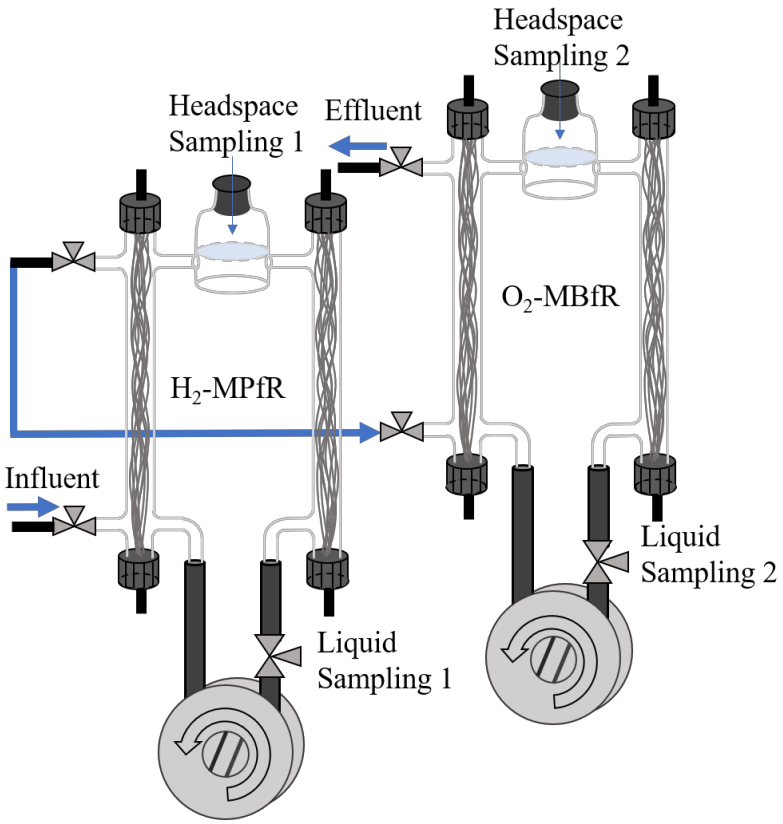

Figure 5.1. The schematic of running H_2-MPfR and O_2-MBfR in sequence.

Figures 5.2 and 5.3 profile concentrations of the major (ethane and 1,4-dioxane) and minor (chlorinated hydrocarbons) electron donors in the O_2-MBfR receiving the effluent from the H_2-MPfR during the 130 days of sequential operation. In Stage 1, once the two reactors were connected and operated in sequence, the degradation of 1,4-dioxane was strongly inhibited (Fig.

5.2). Zhang et al. (2016) investigated the inhibition of 1,4-dioxane degradation by 1,1-DCE, cis-DCE, TCE and TCA, and they showed that 1,1-DCE had the strongest inhibition effect on 1,4-dioxane degradation. Though they did not test DCA and MCA, we hypothesize that these by-products from the H_2-MPfR primarily inhibited 1,4-dioxane degradation in the O_2-MBfR. To attenuate the inhibitive effect, we first increased the H_2 supply from 20 to 30 psig (Days 72 to 85). This did not decrease the production of TCA, DCA and MCA in the H_2-MPfR. Then, we increased the O_2 supply from 10 to 15 psig (Days 85 to 94). Removal of neither 1,4-dioxane nor chlorinated hydrocarbons was enhanced; this indicates that O_2 was not a limiting factor in oxidizing the chlorinated hydrocarbons to eliminate their inhibition on 1,4-dioxane. According to the measured concentrations of chlorinated solvents in the O_2-MBfR (Fig. 5.3 and Table 5.1), most of the chlorinated solvents from the effluent of MPfR were further oxidized to less than 5 μM in the O_2-MBfR, but 1,1-DCA was recalcitrant to oxidation and remained as high as 36 μM (only 60% removal of the effluent from the H_2-MPfR). Since 1,1-DCA has the most similar structure to 1,1-DCE, we further hypothesized that 1,1-DCA probably inhibited 1,4-dioxane oxidation.

We did a batch test in the O_2-MBfR to test if the biofilm could remove dioxane with low ethane concentration. The results, in Figure 5.4, show that the biofilm retained the capacity of dioxane degradation with or without ethane as the primary electron donor, and the reaction rates were similar (83 and 90 mM hr^{-1} with and without ethane, respectively). The results indicate that the inhibition of 1,4-dioxane was reversible, and the biofilm was able to remove 1,4-dioxane even with a low ethane concentration.

In Stage II and based on the previous results, we decreased the influent concentration of TCA and TCE from 1.0 mM to 0.1 mM to minimize the inhibition of TCE, TCA, and their reductive transformation products to the 1,4-dioxane oxidation. The influent concentration of 1,4-dioxane was also decreased from 500 μM to 200 μM to maintain a reasonable TCE/TCA to 1,4-dioxane ratio in reality (Anderson et al. 2012). In the H_2-MPfR, the effluent concentrations of TCA/TCE and all the products were all significantly decreased (Fig. 5.3). In the subsequent O_2-MBfR, these chlorinated hydrocarbons were further removed to undetectable levels. In particular, the 1,1-DCA concentration gradually dropped to 6.8 μM within 10 days. Accordingly, the capacity of 1,4-dioxane biodegradation was recovered from 8% to 97%. This observation further confirms that the presence of chlorinated hydrocarbons, especially 1,1-DCA at a concentration of above 200 μM in our study, inhibited 1,4-dioxane biodegradation, but the inhibition could be removed.

Table 5.1. Concentrations of dissolved VOCs at steady states of Stages I and II in the reactors continuously operated in sequence.

Dissolved VOCs (μM)		TCE	TCA	DCA	MCA	Ethane	Sum
	Influent	778	597	0	0	0	1380
	MPfR	9.7	42.39	60.3	25.3	312	459
Stage I	MBfR	2.1	4.34	36.0	2.85	27.3	73
	Influent	98	103	0	0	0	201
	MPfR	4.1	15.5	6.2	10.5	61.5	98
Stage II	MBfR	1.2	6.4	3.64	0.14	2.4	13.4

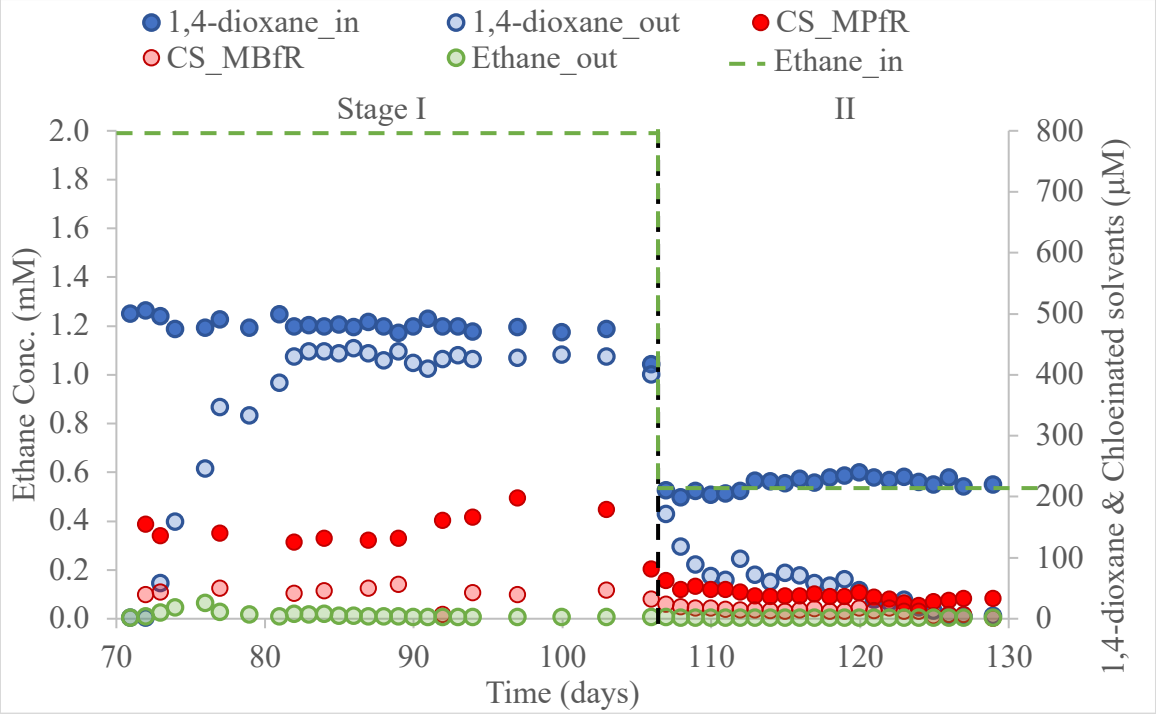

Figure 5.2. The 1,4-dioxane concentration in the O_2-MBfR fed with the effluent from the H_2-MPfR during the 130 days of sequential operation. The vertical black dash line indicates the day when the influent concentrations of all the three substrates were decreased. The red dots indicate the total chlorinated solvent (CS) concentration in both H_2-MPfR and O_2-MBfR.

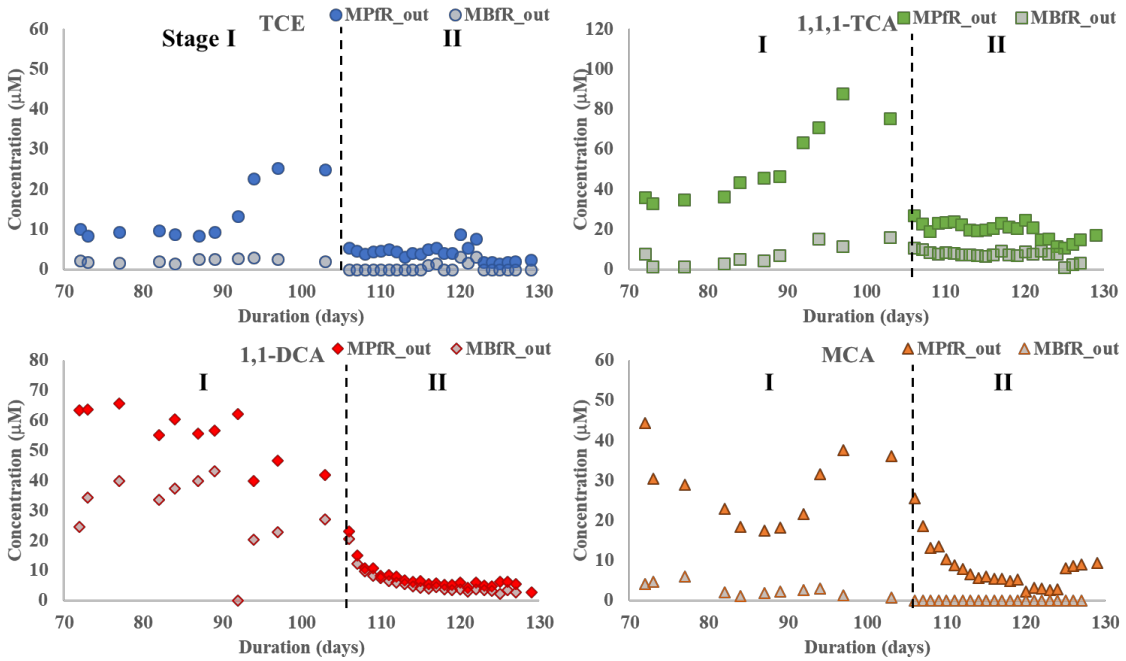

Figure 5.3. Concentration of chlorinated solvents in H_2-MPfR and O_2-MBfR when operated in series. The vertical back dashed line indicates the stage changing from I to II.

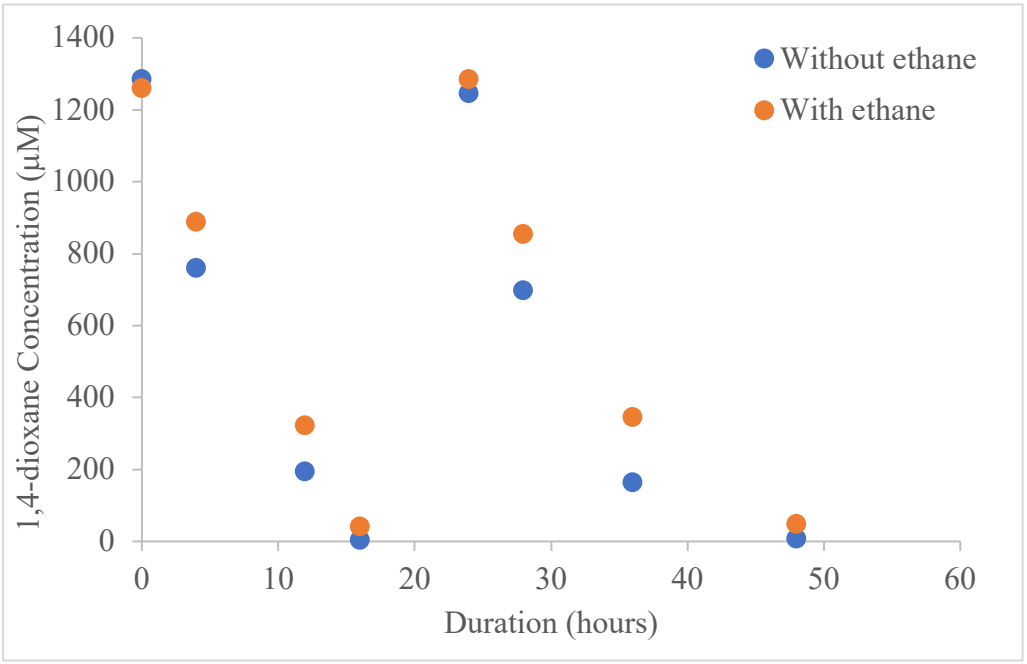

Figure 5.4. A short batch to test the 1,4-dioxane degrading activity of the O_2-MBfR without ethane as primary electron donor.

5.2. Cost analysis

To provide a preliminary estimate of the capital and operating cost of an O_2-based MBfR following the previously estimated H_2-based MPfR, we used the relative area of O_2 membrane to MPfR area in the coupled experiment described above to determine the equipment size and modified APTwater's design models for oxygen in place of H_2. It should be noted that the coupled experiment used a significantly higher 1,4-dioxane concentration than the previous case for cost estimation of the O_2-MBfR (Section 4.5). The cost estimates here are based on the experimental results in this section; they should be considered indicative, but not optimized. Using APTwater's commercial membrane module at 170 m^2 membrane area per module, the resulting module requirement is 318 modules. The estimated capital and annual operating cost for such a system is shown in Table 5.2.

Table 5.2. Estimated capital and operating expense for an O_2-Based MBfR following the H_2-based MPfR at 100 gpm flow rate, 3500 kg 1,4-D/yr

Budgetary Capital Cost		
	Equipment	$2,200,000
	Site improvements and design	$360,000
	Start-up costs	$70,000
	Contingency	$520,000
	Total installed cost	$3,150,000
	Installed cost per kg 1,4-D/yr	$900
Annual Operating Cost		
	Labor	$26,700
	Consumables (oxygen)	$13,300
	Parts and maintenance	$38,500
	Module replacement	$86,900
	Power	$21,800
	Total annual costs	$187,000
	Total operating cost per kg 1,4-D	$53
Note: On the one hand, the cost would be higher at more typical influent 1,4-dioxane concentrations. On the other hand, the cost would be lower at optimized operating conditions.		

5.3. Conclusion for synergistic removal of TCA/TCE and 1,4-dioxane

In this last task, we configured the proposed synergistic platform by linking the TCE/TCA-reducing H_2-MPfR and the 1,4-dioxane-oxidizing O_2-MBfR in sequence. During the 130 days of continuous operation, the ethane produced from TCE and TCA reduction in the H_2-MBfR served

as endogenous primary electron donor for promoting 1,4-dioxane degradation in the O_2-MBfR. Ethane, the desired major products from Pd-catalytic TCE/TCA reduction in the H_2-MPfR, served as the endogenous primary electron donor to promote co-metabolic degradation of 1,4-dioxane in the O_2-MBfR. In addition, the other minor by-products from the H_2-MPfR, including DCA and MCA, also were further degraded through oxidation in the O_2-MBfR. When the concentrations of the 1,1-DCA into in the O_2-MBfR were too high (above 0.2 mM in our study), 1,4-dioxane degradation was significantly inhibited. Once the 1,1-DCA concentration dropped below 0.1 mM (a more field-relevant value), the 1,4-dioxane-degrading capacity was completely recovered, and all MCLs were met. The costs of the overall H_2-MPfR plus O_2-MBfR system for treating a 100-gpm flow were estimated at about $6,600,000 for capital and $480,000 per year for operation. The costs normalized to the amount of 1,4-dioxane removed are around $900/kg-dioxane-year and $53/kg dioxane, respectively.

6. Summary of Publications and Presentations from the Project

6.1. Peer-reviewed publications

1. Wang, B.; Krajmalnik-Brown, R.; Zhou, C.; Luo, Y.; Rittmann, B.E.; Tang, Y. 2018. Modeling the interactions among trichloroethene reduction, methanogenesis, and homoacetogenesis in a H_2-based biofilm. *Biotechnology and Bioengineering* (In review)
2. Wang, B.; Krajmalnik-Brown, R.; Zhou, C.; Luo, Y.; Rittmann, B.E.; Tang, Y. 2018. Complete dechlorination of trichloroethene in the H_2-based biofilm (In preparation)
3. Luo, Y.H., Zhou, C.; Long, X.; Friese, D.; Wang, B.; Tang, Y.; Krajmalnik-Brown, R.; Rittmann, B.E. Synergistic Pd-Catalytic Dechlorination of 1,1,1-Trichloroethane and Trichloroethene Followed by Biodegradation of 1,4-Dioxane (In preparation)

6.2. National and international presentations

Rittmann, B.E. (poster presenter) et al. Synergistic Reductive Dechlorination of 1,1,1-Trichloroethane and Trichloroethene and Aerobic Biodegradation of 1,4-Dioxane. SERDP/ESTCP Symposium 2017, Washington, DC, November 28th, 2017.

Tang, Y. (oral presenter) et al. Synergistic Reductive Dechlorination of 1,1,1-Trichloroethane and Trichloroethene and Aerobic Biodegradation of 1,4-Dioxane. SERDP In-Progress Review Meeting, Washington, DC, November 8th, 2018.

Luo, Y.-H. (poster presenter) et al. A Synergistic Platform for Pd-catalytic Reduction of 1,1,1-Trichloroethane and Trichloroethene Followed by Biological Co-metabolism of 1,4-Dioxane. SERDP & ESTCP Symposium 2018, Washington, DC, November 28th, 2018.

Tang, Y. (poster presenter) et al. Modeling Synergistic Removal of Trichloroethene and 1,4-Dioxane by Two-Stage Membrane Biofilm Reactors. SERDP & ESTCP Symposium 2018, Washington, DC, November 28th, 2018.

Wang, B. (poster presenter) et al. Simulation of intermediate accumulation during trichloroethene dechlorination in a H_2-based biofilm. ACS National Meeting & Expo, Orlando, FL, March 31st, 2019. (In review

7. Future-research Plan

The results from this limited scope project demonstrated the concept of synergistic treatment of TCE, TCA, and 1,4-dioxane: linking the TCE/TCA-reducing H_2-MPfR and the 1,4-dioxane-oxidizing O_2-MBfR in sequence. During the 130 days of continuous operation, the ethane produced from TCE and TCA reduction in the H_2-MPfR served as endogenous primary electron donor for promoting 1,4-dioxane degradation in the O_2-MBfR. Ethane, the desired major product from Pd-catalytic TCE/TCA reduction in the H_2-MPfR, served as the endogenous primary electron donor to promote co-metabolic degradation of 1,4-dioxane in the O_2-MBfR. In addition, the other minor by-products from the H_2-MPfR, including DCA and MCA, also were further degraded through oxidation in the O_2-MBfR. A key part of the project's proof-of-concept came from a mechanistic model we developed for 1,4-dioxane biotransformation in the O_2-MBfR.

From this strong foundation, the team is well-positioned to advance the synergistic platform towards commercial application by a combination of modeling advancements, filling in key knowledge gaps, and pilot scale testing.

The MBfR model puts our team in position to optimize the design of future experiments, to mechanistically interpret experimental results, and to apply our growing knowledge to the design of reliable and cost-effective processes at commercial scale. Developing a similar model for the H_2-based MPfR was outside the scope of the limited scope project, but we will be able to develop that model, which will expand the benefits we can obtain from mechanistic modeling. Thus, advancing the O_2-MBfR model and creating a model for the H_2-MPfR are essential future steps.

While we established that the synergistic platform works as anticipated, we also uncovered a number of fundamental questions that need to be answered in order to ensure that the platform has reliable and cost-effective performance. Part of future work must be directed towards filling in the gaps of fundamental knowledge. Particularly important are these objectives:

- For the O_2-based MBfR, we need to define better what controls the kinetics of 1,4-dioxane biodegradation when ethane is the primary substrate coming from the H_2-based MPfR. Of high importance is relating the delivery capacity of O_2 to the availability of ethane and developing kinetic expressions and parameters for quantifying the effects of 1,4-dioxane, ethane, and O_2. In addition, we will carry out microbial-ecology analyses -- including high-throughput sequencing, qPCR, and metagenomics -- to identify key microbes mediating essential transformation processes and quantify their growth and metabolism.
- For the H_2-based MPfR, we need to define the impacts of Pd-loading, Pd-size, and Pd-coating method on the membranes on Pd's effectiveness as a catalyst for TCE and TCA reduction and its selectivity towards ethane.
- Also for the H_2-based MPfR, we need to define competition among TCE, TCA, and their reduction products for H_2 and reactive sites on the Pd catalyst. These are essential inputs for the mechanistic model of the H_2-based MPfR.

- We need to evaluate the two-stage platform over a much wider range of conditions, including those that we believe are optimized based on modeling simulations. Operating conditions include the input concentrations of TCA, TCE, and 1,4-dioxane; surface loading rates in either stage; and H_2- or O_2-delivery capacities. The wide range of conditions is best tested at the bench-scale and in coordination with modeling.

The culmination of future research is a pilot study of the two-stage platform at a site that has co-contamination of 1,4-dioxane with TCA, TCE, or (preferably) both. Taking advantage of the existing pilot capabilities of APTwater, we can move quickly and efficiently to pilot implementation. While the O_2-based MBfR will need no major modifications from existing APTwater modules, the H_2-based MPfR will need to be modified in a significant way to coat the fibers with Pd catalyst. Thus, the pilot program must include a period for adapting the MBfR to become an MPfR at pilot scale.

We envision a three-year project. The first year will focus on model development and study of the first two fundamental issues at the bench scale. Year two will include adaptation of the APTwater's MBfR modules to become an MPfR, testing the two-stage platform over the wide range of operating conditions, and using the models to find the most favorable designs for the MPfR and MBfR. Year three will focus on the pilot study, and it will be supported by modeling and targeted bench studies. The pilot study will lead to reliable cost estimates for the synergistic system and a field-proven design that is ready to move to field implementation.

8. References

Adamson, D.T., Mahendra, S., Walker Jr, K.L., Rauch, S.R., Sengupta, S. and Newell, C.J. (2014) A multisite survey to identify the scale of the 1, 4-dioxane problem at contaminated groundwater sites. Environmental Science & Technology Letters 1(5), 254-258.

Adamson, D.T., McDade, J.M. and Hughes, J.B. (2003) Inoculation of a DNAPL source zone to initiate reductive dechlorination of PCE. Environmental Science & Technology 37(11), 2525-2533.

Anderson, R.H., Anderson, J.K. and Bower, P.A. (2012) Co-occurrence of 1, 4-dioxane with trichloroethylene in chlorinated solvent groundwater plumes at US Air Force installations: Fact or fiction. Integrated environmental assessment and management 8(4), 731-737.

Aulenta, F., Gossett, J.M., Papini, M.P., Rossetti, S. and Majone, M. (2005) Comparative study of methanol, butyrate, and hydrogen as electron donors for long-term dechlorination of tetrachloroethene in mixed anerobic cultures. Biotechnology and bioengineering 91(6), 743-753.

Bernhardt, D. and Diekmann, H. (1991) Degradation of dioxane, tetrahydrofuran and other cyclic ethers by an environmental Rhodococcus strain. Applied microbiology and biotechnology 36(1), 120-123.

Burback, B.L. and Perry, J.J. (1993) Biodegradation and biotransformation of groundwater pollutant mixtures by Mycobacterium vaccae. Applied and Environmental Microbiology 59(4), 1025-1029.

Chambon, J., Lemming, G., Broholm, M., Binning, P.J. and Bjerg, P.L. (2009) Model assessment of reductive dechlorination as a remediation technology for contaminant sources in fractured clay. Case studies Delrapport III.

Chambon, J.C., Bjerg, P.L., Scheutz, C., Bælum, J., Jakobsen, R. and Binning, P.J. (2013) Review of reactive kinetic models describing reductive dechlorination of chlorinated ethenes in soil and groundwater. Biotechnology and bioengineering 110(1), 1-23.

Chan, W.W., Grostern, A., Löffler, F.E. and Edwards, E.A. (2011) Quantifying the effects of 1, 1, 1-trichloroethane and 1, 1-dichloroethane on chlorinated ethene reductive dehalogenases. Environmental Science & Technology 45(22), 9693-9702.

Chaplin, B.P., Reinhard, M., Schneider, W.F., Schüth, C., Shapley, J.R., Strathmann, T.J. and Werth, C.J. (2012) Critical review of Pd-based catalytic treatment of priority contaminants in water. Environmental Science & Technology 46(7), 3655-3670.

Chen, D.-Z., Jin, X.-J., Chen, J., Ye, J.-X., Jiang, N.-X. and Chen, J.-M. (2016) Intermediates and substrate interaction of 1, 4-dioxane degradation by the effective metabolizer Xanthobacter flavus DT8. International Biodeterioration & Biodegradation 106, 133-140.

Christ, J.A. and Abriola, L.M. (2007) Modeling metabolic reductive dechlorination in dense non-aqueous phase liquid source-zones. Advances in water resources 30(6-7), 1547-1561.

Chung, J., Krajmalnik-Brown, R. and Rittmann, B., E (2007) Bioreduction of trichloroethene using a hydrogen-based membrane biofilm reactor. Environmental science & technology 42(2), 477-483.

Chung, J., Krajmalnik-Brown, R. and Rittmann, B.E. (2008) Bioreduction of trichloroethene using a hydrogen-based membrane biofilm reactor. Environmental Science & Technology 42(2), 477-483.

Chung, J. and Rittmann, B.E. (2007) Bio-reductive dechlorination of 1, 1, 1-trichloroethane and chloroform using a hydrogen-based membrane biofilm reactor. Biotechnology and Bioengineering 97(1), 52-60.

Chung, J. and Rittmann, B.E. (2008) Simultaneous bio-reduction of trichloroethene, trichloroethane, and chloroform using a hydrogen-based membrane biofilm reactor. Water Science and Technology 58(3), 495-501.

Clapp, L.W., Semmens, M.J., Novak, P.J. and Hozalski, R.M. (2004) Model for in situ perchloroethene dechlorination via membrane-delivered hydrogen. Journal of Environmental Engineering 130(11), 1367-1381.

Crawford, J., Jones, D.G., Llados, F., Risher, J. and Tencza, B. (2012) Toxicological profile for 1, 4-dioxane.

Cupples, A.M., Spormann, A.M. and McCarty, P.L. (2004) Vinyl chloride and cis-dichloroethene dechlorination kinetics and microorganism growth under substrate limiting conditions. Environmental science & technology 38(4), 1102-1107.

Davie, M.G., Cheng, H., Hopkins, G.D., LeBron, C.A. and Reinhard, M. (2008) Implementing heterogeneous catalytic dechlorination technology for remediating TCE-contaminated groundwater. Environmental science & technology 42(23), 8908-8915.

Delgado, A.G., Fajardo-Williams, D., Popat, S.C., Torres, C.I. and Krajmalnik-Brown, R. (2014a) Successful operation of continuous reactors at short retention times results in high-density, fast-rate Dehalococcoides dechlorinating cultures. Applied Microbiology and Biotechnology 98(6), 2729-2737.

Delgado, A.G., Kang, D.-W., Nelson, K.G., Fajardo-Williams, D., Miceli III, J.F., Done, H.Y., Popat, S.C. and Krajmalnik-Brown, R. (2014b) Selective enrichment yields robust ethene-producing dechlorinating cultures from microcosms stalled at cis-dichloroethene. PloS one 9(6), e100654.

Delgado, A.G., Parameswaran, P., Fajardo-Williams, D., Halden, R.U. and Krajmalnik-Brown, R. (2012) Role of bicarbonate as a pH buffer and electron sink in microbial dechlorination of chloroethenes. Microbial cell factories 11(1), 128.

Dugat-Bony, E., Biderre-Petit, C., Jaziri, F., David, M.M., Denonfoux, J., Lyon, D.Y., Richard, J.Y., Curvers, C., Boucher, D. and Vogel, T.M. (2012) In situ TCE degradation mediated by complex dehalorespiring communities during biostimulation processes. Microbial biotechnology 5(5), 642-653.

EPA, U. (2009) National Primary Drinking Water Regulations. https://www.epa.gov/ground-water-and-drinking-water/national-primary-drinking-water-regulations.

Fennell, D.E. and Gossett, J.M. (1998) Modeling the production of and competition for hydrogen in a dechlorinating culture. Environmental science & technology 32(16), 2450-2460.

Freeberg, K., Bedient, P. and Connor, J. (1987) Modeling of TCE contamination and recovery in a shallow sand aquifer. Groundwater 25(1), 70-80.

Grostern, A., Chan, W.W. and Edwards, E.A. (2009) 1, 1, 1-Trichloroethane and 1, 1-dichloroethane reductive dechlorination kinetics and co-contaminant effects in a Dehalobacter-containing mixed culture. Environmental Science & Technology 43(17), 6799-6807.

Haston, Z.C. and McCarty, P.L. (1999) Chlorinated ethene half-velocity coefficients (K_s) for reductive dehalogenation. Environmental Science & Technology 33(2), 223-226.

He, J., Holmes, V.F., Lee, P.K. and Alvarez-Cohen, L. (2007) Influence of vitamin B12 and cocultures on the growth of Dehalococcoides isolates in defined medium. Applied and Environmental Microbiology 73(9), 2847-2853.

He, J., Ritalahti, K.M., Yang, K.-L., Koenigsberg, S.S. and Löffler, F.E. (2003) Detoxification of vinyl chloride to ethene coupled to growth of an anaerobic bacterium. Nature 424(6944), 62.

He, J., Sung, Y., Krajmalnik-Brown, R., Ritalahti, K.M. and Löffler, F.E. (2005) Isolation and characterization of Dehalococcoides sp. strain FL2, a trichloroethene (TCE)-and 1, 2-dichloroethene-respiring anaerobe. Environmental Microbiology 7(9), 1442-1450.

Heck, K.N., Nutt, M.O., Alvarez, P. and Wong, M.S. (2009) Deactivation resistance of Pd/Au nanoparticle catalysts for water-phase hydrodechlorination. Journal of Catalysis 267(2), 97-104.

Hirvonen, A., Tuhkanen, T. and Kalliokoski, P. (1996) Treatment of TCE-and PCE contaminated groundwater using UV/H2O2 and O_3/H_2O_2 oxidation processes. Water Science and Technology 33(6), 67-73.

Huang, D. and Becker, J.G. (2009) Determination of intrinsic monod kinetic parameters for two heterotrophic tetrachloroethene (PCE)-respiring strains and insight into their application. Biotechnology and bioengineering 104(2), 301-311.

Isaka, K., Udagawa, M., Sei, K. and Ike, M. (2016) Pilot test of biological removal of 1, 4-dioxane from a chemical factory wastewater by gel carrier entrapping Afipia sp. strain D1. Journal of hazardous materials 304, 251-258.

Johnson, D.R., Nemir, A., Andersen, G.L., Zinder, S.H. and Alvarez-Cohen, L. (2009) Transcriptomic microarray analysis of corrinoid responsive genes in Dehalococcoides ethenogenes strain 195. FEMS microbiology letters 294(2), 198-206.

Kim, Y.-M., Jeon, J.-R., Murugesan, K., Kim, E.-J. and Chang, Y.-S. (2009) Biodegradation of 1, 4-dioxane and transformation of related cyclic compounds by a newly isolated Mycobacterium sp. PH-06. Biodegradation 20(4), 511.

Kotsyurbenko, O.R., Glagolev, M.V., Nozhevnikova, A.N. and Conrad, R. (2001) Competition between homoacetogenic bacteria and methanogenic archaea for hydrogen at low temperature. FEMS microbiology ecology 38(2-3), 153-159.

Leaist, D.G. and Lyons, P.A. (1981) Multicomponent diffusion of electrolytes with incomplete dissociation. diffusion in a buffer solution. The Journal of Physical Chemistry 85(12), 1756-1762.

Liu, Z., Zhou, C., Ontiveros-Valencia, A., Luo, Y.H., Long, M., Xu, H. and Rittmann, B.E. (2018) Accurate O_2 delivery enabled benzene biodegradation through aerobic activation followed by denitrification-coupled mineralization. Biotechnology and Bioengineering.

Lowry, G.V. and Reinhard, M. (1999) Hydrodehalogenation of 1-to 3-carbon halogenated organic compounds in water using a palladium catalyst and hydrogen gas. Environmental Science & Technology 33(11), 1905-1910.

Lowry, G.V. and Reinhard, M. (2001) Pd-catalyzed TCE dechlorination in water: effect of [H2](aq) and H2-utilizing competitive solutes on the TCE dechlorination rate and product distribution. Environmental science & technology 35(4), 696-702.

Maharajh, D.M. and Walkley, J. (1972) Lowering of the saturation solubility of oxygen by the presence of another gas. Nature 236(5343), 165.

Mahendra, S., Petzold, C.J., Baidoo, E.E., Keasling, J.D. and Alvarez-Cohen, L. (2007) Identification of the intermediates of in vivo oxidation of 1, 4-dioxane by monooxygenase-containing bacteria. Environmental Science & Technology 41(21), 7330-7336.

Matteucci, F., Ercole, C. and del Gallo, M. (2015) A study of chlorinated solvent contamination of the aquifers of an industrial area in central Italy: a possibility of bioremediation. Frontiers in microbiology 6, 924.

Maymó-Gatell, X., Chien, Y.-t., Gossett, J.M. and Zinder, S.H. (1997) Isolation of a bacterium that reductively dechlorinates tetrachloroethene to ethene. Science 276(5318), 1568-1571.

Maymó-Gatell, X., Tandoi, V., Gossett, J.M. and Zinder, S.H. (1995) Characterization of an H2-utilizing enrichment culture that reductively dechlorinates tetrachloroethene to vinyl chloride and ethene in the absence of methanogenesis and acetogenesis. Applied and Environmental Microbiology 61(11), 3928-3933.

Moran, M.J., Zogorski, J.S. and Squillace, P.J. (2007) Chlorinated solvents in groundwater of the United States. Environmental science & technology 41(1), 74-81.

Mori, T., Kubo, J. and Morikawa, Y. (2004) Hydrodechlorination of 1, 1, 1-trichloroethane over silica-supported palladium catalyst. Applied Catalysis A: General 271(1-2), 69-76.

Mundle, S.O., Johnson, T., Lacrampe-Couloume, G., Pérez-de-Mora, A., Duhamel, M., Edwards, E.A., McMaster, M.L., Cox, E., Révész, K. and Sherwood Lollar, B. (2012) Monitoring biodegradation of ethene and bioremediation of chlorinated ethenes at a contaminated site using compound-specific isotope analysis (CSIA). Environmental science & technology 46(3), 1731-1738.

Ni, B.J., Liu, H., Nie, Y.Q., Zeng, R.J., Du, G.C., Chen, J. and Yu, H.Q. (2011) Coupling glucose fermentation and homoacetogenesis for elevated acetate production: experimental and mathematical approaches. Biotechnology and bioengineering 108(2), 345-353.

Nutt, M.O., Hughes, J.B. and Wong, M.S. (2005) Designing Pd-on-Au bimetallic nanoparticle catalysts for trichloroethene hydrodechlorination. Environmental science & technology 39(5), 1346-1353.

Parales, R., Adamus, J., White, N. and May, H. (1994) Degradation of 1, 4-dioxane by an actinomycete in pure culture. Applied and Environmental Microbiology 60(12), 4527-4530.

Picioreanu, C., Van Loosdrecht, M.C. and Heijnen, J.J. (2000) Effect of diffusive and convective substrate transport on biofilm structure formation: a two-dimensional modeling study. Biotechnology and bioengineering 69(5), 504-515.

Rittmann and McCarty (2001) Environmental biotechnology: principles and applications. New York: McGrawHill 400.

Scheutz, C., Durant, N.D., Hansen, M.H. and Bjerg, P.L. (2011) Natural and enhanced anaerobic degradation of 1, 1, 1-trichloroethane and its degradation products in the subsurface–a critical review. Water Research 45(9), 2701-2723.

Stewart, P.S. (1993) A model of biofilm detachment. Biotechnology and bioengineering 41(1), 111-117.

Sung, Y., Fletcher, K.E., Ritalahti, K.M., Apkarian, R.P., Ramos-Hernández, N., Sanford, R.A., Mesbah, N.M. and Löffler, F.E. (2006) Geobacter lovleyi sp. nov. strain SZ, a novel metal-reducing and tetrachloroethene-dechlorinating bacterium. Applied and Environmental Microbiology 72(4), 2775-2782.

Tang, Y., Krajmalnik-Brown, R. and Rittmann, B.E. (2013) Modeling trichloroethene reduction in a hydrogen-based biofilm. Water Science and Technology 68(5), 1158-1163.

Tang, Y., Zhao, H., Marcus, A.K., Krajmalnik-Brown, R. and Rittmann, B., E (2012) A steady-state biofilm model for simultaneous reduction of nitrate and perchlorate, part 1: model development and numerical solution. Environmental Science & Technology 46(3), 1598-1607.

Vainberg, S., Condee, C.W. and Steffan, R.J. (2009) Large-scale production of bacterial consortia for remediation of chlorinated solvent-contaminated groundwater. Journal of Industrial Microbiology & Biotechnology 36(9), 1189-1197.

Vainberg, S., McClay, K., Masuda, H., Root, D., Condee, C., Zylstra, G.J. and Steffan, R.J. (2006) Biodegradation of ether pollutants by Pseudonocardia sp. strain ENV478. Applied and Environmental Microbiology 72(8), 5218-5224.

Varfolomeyev, S., Kalyuzhnyy, S. and Spivak, S. (1989) Kinetic regularities of methane production by a methanogenic association. Applied biochemistry and biotechnology 22(3), 351-360.

Vavilin, V., Lokshina, L.Y., Rytov, S., Kotsyurbenko, O., Nozhevnikova, A. and Parshina, S. (1997) Modelling methanogenesis during anaerobic conversion of complex organic matter at low temperatures. Water Science and Technology 36(6-7), 531-538.

Wanner, O. (2006) Mathematical modeling of biofilms, IWA Pub.

Yu, S., Dolan, M.E. and Semprini, L. (2005) Kinetics and inhibition of reductive dechlorination of chlorinated ethylenes by two different mixed cultures. Environmental science & technology 39(1), 195-205.

Yu, S. and Semprini, L. (2004) Kinetics and modeling of reductive dechlorination at high PCE and TCE concentrations. Biotechnology and bioengineering 88(4), 451-464.

Zeebe, R.E. (2011) On the molecular diffusion coefficients of dissolved CO2, HCO3-, and CO32- and their dependence on isotopic mass. Geochimica et Cosmochimica Acta 75(9), 2483-2498.

Zenker, M.J., Borden, R.C. and Barlaz, M.A. (2003) Occurrence and treatment of 1, 4-dioxane in aqueous environments. Environmental Engineering Science 20(5), 423-432.

Zhang, S., Gedalanga, P.B. and Mahendra, S. (2016) Biodegradation kinetics of 1, 4-dioxane in chlorinated solvent mixtures. Environmental science & technology 50(17), 9599-9607.

Zhou, C., Wang, Z., Marcus, A.K. and Rittmann, B.E. (2016a) Biofilm-enhanced continuous synthesis and stabilization of palladium nanoparticles (PdNPs). Environmental Science: Nano 3(6), 1396-1404.

Zhou, Y., Huang, H. and Shen, D. (2016b) Multi-substrate biodegradation interaction of 1, 4-dioxane and BTEX mixtures by Acinetobacter baumannii DD1. Biodegradation 27(1), 37-46.

Ziv-El, M., Delgado, A.G., Yao, Y., Kang, D.W., Nelson, K.G., Halden, R.U. and Krajmalnik-Brown, R. (2011) Development and characterization of DehaloR^2, a novel anaerobic microbial consortium performing rapid dechlorination of TCE to ethene. Applied Microbiology and Biotechnology 92(5), 1063-1071.

Ziv-El, M., Popat, S.C., Cai, K., Halden, R.U., Krajmalnik-Brown, R. and Rittmann, B.E. (2012a) Managing methanogens and homoacetogens to promote reductive dechlorination of trichloroethene with direct delivery of H_2 in a membrane biofilm reactor. Biotechnology and Bioengineering 109(9), 2200-2210.

Ziv-El, M., Popat, S.C., Parameswaran, P., Kang, D.W., Polasko, A., Halden, R.U., Rittmann, B.E. and Krajmalnik-Brown, R. (2012b) Using electron balances and molecular techniques to assess trichoroethene - induced shifts to a dechlorinating microbial community. Biotechnology and Bioengineering 109(9), 2230-2239.

Appendix

Modeling the Interactions among Trichloroethene Reduction, Methanogenesis, and Homoacetogenesis in a H_2-based Biofilm

Boya Wang[1], Rosa Krajmalnik-Brown[2], Chen Zhou[2], Yihao Luo[2], Bruce E. Rittmann[2], Youneng Tang[1, *]

[1] Department of Civil and Environmental Engineering, FAMU-FSU College of Engineering, Florida State University, 2525 Pottsdamer Street, Tallahassee, Florida 32310, United States

[2] Biodesign Swette Center for Environmental Biotechnology, Arizona State University, 1001 South McAllister Ave., Tempe, Arizona 85287, United States

* Corresponding author: Youneng Tang

Phone: +1 (850)410-6119; e-mail: ytang@eng.famu.fsu.edu

Short running title: Modeling TCE reduction in a H_2-based biofilm

Grant numbers: DOD SERDP ER-2721

Abstract

Homoacetogenesis and methanogenesis, which usually occur during anaerobic trichloroethene (TCE) dechlorination, affect the removal of TCE and its daughter products. This work develops a one-dimensional, multi-species H_2-based biofilm model to simulate the interactions among six solid biomass species (*Dehalococcoides*, *Geobacter*, methanogens, homoacetogens, inert biomass, and extracellular polymeric substances) and 10 dissolved chemical species (TCE, dichloroethene (DCE), vinyl chloride (VC), ethene, hydrogen, methane, acetate, bicarbonate, utilization associated products, and biomass associated products). To evaluate and parameterize the model, parameter values from the literature were input into the model to simulate conditions reported for an experiment in which a H_2-based membrane biofilm reactor performed reductive dechlorination of TCE. The biomass species distribution in the biofilm and the chemical species concentrations in the reactor effluent at steady state were consistent between the experiments and the model. The predicted 15-μm biofilm consisted of three layers, each dominated by a different active biomass type: homoacetogens in the layer next to the membrane, *Geobacter* in the biofilm surface layer (next to the water), and *Dehalococcoides* in-between. The biomass distribution is determined by the specific growth rates of the biomass species, which vary along the biofilm depth mainly due to the concentration gradients of TCE and DCE.

Key words: Biofilm model, TCE reduction, methanogenesis, homoacetogenesis

Graphical Abstract

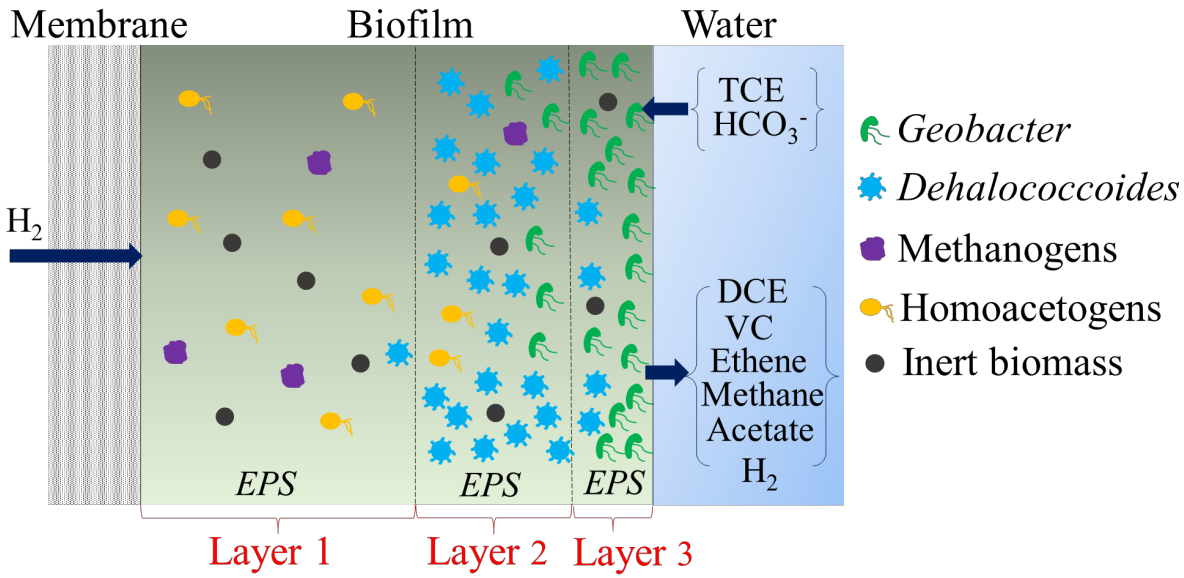

Homoacetogenesis and methanogenesis, which usually occur during anaerobic trichloroethene (TCE) dechlorination, affect removal of TCE and its daughter products. This work develops and parameterizes a multispecies biofilm model to simulate and understand the interactions among TCE dechlorination, homoacetogenesis, and methanogensis in a H_2-based biofilm. Without having any fitted parameters, the model simulates well all trends observed in a membrane biofilm reactor (MBfR).

1 INTRODUCTION

Trichloroethene (TCE) was and is widely used as an industrial solvent and cleaning agent, and it is the most prevalent chlorinated ethene in groundwater aquifers, sediments, and soils worldwide (Mundle et al. 2012). TCE affects human health through liver and kidney damage and by being a carcinogen (Moran et al. 2007). The U.S. Environmental Protection Agency (U.S. EPA) established a drinking-water maximum contaminant level (MCL) of 5 µg/L (3.8×10^{-5} mM) (2009). Because of its prevalence and toxicity, TCE is ranked 16th in the Agency for Toxic Substances and Disease Registry (ATSDR) 2017 Substance Priority List.

TCE can be biologically reduced to a harmless product via stepwise reductive dechlorination to dichloroethene (DCE), vinyl chloride (VC), and finally ethene. DCE and VC also are drinking-water contaminants regulated by U.S. EPA, having MCLs of 70 µg/L (7.2×10^{-4} mM) and 2 µg/L (3.2×10^{-5} mM), respectively. VC is more toxic than TCE and DCE and is ranked in 4th place in the ATSDR (Agency for Toxic Substances and Disease Registry) priority list and as the first organic substance. The species *Dehalococcoides mccartyi* contains the only strains known to reductively dechlorinate TCE to ethene; they use hydrogen gas (H_2) as the electron donor, acetate as carbon source, and chlorinated ethenes as respiratory electron acceptors (Maymó-Gatell et al. 1997, He et al. 2003, He et al. 2005). Some other bacterial genera, such as *Geobacter*, can reduce TCE to DCE using H_2 and acetate as the electron donors and acetate as the carbon source (Sung et al. 2006, Chambon et al. 2013), but they do not reduce DCE to VC or ethene.

The H_2-based membrane biofilm reactor (MBfR) has been proven effective for bio-reduction of TCE (Chung et al. 2007, Chung and Rittmann 2008, Ziv-El et al. 2012a). Because H_2 is a favorable electron donor, hydrogenotrophic methanogenesis and homoacetogenesis usually occur simultaneously (Aulenta et al. 2005, Delgado et al. 2012, Ziv-El et al. 2012a). The presence of a small amount of methanogens and homoacetogens is beneficial, since they generate vitamins and cofactors that help reductive dechlorination (Maymó-Gatell et al. 1995, He et al. 2007, Johnson et al. 2009). Moreover, homoacetogens produce acetate, a carbon source and electron donor for dechlorination. However, too much methanogenesis or homoacetogenesis is undesirable, because these processes compete with dechlorination for H_2. Additionally, electrons channeled to methanogenesis are lost as CH_4, which is combustible and a greenhouse gas. Therefore, optimizing homoacetogenesis and minimizing methanogens are key objectives when using an MBfR for TCE reduction. Another important objective is minimizing the accumulation of DCE

and VC, since VC is more toxic than TCE (Dugat-Bony et al. 2012, Matteucci et al. 2015).

The goal of this study is to develop and parameterize a model that considers the key H_2-based interactions among TCE reduction, methanogenesis, and homoacetogenesis. To evaluate the model, we simulated a bench-scale experiment conducted with a H_2-based MBfR (Ziv-El et al. 2012a).

2 MATHEMATICAL MODEL

This model builds on the one-dimensional, multispecies framework for simulating the simultaneous reductions of nitrate and perchlorate in a H_2-based membrane biofilm (Tang et al. 2012). The model for this work has six solid biomass species (*Dehalococcoides*, *Geobacter,* methanogens, homoacetogens, inert biomass (IB), and extracellular polymeric substances (EPS), noted with subscript *j* from 1 to 6, respectively) and 10 dissolved chemical species (TCE, DCE, VC, ethene, H_2, methane, acetate, HCO_3^-, utilization associated products (UAP), and biomass associated products (BAP), noted with subscript *i* from 1 to 10, respectively).

2.1 Model Components and Their Interactions

Figure 1 summarizes the interactions among all the microbiological and chemical species. A special feature for TCE reductive dechlorination is that the chlorinated ethenes inhibit the reduction kinetics of the downstream chlorinated species: i.e., TCE inhibits DCE and VC dehalogenations, and DCE inhibits VC dehalogenation (Yu et al. 2005). The interactions among the species are tabulated in matrix form in Table I for the biomass species and Table II for the dissolved chemical species. Symbols used in the mathematical expressions are defined in Tables III (model inputs: constants), IV (model inputs: operating conditions), and V (model outputs). For consistency, chemical oxygen demand (COD) is used as the mass unit for all species. When used for electron acceptors, COD has a negative sense. Unit conversions are summarized in Table VI.

2.2 Mass Balances and Kinetics

The governing equation for any dissolved chemical species in the biofilm is:

$$\frac{dS_{fi}}{dt} = D_{fi}\frac{d^2S_{fi}}{dz^2} + r_i \qquad (i = 1,2,3,...,10) \qquad 1$$

(All symbols are defined in Tables I – V.) The change in concentration of a chemical species is governed by diffusion (first term on the right side of the equation) and reaction (second term). The boundary condition at the interface of biofilm and membrane is flux continuity for H_2 (Equation 2) and no flux for the other 9 species (Equation 3):

$$\frac{D_m}{L_m}(S_{g5} - \frac{S_{f5}\Big|_{z=0}}{k_H}) = -D_{f5}\left.\frac{dS_{f5}}{dz}\right|_{z=0} \qquad 2$$

$$\left.\frac{dS_{fi}}{dz}\right|_{z=0} = 0 \qquad (i \neq 5) \qquad 3$$

The boundary condition at the interface of biofilm and water diffusion layer is flux continuity for all chemical species:

$$\frac{D_i}{L_d}(S_{bi} - S_{fi}\Big|_{z=L_f}) = D_{fi}\left.\frac{dS_{fi}}{dz}\right|_{z=L_f} \qquad (i = 1,2,3,...,10) \qquad 4$$

where S_{bi} is calculated using Equation 5 based on mass balance applied to the reactor:

$$S_{bi} = \frac{S_i\frac{Q}{A} + S_{fi}\Big|_{z=L_f}\frac{D_i}{L_d}}{(\frac{D_i}{L_d} + \frac{Q}{A})} \qquad (i = 1,2,3,...,10) \qquad 5$$

The governing equation to simulate the fraction variation of biomass species at a location in the biofilm is:

$$\frac{df_j}{dt} = (\mu_j - \bar{\mu})f_j - u_L\frac{df_j}{dz} \qquad (j = 1,2,3,4,5,6) \qquad 6$$

where the first term on the right side describes the fraction variation of a biomass species j at the biofilm depth z due to the comparison of its specific growth rate (μ_j) and the average growth rate of all biomass species at the biofilm depth z ($\bar{\mu}$):

$$\bar{\mu} = \sum_{j=1}^{j=6} (\mu_j f_j) \qquad 7$$

The second term on the right side of Equation 6 describes the fraction variation of the biomass species *j* at the biofilm depth *z* due to the biofilm expansion or shrinkage (i.e., biomass advection). It is proportional to the biofilm moving speed, u_L:

$$u_L = \frac{dL}{dt} = \int_0^z \sum_{j=1}^{j=6} (\mu_j f_j) dz - k_{\text{det}} \times \mathrm{L}_f^2 \times \frac{L}{L_f} \qquad 8$$

The boundary condition for Equation 6 at the interface between the membrane and the biofilm and the interface between the water diffusion layer and the biofilm is no flux. Therefore, Equation 6 is simplified to Equation 9 at the boundaries:

$$\left.\frac{df_j}{dt}\right|_{z=0 \text{ or } L_f} = (\mu_j - \bar{\mu}) f_j \qquad (j = 1,2,3,4,5,6) \qquad 9$$

The biofilm thickness is simulated by Equation 10, which is the biofilm surface form of Equation 8:

$$\frac{dL_f}{dt} = \int_0^{L_f} \sum_{j=1}^{j=6} (\mu_j f_j) dz - k_{\text{det}} \times \mathrm{L}_f^2 \qquad 10$$

The first term on the right side of Equation 10 represents the biofilm expansion due to biomass growth, and the second term represents the biofilm shrinkage due to biomass detachment that is described by a second-order function of $\mathrm{L_f}$ (Stewart 1993, Tang et al. 2012). At steady state, the biofilm surface remains stationary as biofilm expansion by growth balances biofilm shrinkage by detachment.

2.3 Numerical Solution

This problem includes two dynamic processes that occur at very different time scales: biofilm development, which takes place over days, and diffusion and reaction of dissolved chemical species, which occur with a time scale of seconds to minutes. Therefore, equations for these two processes can be decoupled and solved sequentially (Picioreanu et al. 2000). The equations for the dissolved chemical species (Equations 1-5) are solved to a pseudo-steady state using the finite difference method and with the biomass species assumed to be in in "frozen" state that does not

change over the seconds to minutes needed to establish the pseudo-steady state for the dissolved species (Wanner 2006). The chemical species concentrations from the pseudo-steady state solution are then used to solve Equations 6-10 for updating the biomass species distribution and the biofilm thickness at the next time step for the solid components (e.g., after 1 day). With the updated biofilm thickness and biomass fractions, the concentrations of the chemical species at the new time step can be solved to a new pseudo-steady state. The process is repeated until the solution reaches a global steady state, in which the biofilm thickness, concentrations of chemical species, and fractions of biomass species do not change with time.

2.4 Parameterization

The model inputs in Table III can be divided into two categories: 1) biological parameters, including the half-maximum-rate concentration (K), the maximum specific growth rate (μ_{max}), the biomass yield coefficient (Y), and the endogenous-decay coefficient (b); and 2) physical and transport constants, including the diffusion coefficients (D and D_f), the biofilm density (X_f), and the Henry's law constant (K_H). Values of the biological parameters, taken from the literature, depend on the specific microbial species and reaction. For instance, the values of the decay coefficient for methanogens (b_2) are reported to be 0.015 day^{-1} (Clapp et al. 2004), 0.024 day^{-1} (Fennell and Gossett 1998), and 0.05 day^{-1} (Christ and Abriola 2007). We chose the median value 0.024 day^{-1} as the model input. Reported values of maximum specific growth rate for *Dehalococcoides* performing TCE reduction (μ_{1_max}) are 0.33 day^{-1} (Cupples et al. 2004), 0.49 day^{-1} (Tang et al. 2013), and 0.75 day^{-1} (Yu and Semprini 2004). We chose the median value 0.49 day^{-1} as the model input for *Dehalococcoides* (μ_{1_max}). The variability of the physical and transport constants is generally smaller than that of the biological kinetic parameters. One exception is the density of active biomass in the biofilm, X_f, which can span a wide range, 5 - 200 mg volatile solids/cm^3 (Rittmann and McCarty 2001). We chose a typical value for X_f, 40 mg volatile solids/cm^3 = 79 mg COD/cm^3. We did not fit any parameters to achieve a good match to experimental results; thus, the modeling output are predictions based on literature-derived parameter values.

2.5 Simulation of an Experiment

To evaluate the model, we simulated a bench-scale H_2-MBfR experiment conducted by Ziv-El et al. (Ziv-El et al. 2012a). The reactor treated a synthetic groundwater containing TCE until steady

state was achieved. At steady state, the biofilm was sampled and analyzed by quantitative polymerase chain reaction (qPCR) to quantify the relative abundance of *Dehalococcoides*, *Geobacter*, homoacetogens, and methanogens. Concentrations in the reactor effluent were reported for acetate, TCE, DCE, VC, and ethene. We compare the modeled steady-state results, including the relative abundance of the biomass species in the biofilm and the concentrations of the dissolved chemical species in the reactor effluent, with the analogous experimental results in Results and Discussion.

3 RESULTS AND DISCUSSION

The mathematical model was evaluated by simulating conditions reported for a bench-scale H_2-MBfR experiment with TCE (Ziv-El et al. 2012a). Figure 2(a) shows the model-generated biomass fractions along a biofilm depth of 15 μm, the steady-state thickness. The corresponding specific growth rates are plotted in Figure 2(b), and concentrations of dissolved-species are in Figure 3. The biofilm can be divided into three layers that are characterized by one dominant type of microorganism. Layer 1, next to the membrane, is dominated by homoacetogens. *Dehalococcoides* and *Geobacter* are suppressed due to the low concentration of TCE and DCE in this layer (Figure 3). A biomass species can exist at the biofilm-membrane interface only if its specific growth rate is high enough to be the same as the average specific growth rate of all biomass species ($\mu_j - \bar{\mu} = 0$); homoacetogens, inert biomass, and EPS meet this criterion and are present at this boundary, Figure 2(b)). A species is out-competed when its specific growth rate is smaller than the average, and $f_j = 0$ is true for *Dehalococcoides*, *Geobacter*, and methanogens at the membrane boundary, Figure 2(b).

Dehalococcoides dominate in Layer 2 due to the presence of TCE and DCE in this layer (Figure 3). *Dehalococcoides* outcompete *Geobacter* in this layer because *Dehalococcoides* can utilize TCE, DCE, and VC as election acceptors, while *Geobacter* can utilize only TCE.

Geobacter dominates in Layer 3 (next to the water diffusion layer) due to the high TCE concentration (Figure 3) and because *Geobacter* has a faster specific growth rate with TCE reduction than *Dehalococcoides*. *Geobacter*, homoacetogens, and IB can exist on this boundary due to them having higher specific growth rates than the other biomass species (Figure 2(b)). Methanogens are nearly absent in Layer 3, because they are out-competed by homoacetogens,

which have a much higher maximum specific growth rate.

The supplied electron donor, H_2, is not limiting anywhere in the biofilm, since its concentration is about 13 mg COD/L, orders of magnitude higher than the half-maximum-rate constants for all active biomass species (3.2×10^{-4} – 0.21 mg COD/L). The variation of the active biomass species in the biofilm is mainly caused by the high TCE and DCE concentration gradients in the biofilm (Figure 3), as well as their concentrations being smaller than their corresponding half-maximum-rate constants.

The non-active biomass species (i.e., EPS and inert biomass) accumulate mostly near the membrane (Layer 1). Since the growth-limiting substrates (i.e., the electron acceptors) for the active components are at higher concentrations near the water side (Figure 3), the active biomass components have an advantage in Layers 2 and 3. Not needing an electron acceptor, the inactive components are able to accumulate in Layer 1.

Dissolved chemical species other than TCE and DCE do not change significantly in the relatively thin biofilm (15 μm). Their consumption reactions are too slow, production reactions are too fast, or both to bring about concentration gradients. Acetate is an example of fast production and slow consumption. Homoacetogens produce 165 mmole of acetate/day, per Equation 11:

$$\left[Generated\ acetate\right] = \frac{1}{64} A\eta_{77} \int_0^{L_f} R_7 dz \qquad 11$$

(Symbols in Equations 11 - 14 are defined in Tables I - III.) *Dehalococcoides* and *Geobacter* utilize acetate at a rate of 3.7 mmole of acetate/day (i.e., 2.3% of total produced acetate) as their carbon source (Eqn. 12), and *Geobacter* also utilizes 2.6 mmole of acetate/day (i.e., 1.6% of total produced acetate) as its electron donor (Eqn. 13). Together, they consume only ~4% of the generated acetate, and 96% diffuses out of the biofilm and leaves in the reactor effluent (158 mmole of acetate/day, Equation 14).

$$\left[Carbon\ source\right] = \frac{1}{64} A\eta_c \int_0^{L_f} \left(R_1 + R_2 + R_3 + R_{10} + R_{11}\right) dz \qquad 12$$

$$\left[Electron\ donor\right] = \frac{1}{64} A\eta_{7-11} \int_0^{L_f} R_{11} dz \qquad 13$$

$$[Effluent] = \frac{1}{64} S_{b7} Q \qquad 14$$

How do the mathematical modeling results compare to the results from the MBfR experiments (Ziv-El et al. 2012a)? Table VII compares the analogous results side-by-side. In general, the experiment and the model simulation are consistent. The model and experiments agree that the active biomass was dominated by *Dehalococcoides* (43% of 16S rRNA gene reads in experiment and 49% of the active biomass in model) and *Geobacter* (39% in experiment and 32% in model). Methanogens were negligible (0.4% in the experiment and 1.0% in the model) because they were outcompeted by homoacetogens, whose maximum specific growth rate is twice that of methanogens.

The model and experiments also coincide in terms of the fate of the chlorinated ethenes: TCE reduction was >98% of the input 0.33 mM TCE in the model and experiment, accumulation of DCE was minor (0.00062 mM in model and 0.013 mM in experiment, VC had the largest accumulation (0.07 mM in model and 0.1 mM in experiment, about 1/3 of the TCE in the influent), and ethene was 0.25 mM in model and 0.21 mM in the experiments (about 2/3rds of the TCE in the influent). The model explains that the accumulations of DCE and VC were due to the important role of *Geobacter*, which reduces TCE, but not DCE and VC. VC accumulation was greater than DCE because *Dehalococcoides* has a ~30-fold higher half-maximum-rate concentration (K) for VC than for DCE.

Acetate in the effluent was significant (4.5 mM in the experiment and 2.2 mM in the model), since its production rate by homoacetogens ($\mu_5 \times \eta_{77}$) was much greater than the acetate utilization rate by *Geobacter* and *Dehalococcoides*. Model-predicted methane also was negligible in the effluent due to the lack of methanogens.

4 CONCLUSIONS

We developed and parameterized a multispecies biofilm model to simulate and understand the interactions among TCE dechlorination, homoacetogenesis, and methanogensis in a H_2-based biofilm. Without having any fitted parameters, the model simulated well all trends observed in a MBfR not limited by H_2 supply. *Dehalococcoides* and *Geobacter*, the dominant active biomass species, accumulated away from the membrane surface and reduced >98% of the TCE. About two thirds of the TCE was converted to ethene and one third to VC due to the large half-maximum-

rate concentration of VC. Homoacetogens mainly lived near the membrane surface, generating acetate that was used as an electron donor by the *Geobacter* (2.4%) and carbon source by *Geobacter* and *Dehalococcoides* (1.3%), although most of the acetate diffused out of the biofilm. The two TCE-reducing biomass species and homoacetogens outcompeted hydrogenotrophic methanogens, resulting in insignificant methane generation.

5 ACKNOWLEDGEMENTS

The authors gratefully thank the U.S. Department of Defense's Strategic Environmental Research and Development Program (SERDP) for funding the research through Project ER-2721.

REFERENCES

Aulenta, F., J. M. Gossett, M. P. Papini, S. Rossetti and M. Majone (2005). Comparative study of methanol, butyrate, and hydrogen as electron donors for long-term dechlorination of tetrachloroethene in mixed anerobic cultures. *Biotechnol. Bioeng.* 91(6): 743-753.

Chambon, J., G. Lemming, M. Broholm, P. J. Binning and P. L. Bjerg (2009). Model assessment of reductive dechlorination as a remediation technology for contaminant sources in fractured clay: Modeling Tool Delrepport II. Danish Environmental Protection Agency.

Chambon, J. C., P. L. Bjerg, C. Scheutz, J. Bælum, R. Jakobsen and P. J. Binning (2013). Review of reactive kinetic models describing reductive dechlorination of chlorinated ethenes in soil and groundwater. *Biotechnol. Bioeng.* 110(1): 1-23.

Christ, J. A. and L. M. Abriola (2007). Modeling metabolic reductive dechlorination in dense non-aqueous phase liquid source-zones. *Adv. Water Resour.* 30(6-7): 1547-1561.

Chung, J., R. Krajmalnik-Brown and B. Rittmann, E (2007). Bioreduction of trichloroethene using a hydrogen-based membrane biofilm reactor. *Environ. Sci. Technol.* 42(2): 477-483.

Chung, J. and B. E. Rittmann (2008). Simultaneous bio-reduction of trichloroethene, trichloroethane, and chloroform using a hydrogen-based membrane biofilm reactor. *Water Sci. Technol.* 58(3): 495-501.

Clapp, L. W., M. J. Semmens, P. J. Novak and R. M. Hozalski (2004). Model for in situ perchloroethene dechlorination via membrane-delivered hydrogen. *J. Environ. Eng.* 130(11): 1367-1381.

Cupples, A. M., A. M. Spormann and P. L. McCarty (2004). Vinyl chloride and cis-dichloroethene dechlorination kinetics and microorganism growth under substrate limiting conditions. *Environ. Sci. Technol.* 38(4): 1102-1107.

Delgado, A. G., P. Parameswaran, D. Fajardo-Williams, R. U. Halden and R. Krajmalnik-Brown (2012). Role of bicarbonate as a pH buffer and electron sink in microbial dechlorination of chloroethenes. *Microb. Cell Fact.* 11(1): 128.

Dugat-Bony, E., C. Biderre-Petit, F. Jaziri, M. M. David, J. Denonfoux, D. Y. Lyon, J. Y. Richard, C. Curvers, D. Boucher and T. M. Vogel (2012). In situ TCE degradation mediated by complex dehalorespiring communities during biostimulation processes. *Microb. Biotechnol.* 5(5): 642-653.

Fennell, D. E. and J. M. Gossett (1998). Modeling the production of and competition for hydrogen in a dechlorinating culture. *Environ. Sci. Technol.* 32(16): 2450-2460.

He, J., V. F. Holmes, P. K. Lee and L. Alvarez-Cohen (2007). Influence of vitamin B12 and cocultures on the growth of Dehalococcoides isolates in defined medium. *Appl. Environ. Microbiol.* 73(9): 2847-2853.

He, J., K. M. Ritalahti, K.-L. Yang, S. S. Koenigsberg and F. E. Löffler (2003). Detoxification of vinyl chloride to ethene coupled to growth of an anaerobic bacterium. *Nature* 424(6944): 62.

He, J., Y. Sung, R. Krajmalnik-Brown, K. M. Ritalahti and F. E. Löffler (2005). Isolation and characterization of Dehalococcoides sp. strain FL2, a trichloroethene (TCE)-and 1, 2-dichloroethene-respiring anaerobe. *Environ. Microbiol.* 7(9): 1442-1450.

Huang, D. and J. G. Becker (2009). Determination of intrinsic monod kinetic parameters for two heterotrophic tetrachloroethene (PCE)-respiring strains and insight into their application.

Biotechnol. Bioeng. 104(2): 301-311.

Johnson, D. R., A. Nemir, G. L. Andersen, S. H. Zinder and L. Alvarez-Cohen (2009). Transcriptomic microarray analysis of corrinoid responsive genes in Dehalococcoides ethenogenes strain 195. *FEMS Microbiol. Lett.* 294(2): 198-206.

Kotsyurbenko, O. R., M. V. Glagolev, A. N. Nozhevnikova and R. Conrad (2001). Competition between homoacetogenic bacteria and methanogenic archaea for hydrogen at low temperature. *FEMS Microbiol. Ecol.* 38(2-3): 153-159.

Leaist, D. G. and P. A. Lyons (1981). Multicomponent diffusion of electrolytes with incomplete dissociation. diffusion in a buffer solution. *J. Phys. Chem.* 85(12): 1756-1762.

Maharajh, D. M. and J. Walkley (1972). Lowering of the saturation solubility of oxygen by the presence of another gas. *Nature* 236(5343): 165.

Matteucci, F., C. Ercole and M. del Gallo (2015). A study of chlorinated solvent contamination of the aquifers of an industrial area in central Italy: a possibility of bioremediation. *Front. Microbiol.* 6: 924.

Maymó-Gatell, X., Y.-t. Chien, J. M. Gossett and S. H. Zinder (1997). Isolation of a bacterium that reductively dechlorinates tetrachloroethene to ethene. *Science* 276(5318): 1568-1571.

Maymó-Gatell, X., V. Tandoi, J. M. Gossett and S. H. Zinder (1995). Characterization of an H2-utilizing enrichment culture that reductively dechlorinates tetrachloroethene to vinyl chloride and ethene in the absence of methanogenesis and acetogenesis. *Appl. Environ. Microbiol.* 61(11): 3928-3933.

Moran, M. J., J. S. Zogorski and P. J. Squillace (2007). Chlorinated solvents in groundwater of the United States. *Environ. Sci. Technol.* 41(1): 74-81.

Mundle, S. O., T. Johnson, G. Lacrampe-Couloume, A. Pérez-de-Mora, M. Duhamel, E. A. Edwards, M. L. McMaster, E. Cox, K. Révész and B. Sherwood Lollar (2012). Monitoring biodegradation of ethene and bioremediation of chlorinated ethenes at a contaminated site using compound-specific isotope analysis (CSIA). *Environ. Sci. Technol.* 46(3): 1731-1738.

Ni, B. J., H. Liu, Y. Q. Nie, R. J. Zeng, G. C. Du, J. Chen and H. Q. Yu (2011). Coupling glucose fermentation and homoacetogenesis for elevated acetate production: experimental and mathematical approaches. *Biotechnol. Bioeng.* 108(2): 345-353.

Picioreanu, C., M. C. Van Loosdrecht and J. J. Heijnen (2000). Effect of diffusive and convective substrate transport on biofilm structure formation: a two-dimensional modeling study. *Biotechnol. Bioeng.* 69(5): 504-515.

Rittmann and McCarty (2001). Environmental biotechnology: principles and applications. New York: McGrawHill.

Stewart, P. S. (1993). A model of biofilm detachment. *Biotechnol. Bioeng.* 41(1): 111-117.

Sung, Y., K. E. Fletcher, K. M. Ritalahti, R. P. Apkarian, N. Ramos-Hernández, R. A. Sanford, N. M. Mesbah and F. E. Löffler (2006). Geobacter lovleyi sp. nov. strain SZ, a novel metal-reducing and tetrachloroethene-dechlorinating bacterium. *Appl. Environ. Microbiol.* 72(4): 2775-2782.

Tang, Y., R. Krajmalnik-Brown and B. E. Rittmann (2013). Modeling trichloroethene reduction in a hydrogen-based biofilm. *Water Sci. Technol.* 68(5): 1158-1163.

Tang, Y., H. Zhao, A. K. Marcus, R. Krajmalnik-Brown and B. Rittmann, E (2012). A steady-state

biofilm model for simultaneous reduction of nitrate and perchlorate, part 1: model development and numerical solution. *Environ. Sci. Technol.* 46(3): 1598-1607.

U.S. Environmental Protection Agency, National Primary Drinking Water Regulations. 2009, https://www.epa.gov/ground-water-and-drinking-water/national-primary-drinking-water-regulations.

Varfolomeyev, S., S. Kalyuzhnyy and S. Spivak (1989). Kinetic regularities of methane production by a methanogenic association. *Appl. Environ. Microbiol.* 22(3): 351-360.

Vavilin, V., L. Y. Lokshina, S. Rytov, O. Kotsyurbenko, A. Nozhevnikova and S. Parshina (1997). Modelling methanogenesis during anaerobic conversion of complex organic matter at low temperatures. *Water Sci. Technol.* 36(6-7): 531-538.

Wanner, O. (2006). Mathematical modeling of biofilms. IWA Publishing.

Yu, S., M. E. Dolan and L. Semprini (2005). Kinetics and inhibition of reductive dechlorination of chlorinated ethylenes by two different mixed cultures. *Environ. Sci. Technol.* 39(1): 195-205.

Yu, S. and L. Semprini (2004). Kinetics and modeling of reductive dechlorination at high PCE and TCE concentrations. *Biotechnol. Bioeng.* 88(4): 451-464.

Zeebe, R. E. (2011). On the molecular diffusion coefficients of dissolved CO2, HCO3-, and CO32- and their dependence on isotopic mass. *Geochim. Cosmochim. Acta.* 75(9): 2483-2498.

Ziv-El, M., S. C. Popat, K. Cai, R. U. Halden, R. Krajmalnik-Brown and B. E. Rittmann (2012). Managing methanogens and homoacetogens to promote reductive dechlorination of trichloroethene with direct delivery of H2 in a membrane biofilm reactor. *Biotechnol. Bioeng.* 109(9): 2200-2210.

Table I. Process, solid biomass species, and rate matrix

Process (p)		Coefficient of species j in process p (η_{jp})						Conversion rate R_p[1]
		Solid biomass species (j)						
		1	2	3	4	5	6	
		Dehalococ-coides	*Geobacter*	Methanogens	Homoaceto-gens	IB	EPS	
Dehalococcoides	1 Growth on TCE	k_1					k_3/Y_1	R_1
	2 Growth on DCE	k_1					k_3/Y_2	R_2
	3 Growth on VC	k_1					k_3/Y_3	R_3
	4 Inactivation	-1				$(1-f_d)$		$b_1 f_1 X_f$
Methanogens	5 Growth			k_1			k_3/Y_5	R_5
	6 Inactivation			-1		$(1-f_d)$		$b_2 f_2 X_f$
Homoacetogens	7 Growth				k_1		k_3/Y_7	R_7
	8 Inactivation				-1	$(1-f_d)$		$b_3 f_3 X_f$
EPS	9 Hydrolysis						-1	$k_{hyd} f_5 X_f$
Geobacter	10 Growth on H_2		k_1				k_3/Y_{10}	R_{10}
	11 Growth on acetate		k_1				k_3/Y_{11}	R_{11}

	12 Inactivation	-1 (1-f_d)	$b_6 f_6 X_f$
Summed specific growth rate of solid species *j*	$\mu_j = \frac{\sum_p (\eta_{jp} R_p)}{f_j X_f}$		

Notes:

1. $R_1 = \mu_{1\_max} f_1 X_f \frac{S_{f1}}{K_1 + S_{f1}} \frac{S_{f5}}{K_{51} + S_{f5}}$, $R_2 = \mu_{2\_max} f_1 X_f \frac{S_{f2}}{K_2\left(1 + \frac{S_{f1}}{K_{12i}}\right) + S_{f2}} \frac{S_{f5}}{K_{52} + S_{f5}}$, $R_3 = \mu_{3\_max} f_1 X_f \frac{S_{f3}}{K_3\left(1 + \frac{S_{f1}}{K_{13i}} + \frac{S_{f2}}{K_{23i}}\right) + S_{f3}} \frac{S_{f5}}{K_{53} + S_{f5}}$,

$R_5 = \mu_{4\_max} f_2 X_f \frac{S_{f5}}{K_{55} + S_{f5}} \frac{S_{f8}}{K_{85} + S_{f8}}$, $R_7 = \mu_{5\_max} f_3 X_f \frac{S_{f5}}{K_{57} + S_{f5}} \frac{S_{f8}}{K_{87} + S_{f8}}$, $R_{10} = \mu_{6\_max} f_6 X_f \frac{S_{f1}}{K_{1-10} + S_{f1}} \frac{S_{f5}}{K_{5-10} + S_{f5}}$, $R_{11} = \mu_{7\_max} f_6 X_f \frac{S_{f1}}{K_{1-11} + S_{f1}} \frac{S_{f7}}{K_{7-11} + S_{f7}}$

Table II. Process, dissolved chemical species, and rate matrix[1]

Process (p)		Coefficient of chemical species *i* in process p (η_{ip}[2])										Conversion rate R_p[2]
		Chemical species (*i*)										
		1	2	3	4	5	6	7	8	9	10	
		TCE	DCE	VC	Ethene	H_2	CH_4	Acetate	HCO_3^-	UAP	BAP	
Dehalo-coccoides	1 Growth on TCE	η_{11}	η_{21}			η_{51}		η_c		η_{91}		R_1
	2 Growth on DCE		η_{22}	η_{32}		η_{52}		η_c		η_{92}		R_2
	3 Growth on VC			η_{33}	η_{43}	η_{53}		η_c		η_{93}		R_3
	4 Inactivation											$b_1 f_1 X_f$
Methanogens	5 Growth					η_{55}	η_{65}		η_{85}	η_{95}		R_5
	6 Inactivation											$b_2 f_2 X_f$
Homoaceto-gens	7 Growth					η_{57}		η_{77}	η_{87}	η_{97}		R_7
	8 Inactivation											$b_3 f_3 X_f$
EPS	9 Hydrolysis										1	$k_{hyd} f_5 X_f$
Geobacter	10 Growth on H_2	η_{1-10}	η_{2-10}			η_{5-1}		η_c		η_{9-10}		R_{10}
	11 Growth on acetate	η_{1-11}	η_{2-11}					$\eta_{7-11} + \eta_c$		η_{9-11}		R_{11}
	12 Inactivation											$b_6 f_6 X_f$

Summed reaction rate of dissolved chemical species *i*	$r_i = \sum_p (\eta_{ip} R_p)$	

Notes:

1. Reactions:

Dehalococcoides: TCE + H_2 → H^+ + Cl^- + DCE DCE + H_2 → H^+ + Cl^- + VC VC + H_2 → H^+ + Cl^- + ethene

Metahnogens: HCO_3^- + $4H_2$ + H^+ → CH_4 + $3H_2O$ Homoacetogens: $2HCO_3^-$ + $4H_2$ + H^+ → CH_3COO^- + $4H_2O$

Geobacter: TCE + H_2 → H^+ + Cl^- + DCE CH_3COO^- + 4 TCE + $4H_2O$ → 4DCE + $2HCO_3^-$ + $5H^+$ + $4Cl^-$

2. $\eta_{11} = \frac{4(Y_1-1)k_1}{Y_1}, \eta_{1-10} = \frac{4(Y_{10}-1)k_1}{Y_{10}}, \eta_{1-11} = \frac{4(Y_{11}-1)k_1}{Y_{11}}, \eta_{21} = \frac{3(1-Y_1)k_1}{Y_1}, \eta_{22} = \frac{3(Y_2-1)k_1}{Y_2}, \eta_{2-10} = \frac{3(1-Y_{10})k_1}{Y_{10}}, \eta_{2-11} = \frac{3(1-Y_{11})k_1}{Y_{11}}, \eta_{32} = \frac{2(1-Y_2)k_1}{Y_2}, \eta_{33} = \frac{2(Y_3-1)k_1}{Y_3}, \eta_{43} = \frac{(1-Y_3)k_1}{Y_3}, \eta_{51} = -\frac{1}{Y_1}, \eta_{52} = -\frac{1}{Y_2}, \eta_{53} = -\frac{1}{Y_3}, \eta_{55} = -\frac{1}{Y_5}, \eta_{57} = -\frac{1}{Y_7}, \eta_{5-10} = -\frac{1}{Y_{10}}, \eta_{65} = \frac{(1-Y_5)k_1}{Y_5}, \eta_{77} = \frac{(1-Y_7)k_1}{Y_7}, \eta_{7-11} = -\frac{1}{Y_{11}}, \eta_{85} = \frac{(Y_5-1)k_1}{Y_5}, \eta_{87} = \frac{2(Y_7-1)k_1}{Y_7}, \eta_{91} = \frac{k_2}{Y_1}, \eta_{92} = \frac{k_2}{Y_2}, \eta_{93} = \frac{k_2}{Y_3}, \eta_{95} = \frac{k_2}{Y_5}, \eta_{97} = \frac{k_2}{Y_7}, \eta_{9-10} = \frac{k_2}{Y_{10}}, \eta_{9-11} = \frac{k_2}{Y_{11}}, \eta_c = -\frac{2.5\ mmol\ C_2H_4O_2}{1\ mmol\ C_5H_7O_2N} \frac{\frac{64\ mg\ COD}{1\ mmol\ C_2H_4O_2}}{\frac{160\ mg\ COD}{1\ mmol\ C_5H_7O_2N}} = -1$ (carbon source)

Table III. Model inputs

Symbols	Description	Units	Values	References
K_{11}	Half-maximum-rate concentration for TCE reduction by *Dehalococcoides*	mg-COD/cm^3	9.0×10^{-5}	(Chambon et al. 2009)
K_{1-10}	Half-maximum-rate concentration for TCE reduction by *Geobacter* using H_2	mg-COD/cm^3	3.5×10^{-5}	(Huang and Becker 2009)
K_{1-11}	Half-maximum-rate concentration for TCE reduction by *Geobacter* using acetate	mg-COD/cm^3	3.5×10^{-5}	
K_{22}	Half-maximum-rate concentration for DCE	mg-COD/cm^3	3.3×10^{-4}	(Chambon et al. 2009)
K_{33}	Half-maximum-rate concentration for VC	mg-COD/cm^3	9.3×10^{-3}	
K_{51}	Half-maximum-rate concentration for H_2 in TCE reduction	mg-COD/cm^3	8.0×10^{-6}	(Tang et al. 2013)
K_{52}	Half-maximum-rate concentration for H_2 in DCE reduction	mg-COD/cm^3	8.0×10^{-6}	
K_{53}	Half-maximum-rate concentration for H_2 in VC reduction	mg-COD/cm^3	8.0×10^{-6}	
K_{55}	Half-maximum-rate concentration for H_2 in methanogenesis	mg-COD/cm^3	1.6×10^{-5}	(Chambon et al. 2009)
K_{57}	Half-maximum-rate concentration for H_2 in homoacetogenesis	mg-COD/cm^3	2.1×10^{-4}	(Kotsyurbenko et al. 2001)
K_{5-10}	Half-maximum-rate concentration for H_2 in TCE reduction by *Geobacter*	mg-COD/cm^3	3.2×10^{-7}	(Chambon et al. 2009)
K_{7-11}	Half-maximum-rate concentration for acetate in TCE reduction by *Geobacter*	mg-COD/cm^3	3.7×10^{-4}	(Huang and Becker 2009)
K_{85}	Half-maximum-rate concentration for HCO_3^- in methanogenesis	mg-COD/cm^3	9.6×10^{-2}	(Varfolomeyev et al. 1989)
K_{87}	Half-maximum-rate concentration for	mg-COD/cm^3	1.1×10^{-2}	(Vavilin et

	HCO_3^- in homoacetogenesis			al. 1997)
K_{12i}	Inhibition coefficient of TCE on DCE reduction	mg-COD/cm^3	9.0×10^{-5}	(Tang et al. 2013)
K_{13i}	Inhibition coefficient of TCE on VC reduction	mg-COD/cm^3	9.0×10^{-5}	
K_{23i}	Inhibition coefficient of DCE on VC reduction	mg-COD/cm^3	5.1×10^{-5}	
μ_{1_max}	Maximum specific growth rate of *Dehalococcoides* in TCE reduction	d^{-1}	0.49	
μ_{2_max}	Maximum specific growth rate of *Dehalococcoides* in DCE reduction	d^{-1}	0.43	
μ_{3_max}	Maximum specific growth rate of *Dehalococcoides* in VC reduction	d^{-1}	0.22	(Chambon et al. 2009)
μ_{4_max}	Maximum specific growth rate of Methanogens	d^{-1}	0.15	
μ_{5_max}	Maximum specific growth rate of Homoacetogens	d^{-1}	0.29	(Ni et al. 2011)
μ_{6_max}	Maximum specific growth rate of *Geobacter* using H_2	d^{-1}	1.6	(Huang and Becker 2009)
μ_{7_max}	Maximum specific growth rate of *Geobacter* using acetate	d^{-1}	0.6	
Y_1	Yield of *Dehalococcoides* growing on TCE	mg-COD/ mg-COD	0.060	(Tang et al. 2013)
Y_2	Yield of *Dehalococcoides* growing on DCE	mg-COD/ mg-COD	0.090	
Y_3	Yield of *Dehalococcoides* growing on VC	mg-COD/ mg-COD	0.14	(Chambon et al. 2009)
Y_5	Yield of Methanogens	mg-COD/ mg-COD	0.080	
Y_7	Yield of Homoacetogens	mg-COD/ mg-COD	0.010	(Vavilin et al. 1997)
Y_{10}	Yield of *Geobacter* using H_2	mg-COD/ mg-	0.160	(Huang and

		COD		Becker 2009)
Y_{11}	Yield of *Geobacter* using acetate	mg-COD/ mg-COD	0.06	
b_1	Inactivation coefficient for *Dehalococcoides*	d^{-1}	0.0030	(Tang et al. 2013)
b_2	Inactivation coefficient for Methanogens	d^{-1}	0.024	(Fennell and Gossett 1998)
b_3	Inactivation coefficient for Homoacetogens	d^{-1}	0.030	(Ni et al. 2011)
b_6	Inactivation coefficient for *Geobacter*	d^{-1}	0.0030	(Chambon et al. 2009)
k_1	Coefficient for electrons used for biomass production		0.77	(Rittmann and McCarty 2001)
k_2	Coefficient for electrons going to UAP		0.050	
k_3	Coefficient for electrons going to EPS		0.18	
k_{det}	Biofilm detachment coefficient	$cm^{-1}d^{-1}$	36	(Tang et al. 2013)
D_1	TCE diffusion coefficient within the diffusion layer	cm^2/d	0.54	
D_2	DCE diffusion coefficient within the diffusion layer	cm^2/d	0.61	
D_3	VC diffusion coefficient within the diffusion layer	cm^2/d	0.71	
D_4	ethene diffusion coefficient within the diffusion layer	cm^2/d	1.4	
D_5	H_2 diffusion coefficient within the diffusion layer	cm^2/d	4.4	
D_6	methane diffusion coefficient within the diffusion layer	cm^2/d	1.4	(Maharajh and Walkley 1972)
D_7	acetate diffusion coefficient within the	cm^2/d	1.0	(Leaist and Lyons

	diffusion layer			1981)
D_8	HCO_3^- diffusion coefficient within the diffusion layer	cm^2/d	1.0	(Zeebe 2011)
D_9	UAP diffusion coefficient within the diffusion layer	cm^2/d	1.0	(Tang et al. 2013)
D_{10}	BAP diffusion coefficient within the diffusion layer	cm^2/d	0.60	
D_{f1}	TCE diffusion coefficient within the biofilm	cm^2/d	0.43	$D_f = 0.8 \times D$ (Tang et al. 2012)
D_{f2}	DCE diffusion coefficient within the biofilm	cm^2/d	0.49	
D_{f3}	VC diffusion coefficient within the biofilm	cm^2/d	0.57	
D_{f4}	ethene diffusion coefficient within the biofilm	cm^2/d	1.1	
D_{f5}	H_2 diffusion coefficient within the biofilm	cm^2/d	3.5	
D_{f6}	methane diffusion coefficient within the biofilm	cm^2/d	1.1	
D_{f7}	acetate diffusion coefficient within the biofilm	cm^2/d	0.82	
D_{f8}	HCO_3^- diffusion coefficient within the biofilm	cm^2/d	0.81	
D_{f9}	UAP diffusion coefficient within the biofilm	cm^2/d	0.80	
D_{f10}	BAP diffusion coefficient within the biofilm	cm^2/d	0.48	
k_{hyd}	Hydrolysis rate of EPS	d^{-1}	0.22	(Tang et al. 2013)
f_d	Fraction of biomass that is biodegradable		0.80	
X_f	Biomass density	$mg\text{-}COD/cm^3$	79	

L_d	Thickness of effective diffusion layer	cm	0.010	
K_H	Dimensionless Henry's Law constant of H_2		0.019	

Table IV. Reactor operation parameters in Ziv-El's experiment (Ziv-El et al. 2012a)

Symbols	Description	Units	Values
A	Total membrane surface area	cm^2	112
Q	Flow rate	cm^3/d	72
V	Volume of MBfR	cm^3	70
S_1	TCE concentration in the influent	mg-COD/cm^3	0.0208
S_8	HCO_3^- concentration in the influent	mg-COD/cm^3	0.48
S_{g5}	H_2 concentration in the bulk gas	mg-COD/cm^3	0.766[1]
D_m	Hydrogen diffusion coefficient within the membrane	cm^2/d	0.014
L_m	Thickness of membrane	cm	0.005

Note: 1. For consistency, H_2 concentration in the fiber lumen, instead of H_2 pressure, is used. H_2 concentration is calculated using the ideal gas law: S_{g5} = 1.17 atm ÷ 82.057 cm^3-atm/K-mol ÷ 298 K × 16 g COD/mol × 10^3 mg/g = 0.766 mg-COD/cm^3.

Table V. Model outputs

Symbols	Description	Units
L_f	Thickness of biofilm	cm
L	distance from the attachment surface to position z in the biofilm	cm
μ_L	moving speed of biofilm at position z	cm/d
$\bar{\mu}$	average specific growth rate of all solid species	d^{-1}
f_1	fraction of *Dehalococcoides*	--
f_2	fraction of Methanogens	--
f_3	fraction of Homoacetogens	--
f_4	fraction of IB	--
f_5	fraction of EPS	--
f_6	fraction of *Geobacter*	--
S_{f1}	TCE concentration in the biofilm	mg-COD/cm^3
S_{f2}	DCE concentration in the biofilm	mg-COD/cm^3
S_{f3}	VC concentration in the biofilm	mg-COD/cm^3
S_{f4}	ethene concentration in the biofilm	mg-COD/cm^3
S_{f5}	H_2 concentration in the biofilm	mg-COD/cm^3
S_{f6}	methane concentration in the biofilm	mg-COD/cm^3
S_{f7}	acetate concentration in the biofilm	mg-COD/cm^3
S_{f8}	HCO_3^- concentration in the biofilm	mg-COD/cm^3
S_{f9}	UAP concentration in the biofilm	mg-COD/cm^3
S_{f10}	BAP concentration in the biofilm	mg-COD/cm^3
S_{b1}	TCE concentration in the effluent	mg-COD/cm^3
S_{b2}	DCE concentration in the effluent	mg-COD/cm^3

S_{b3}	VC concentration in the effluent	mg-COD/cm^3
S_{b4}	ethene concentration in the effluent	mg-COD/cm^3
S_{b5}	H_2 concentration in the effluent	mg-COD/cm^3
S_{b6}	methane concentration in the effluent	mg-COD/cm^3
S_{b7}	acetate concentration in the effluent	mg-COD/cm^3
S_{b8}	HCO_3^- concentration in the effluent	mg-COD/cm^3
S_{b9}	UAP concentration in the effluent	mg-COD/cm^3
S_{b10}	BAP concentration in the effluent	mg-COD/cm^3

Table VI. Unit conversions from mmol to mg COD

Dissolved chemical species	Basis for COD conversion	mg COD/mmol
TCE (C_2HCl_3)	Ethane (C_2H_6)	-64
DCE ($C_2H_2Cl_2$)	Ethane (C_2H_6)	-48
VC (C_2H_3Cl)	Ethane (C_2H_6)	-32
Ethene (C_2H_4)	Ethane (C_2H_6)	-16
Bicarbonate (HCO_3^-)	Methane (CH_4)	-64
Acetate ($C_2H_4O_2$)	CO_2	64
UAP & BAP[1]	CO_2	160

Methane (CH_4)	CO_2	64
H_2	H_2O	16

Note: 1. Assume UAP and BAP have the same chemical composition as microbial cells, $C_5H_7O_2N$. (Rittmann and McCarty 2001)

Table VII. Comparison of simulated results to experimental effluent concentrations and relative microbial fractions in Ziv-El et al. (Ziv-El et al. 2012a)

	Experiment Results	Simulation Results
TCE (mM)	<0.00001	0.0039
DCE (mM)	0.013	0.00062
VC (mM)	0.10	0.071
ethene (mM)	0.21	0.25
methane (mM)	Not measured	0.0067
acetate (mM)	4.5	2.20
Dehalococcoides (%)[1]	43.3	49.3
methanogens(%)[1]	0.4	1.1
homoacetogens (%)[1]	17.3	17.7
Geobacter (%)[1]	39.0	32.0

Note: 1. To be consistent with Ziv-El et al., (Ziv-El et al. 2012a) the fraction of each solid biomass species is mass of one active biomass species in the biofilm divided by the mass of total active biomass species in the biofilm.

LIST OF FIGURES AND THEIR LEGENDS

Figure 1. Model components and their interactions in the H_2-based membrane biofilm. Notes: The blue square symbols represent dissolved chemical species and green round symbols represent solid biomass species

Figure 2. Simulation of the experiment in Ziv-El et al (Ziv-El et al. 2012a). (a) Distribution of (solid) biomass species along the biofilm depth; (b) Specific growth rates of (solid) biomass species along the biofilm depth

Figure 3. Dissolved chemical species concentrations along the biofilm depth in the simulation of the experiment in Ziv-El et al (Ziv-El et al. 2012a).

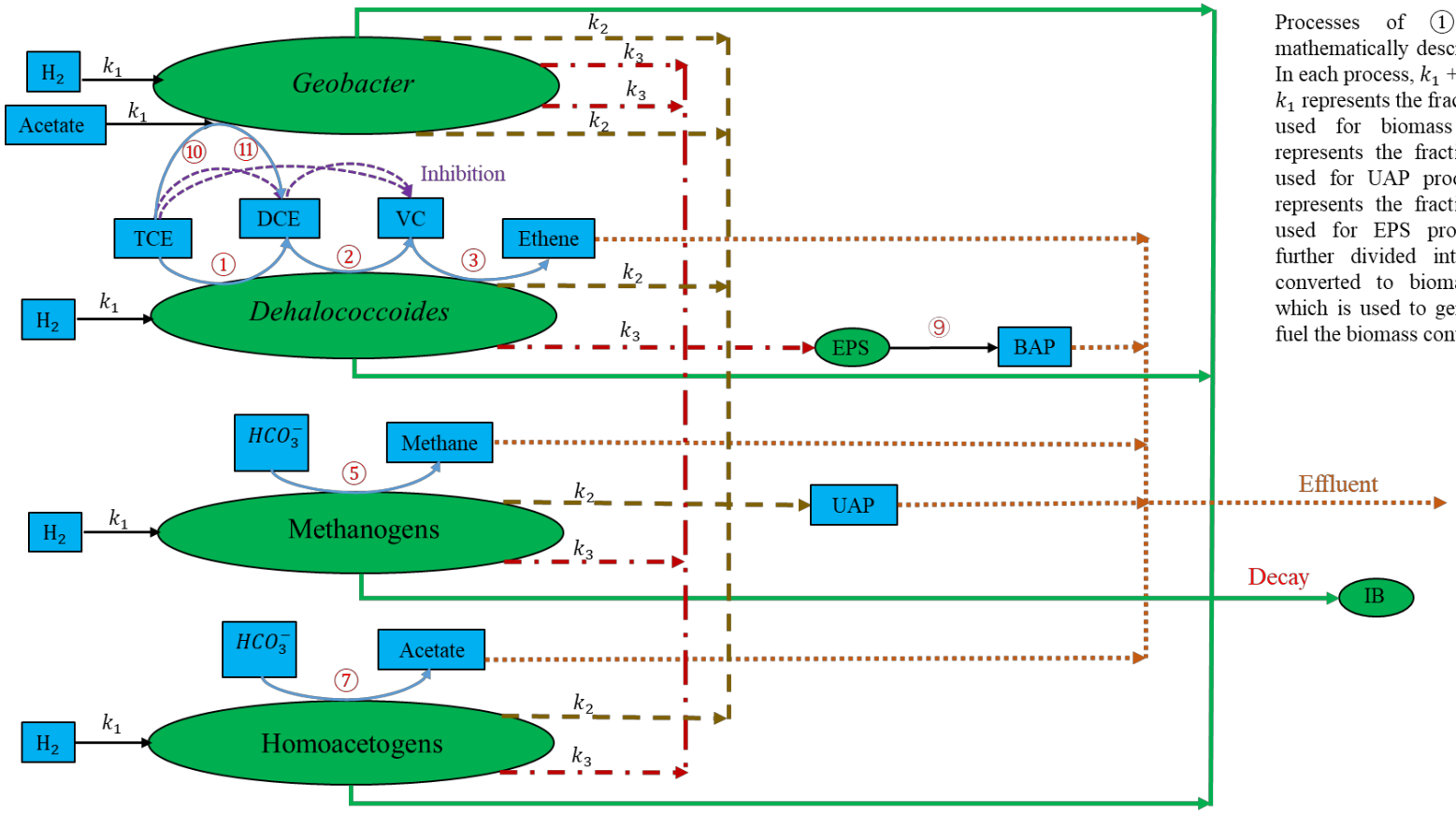

Processes of ① to ⑪ are mathematically described in Table 1. In each process, $k_1 + k_2 + k_3 = 1$. k_1 represents the fraction of electrons used for biomass synthesis, k_2 represents the fraction of electrons used for UAP production, and k_3 represents the fraction of electrons used for EPS production. k_1 is further divided into Y, which is converted to biomass, and (1-Y), which is used to generate energy to fuel the biomass conversion.

Figure 1. Model components and their interactions in the H_2-based membrane biofilm. Notes: The blue square symbols represent dissolved chemical species and green round symbols represent solid biomass species

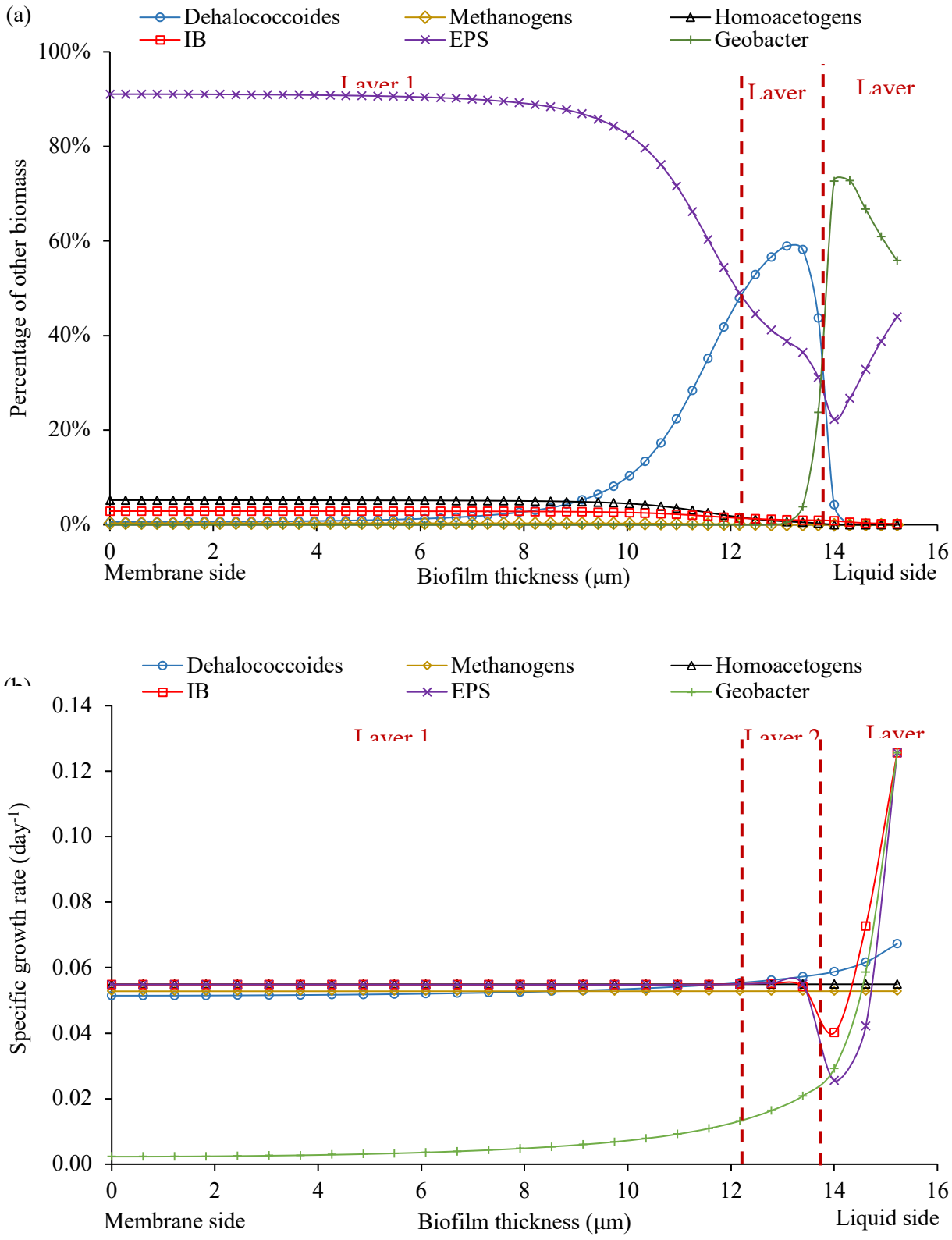

Figure 2. Simulation of the experiment in Ziv-El et al. (Ziv-El et al. 2012a). (a) Distribution of (solid) biomass species along the biofilm depth; (b) Specific growth rates of (solid) biomass

species along the biofilm depth

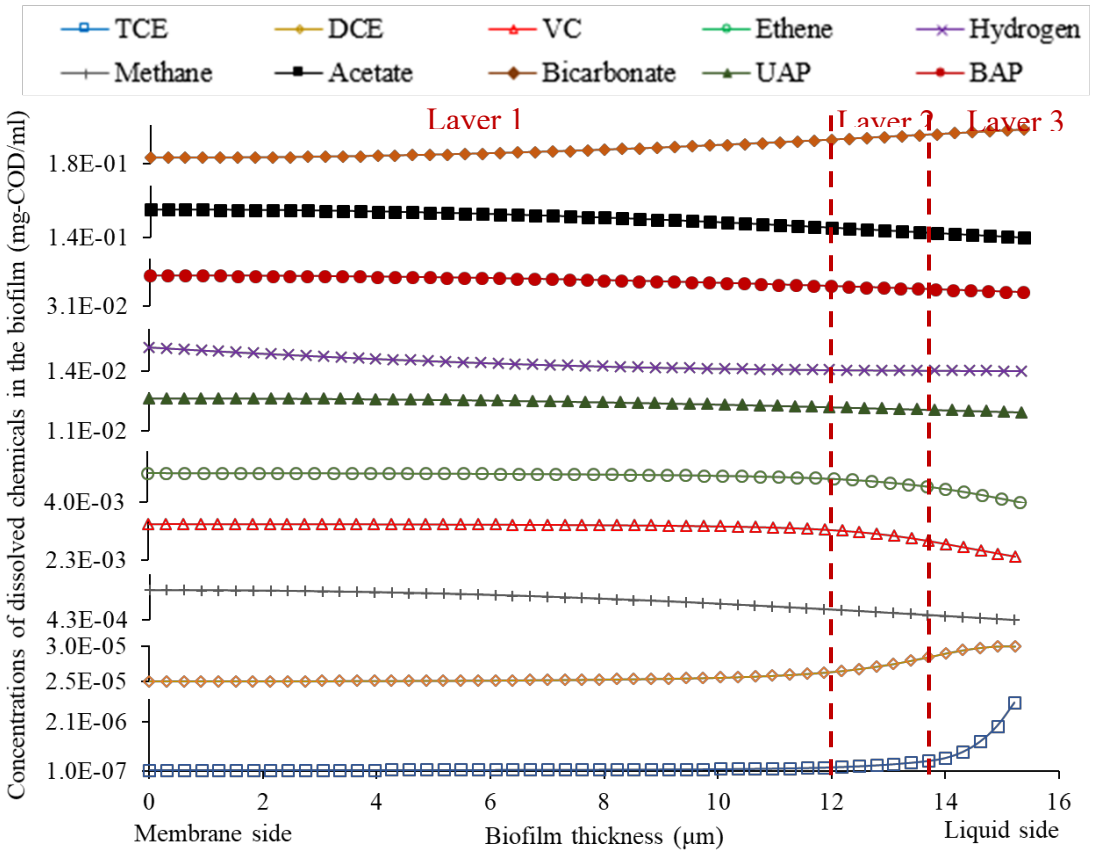

Figure 3. Dissolved chemical species concentrations along the biofilm depth in the simulation of the experiment in Ziv-El et al. (Ziv-El et al. 2012a)